Dual responsive physical networks from asymmetric biosynthetic triblock copolymers

Thao Thi Hien Pham

Dual responsive physical networks from asymmetric biosynthetic triblock copolymers

Thao Thi Hien Pham

CONTENTS

iii

iv

Chapter 1

Introduction

1.1.   Hydrogels

Hydrogels are crosslinked polymer networks that swell in water (Figure 1.1). Hydrogels can be made from any water-soluble polymer, encompassing a wide range of chemical compositions and bulk physical properties. Hydrogels also possess a degree of flexibility very similar to natural tissue, due to their significant water content [1].
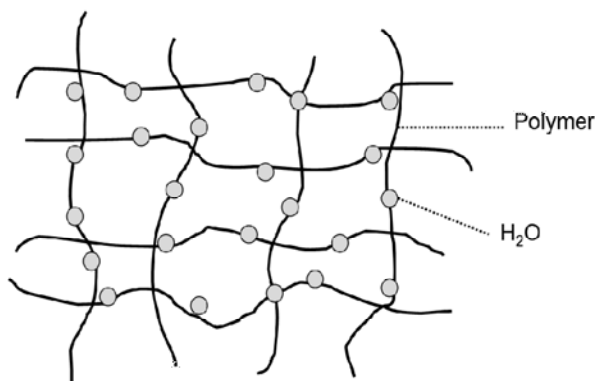
Figure 1.1 Hydrogel.

There are various types of hydrogels that are different in crosslinks, linker chains, and chain flexibility. These features determine the hydrogel properties. Regarding the forces involved in the building up of networks, hydrogels can be distinguished as chemical hydrogels and physical hydrogels [2]. The network of chemical links joining different chains can be obtained by covalently cross-linking bulk polymers or polymers in solution, whereas in physical hydrogels, chains are held together by ionic, hydrogen bonding and hydrophobic interactions. In both cases, the density of cross-links is crucial in determining the properties and applications of the gels.

1.2.   Applications

Hydrogels in food

In the food industry, the popular applications of hydrogels are as a gelling agent and food thickener. Hydrogels such as gelatin give better elastic properties. Hydrogels are used as food thickening agent such as xanthan gum to give the pleasant texture (ice-cream,

yoghurt) or to facilitate using food products (salad dressings, sauces). Moreover, the use of food proteins to develop environment-sensitive hydrogels for nutraceutical delivery constitutes a promising strategy. A fundamental advantage of this approach is that nutraceutical carrier gels can stabilize food texture, which is a highly desirable characteristic in the manufacturing of food products [3]. Hydrogel-based delivery brings about the possibility to achieve site specific release of the agent. The porous structure of hydrogels, along with their water content, are extremely suitable properties to accommodate high loads of water-soluble compounds, like therapeutically active proteins and peptides [4].

Hydrogels in biomedical applications

Hydrogels which possess a degree of flexibility very similar to natural tissues are generally regarded as biocompatible materials in regenerative medicine; their high water content and soft nature render them similar to natural extracellular matrices, so that they minimize tissue irritation and cell adherence [5]. Furthermore, hydrogels may affect the fields of biotechnology, pharmacology, and biosensors by providing solutions for large-scale protein production, drug screening techniques, and individualized chemo-sensitivity assays.

Tissue engineering or regenerative medicine is an emerging multidisciplinary field involving biology, medicine, and engineering by manipulating cells via their extracellular microenvironment (Figure 1.2). It is involved combination of cells, engineering and materials methods with suitable biochemical and physio-chemical factors for the development of substitutes that replace, repair or enhance the biological function of diseased or damaged human body parts [1].

Hydrogels have many different functions in the field of tissue engineering. They are applied as space filling agents, delivery vehicles for bioactive molecules, and three-dimensional structures that organize cells and present stimuli to direct the formation of a desired tissue [6]. Hydrogels in tissue engineering must meet a number of design criteria to function appropriately and promote new tissue formation such as biocompatibility, mechanical properties and controllable degradation [7]. In medical application, biocompatibility is especially problematic as the inflammatory response to a hydrogel can lead to immunological rejection of the transplanted cells. The mechanical properties of

hydrogels are also important parameters, as the gel must create and maintain adequate space for tissue development. The controlled degradation of hydrogels is also critical in tissue engineering, which should match the healing time of the tissue.
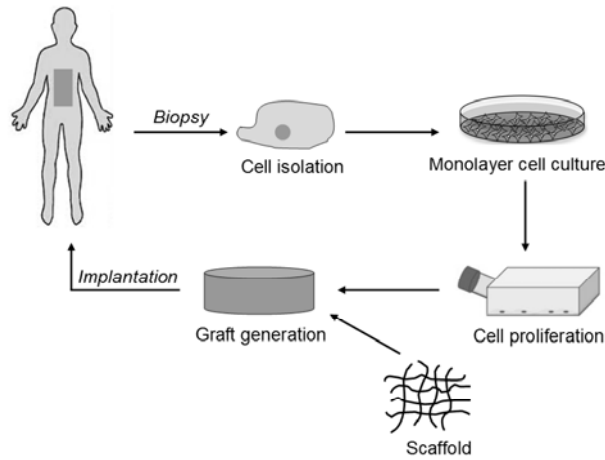
Figure 1.2 Basic principle of tissue engineering.

Both natural and synthetic gel-forming polymers are used as materials for tissue engineering. Natural polymers commonly studied for potential hydrogels derive from diverse sources, including mammalian fibrous tissues (collagen, gelatin), mammalian wound healing matrices (hyaluronate, fibrin), algae (alginate, agarose) and exoskeleton of crustaceans and cell walls of fungi (chitosan). Natural hydrogels are either components of the extra cellular matrix (ECM), or have macromolecular properties similar to the natural ECM [6]. Thus, they frequently demonstrate more biocompatibility and biodegradability than synthetic ones. Peptide-derived polymer gels might also prevent postoperative adhesion formation, [8] which is a common problem of using sheet-based synthetic hydrogels, thus improving wound healing processes.

1.3.   Physical hydrogels

A hydrogel consists of a three-dimensional network that spans the volume of a liquid medium. This internal network structure may result from physical bonds in physical gels. When the gels are formed by strong chemical bonds, they cannot be re-dissolved and are responsively irreversible, whereas gels formed by weak noncovalent interactions are

usually reversible [9, 10]. The physical joints provide extra tunability due to the controllable association/dissociation of the network. A physical gel can also form by the self-assembly of block copolymers, thus resulting in improved degradability.

Gel-forming block copolymers typically consist of two- or more- covalently linked blocks (often with an inert spacer between them) with different physical and chemical properties. They self-assemble both in solution and in bulk, and generate a variety of microdomain morphologies. Block copolymers undergo two basic processes in solvent media: micellization and gelation [11]. Otherwise, gelation likely occurs from the semi-dilute to the high concentration regime of block copolymer solutions and results from an arrangement of ordered structures.

Different methods have been investigated to create physically crosslinked gels, including ionic interaction, crystallization, hydrophobic interaction, hydrogen bonds, and composite interaction (often with proteins). In physical gels, depending on the nature of each gelling system, the junction formation can be reversibly controlled, which allows changing the shape and mechanical properties of the gels. Such controllable crosslinks widen the application of the physical gels [4, 12, 13]. Moreover, a reversible sol-gel transition (upon changing temperature, pH) in aqueous solutions may provide a user-friendly means for drug delivery, because the material is injected as a solution after which it gels in situ. This is particularly important for delivery of labile biomacromolecules [14].

Responsive hydrogels

Responsive hydrogels can exhibit swelling/collapse of the chain of the network former. This sort of responsive hydrogels have enormous potential in various applications where they can undergo a reversible and controllable shape change in response to an applied stimulus (Figure 1.3). Such hydrogels can exhibit dramatic changes in their swelling behavior, permeability or mechanical strength in response to different stimuli, both internal and external stimuli such as changes in pH, temperature, ionic strength, solvent type, electric and magnetic field, and light [10, 15, 16].

Another type of responsive hydrogels is based on the association/dissociation of crosslinks, thus exhibiting a sol-gel transition (Figure 1.4). This sol-gel process involves conversion of monomers into a colloidal solution (sol) that acts as the precursor for an

integrated network (or gel) of either discrete particles or network polymers [14]. Aqueous polymer solutions are transformed into gels by changes in environmental conditions, such as temperature, pH, and additives, thus resulting in in-situ hydrogel formation. In polymer-forming gels, the network former consists of two reactive blocks, which can associate or dissociate upon physico-chemical triggering.
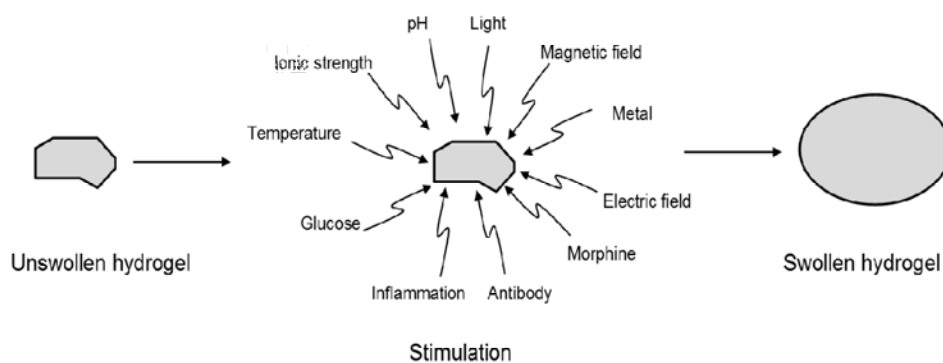
Figure 1.3 Stimuli-responsive swelling of hydrogels.
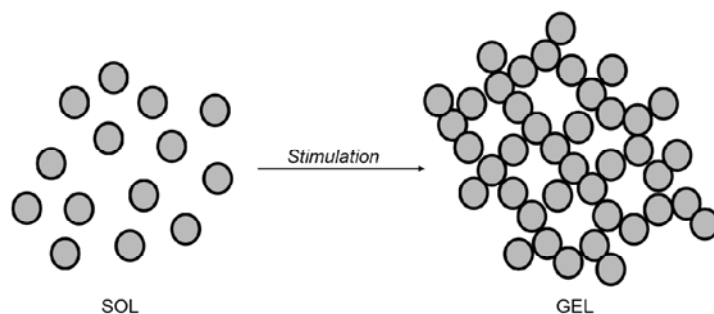
Figure 1.4 Sol-gel transition of responsive hydrogels.

Thermo-responsive hydrogels

Temperature-responsive polymers are characterized by a critical transition temperature in aqueous solutions, where the polymers switch solubility so that phase separation is observed. The gelation of temperature-responsive polymers is based on the water-solubility of the polymer chain [17], and concomitant gel swelling or collapse. Two different types of

temperature-sensitive materials can be distinguished: lower critical solution temperature (LCST) materials, and upper critical solution temperature (UCST) materials. The LCST polymer chains possess moderately hydrophobic groups or contain a mixture of hydrophilic and hydrophobic segments [17]. At low temperature, hydrogen bonds between hydrophilic segments of the polymer chain and water are dominant, leading to enhanced dissolution in water. As the temperature increases, hydrophobic interactions become strengthened while hydrogen bonds get weaker. The result is shrinking of the hydrogels or phase separation due to inter-polymer chain association through hydrophobic segments. In contrast, UCST polymers feature the formation of intramolecular hydrogen bonds below a critical temperature, which break upon increasing the temperature. This leads to phase separation upon cooling. Thus, hydrogels made from the polymers with UCST shrink when cooled below their UCST and melt (swell) upon heating.

Thermo-responsive polymer gels show a discontinuous change of the degree of swelling with temperature. If the polymer chains in the hydrogels are not covalently crosslinked, temperature-sensitive hydrogels might undergo sol-gel phase transitions, instead of swelling-shrinking transitions [17]. Sol-gel reversible hydrogels are usually based on block or graft copolymers [18]. For example, a thermo-sensitive sol-gel transition might happen in a telechelic copolymer where the two 'reactive' end-blocks are thermo-sensitive.

Gellan (composed of glucose and β-D-glucuronic acid and α-L-rhamnose), gelatine (protein obtained from the collagen hydrolysis), amylopectin, amylose and agarose are some biopolymers that also exhibit temperature sensitivity. They all have different gelation mechanisms which involves the formation of helices that act as physical crosslinks [19]. These polymers are sols at high temperature and become gel at lower temperature.

pH-responsive hydrogels

pH-sensitive hydrogels rely on changing a protonation/deprotonation equilibrium, which depends on the pKa of the acidic and/or basic moieties present in the polymer. This property is found in both synthetic polymers such as hydrolyzed poly(acrylamide), poly(acrylic acid), poly(methacrylic acid); and natural polymers (xanthan, DNA, chitosan). The formation of these hydrogels is due to the electrostatic interaction of polymers with opposite charge. Small changes in pH can result in a significant change in the mesh size of the polymeric networks. The topology of the pH-sensitive polymers governs the kind of

responsiveness (*e.g.* sol–gel transition) that will appear upon pH variation [20]. Other factors also affect the pH-responsive properties of the hydrogels such as cross-link density, ionic strength and the hydrophilicity / hydrophobicity of the counterion (Hofmeister effect).

The ionisable polymers with a pKa value between 3 to 10 are candidates for pH-responsive delivery system [21]. Application of pH-responsive hydrogels commonly takes advantages of gel swelling/collapse due to changes in pH of the external environment. Many such applications can be found in oral drug-delivery. For example, the pH-sensitive insulin-polymeric complexes swell and release insulin in the basic and neutral environments of the intestine [22, 23], but not in the acidic stomach.

Salt-responsive hydrogels

Salt-responsive network formers are usually ionic polymers containing charged groups. They exhibit varied solubility in aqueous solution depending on the salt concentration (or ionic strength). These responsive properties have been reported in synthetic block copolymers such as salt-responsive micellization [24], salt-dependent solubility [25] and pH/salt responsive system [26]. Salt-responsive hydrogels might be derived from natural polymers such as cellulose [27], xanthan [28], alginate [29] and elastin [30].

Many researches have been paid attention to single-stimulus-responsive hydrogels, which might not be very advantageous for biomedical applications since there are at least several physiological stimuli associated with pathological conditions [15]. For instance, the combination of a thermo-responsive and pH-responsive system can alter the hydrophilic/hydrophobic balance more strongly, making the polymer switch from an entirely inactive to an active state at a specific temperature or pH. This widens the range of possible application.

1.4.   Hybrid hydrogels: symmetric versus asymmetric

An emerging class of physical hydrogels with controllable self-assembly features is formed by associative triblock copolymers. These molecules have functional groups as their end blocks that can exclusively assemble into supramolecular structures upon a suitable trigger. The gel from this type of ABA triblock is formed by, e.g. hydrophobically driven self-assembly [31], charge-driven association [32], or hydrogen-bonds [33, 34]. In such symmetric networks, the nodes formed by the end blocks largely determine the network

properties. The connectors (B) in these symmetric networks can return to the same node. This leads to the formation of a loop. They may also cross over a neighboring domain, resulting in the formation of a bridge (Figure 1.5a). The molecular mechanical imperfection due to loop formation has a critical impact on the polymer networks built from an end-linked architecture [35, 36].

To remediate this effect, the asymmetry can be introduced into the network former; this implies a triblock telechelic consisting of two different end blocks. Now, each end block can only form nodes with itself, thereby, preventing loop formation (Figure 1.5b). This ABC architecture is likely to have advantages over the ABA architecture, due to greater efficiency of inter-micellar interactions and mechanical properties, especially at low concentrations [37-39].
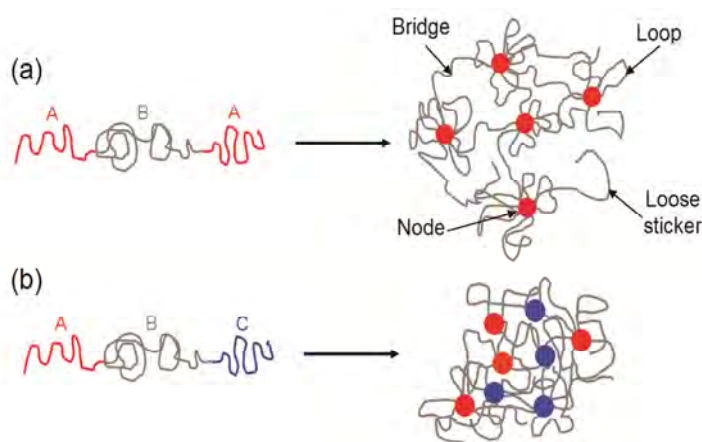
Figure 1.5 (a) Network formed by a symmetric triblock polymer (ABA) showing nodes (red dots), loops, loose sticker and bridges, (b) A hybrid network from an asymmetric triblock polymer: red nodes only connect to blue nodes. Loops are largely suppressed.

The ABC molecules consist of two distinct functional groups at two end blocks, which results in dual responsive properties and tunability. The hydrogels formed from this type of asymmetric telechelics constitute a relatively new and interesting class of hybrid hydrogels. Hydrid networks are usually referred to as hydrogel systems that possess components from at least two distinct classes of molecules [16]. This design also imparts more stimuli-responsive properties by optimizing the functional groups at the end blocks.

1.5.   Genetic engineering to produce bio-inspired network formers

Peptides and peptide derivatives that self-assemble into fibrillar gels have received increasing interest as synthetic extracellular matrices for applications in 3D cell culture and regenerative medicine. In regenerative medicine, scaffolds seek to recapitulate the function of natural ECMs by providing supramolecular frameworks capable of bringing about desired cellular or tissue level responses. The peptide-based materials have advantages over polymeric or other covalently built synthetic ECMs in that once a self-assembling material is designed, many different modifications of the base material (e.g. containing ligands, cross-linking domains, degradable sequences, drug-releasing components, etc.) can then be co-assembled into integrated multi-functional scaffolds [40]. Because the materials are constructed non-covalently, the incorporated factors can in principle be explored as combinations, which can be done much more efficiently than within covalent or polymerized materials. Further, a change in the peptide properties is caused by a conformational transition, leading to, e.g. a spatial redistribution of hydrophobic and hydrophilic residues, thus allowing to control the self-assembly of peptides [41].

Peptides as a more synthetically accessible class of compounds have been evaluated as building blocks for stimuli responsive materials. Conjugation of peptide domains and synthetic polymers may also lead to novel hybrid materials with properties superior to those of individual components. Proteins and protein modules have well defined and homogeneous structures, consistent mechanical properties, and cooperative folding/unfolding transitions. However, long and complicated polypeptides can not be produced by the conventional synthetic chemistry. The hybrid of two different responsive protein motifs in one block protein copolymer is comprehensive due to genetic engineering. Genetic engineering allows the apriority design of appropriate amino acid sequences for the various protein domains as the end blocks [34, 42-44] and the connector as the middle block into various structures of desired asymmetric (and symmetric) telechelics. Protein-based polymers can be designed to incorporate a variety of functionalities, including responsiveness to micro-environmental stimuli, controlled biodegradation and the presentation of informational motifs for cellular and subcellular interactions [45].

By designing the nucleotide sequence of the DNA template which encodes the amino acid sequence of the complete designed polypeptide, artificial co-block polypeptides with

precisely-controlled composition and sequence are achieved. Then during biosynthesis, each protein-coding gene is transcribed into a molecule of the related RNA polymer. In prokaryotes, this RNA functions as messenger RNA or mRNA. The synthesis of proteins is known as translation, when the mRNA is decoded to produce a specific polypeptide according to the rules specified by the tri-nucleotide genetic code. The genetic codes in the mRNA sequence guide the synthesis of a chain of amino acids that form a protein.
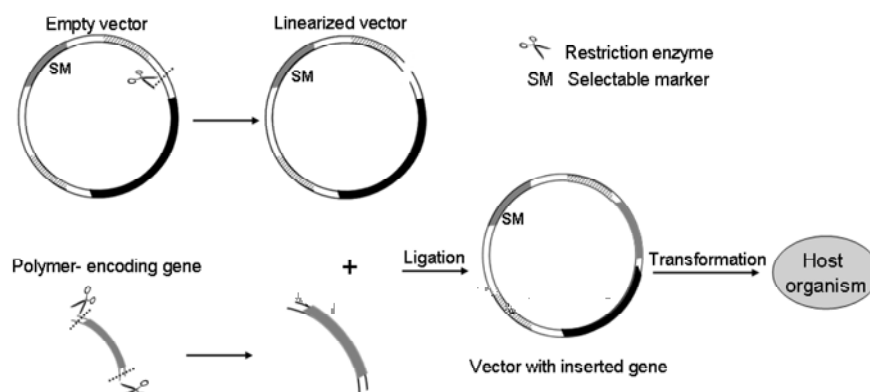
Figure 1.6 Schematic representation of the procedure to insert the constructed gene, and to introduce it into a host cell.

In order to produce protein block copolymer, such DNA-based synthesis is used. The gene is constructed by either copying the genetic codes from existing natural genes or using entirely artificial sequences with chemically synthesized nucleotide fragments. Using tools of molecular biology such as restriction enzymes (which cleave DNA) and ligation enzymes (which ligate DNA fragments), DNA fragments are combined into a desired artificial gene. The artificial gene is then inserted into a vector, a modified plasmid consisting of small circular, double-stranded DNA molecules that can replicate independently of chromosomal DNA. The plasmid containing the designed gene is finally transferred in to the host organism to produce the protein product [46]. This genetic technology provides not only the potential to combine different natural motifs into one protein polymer but also to yield monodisperse, in fact, exactly identical molecules.

1.6.   The aim and organization of the thesis

This thesis deals with a new class of hydrogels based on biomimetic protein polymers. The aim is to design, produce and understand multiscale static and dynamic physics of these hydrogels *in terms of molecular details*. The materials are made of amino acid sequences consisting of three functional parts: a *connector* (C) and two *different stickers* (S_A, S_B) in the order S_A-C-S_B, thus producing asymmetric triblock copolymers. The connector is a water soluble sequence that does not respond to physicochemical triggers like temperature, pH or additives, assuming in water a random coil structure under all conditions. The S_A and S_B sequences self-assemble upon appropriate changes in conditions. The central aim of the project is to generate new insights into structure/property relationships of the designed biopolymers in this class, and the potential of hybrid networks to produce soft materials with specific and desired properties.

Such asymmetric telechelics might also introduce various new and physically interesting features. The asymmetry causes nodes of type A to be surrounded by nodes of type B, and vice versa. Hence, a connected path through the network alternatingly visits A and B nodes; loops connecting the ends of a single molecule (which are common in the symmetric version) can be eliminated. Therefore, these systems will probably show a higher degree of attraction between nodes, and a concomitant stronger tendency to phase separation. Furthermore, the selective triggering of separate stickers leads to micelle-to-network transitions along different pathways, such as 'first A then B' or 'first B then A', that do not necessarily (and are in fact unlikely to) lead to the same final structure. It will then depend on the kinetics and the tendency of the system to relax what final structure results, and it should be possible to prepare various structures depending on the path chosen. Such history-dependent structures are particularly likely to occur for telechelic protein polymers as their associated structures typically have very long relaxation times.

Various domains inspired from natural protein polymers are combined in the asymmetric triblock protein polymers, including silklike/random-coil/elastinlike, triple helix/random-coil/cationic block, and triple helix/random-coil/triple helix with one cysteine. The molecular design including genetic engineering, production and purification of different asymmetric protein polymer will be discussed in **chapter 2**.

12

There are three different combinations of asymmetric triblock protein polymer physico-chemically studied here. The properties of hybrid molecules of silk-like and elastin-like sequences are presented in **chapter 3** and **4**. In **Chapter 3**, we investigate the pH-triggered fibril growth due to the silk-like blocks, and the effects of elastin-like blocks, regarding their thermo-responsive property. We compare the fibril formation kinetics of the triblock (silklike/random-coil/elastinlike triblock) with a diblock (silklike-elastinlike diblock), from which the outcomes reveal the important role of the random-coiled mid-block in decoupling the local interaction of the two end-blocks. The self-assembly of these sensitive blocks is further studied in **chapter 4** under conditions where both of them are reversibly responsive to physical triggers. By selectively regulating the experimental conditions, we find that the final structure of the hybrid system is dependent on the triggering pathway. The results reveal a rather complex behavior, leaving as a challenge to get more insights into this non-equilibrium self-assembly. The second asymmetric triblock protein polymer which consists of a collagen-like triple-helix former and a cationic block, bridged by a random-coiled mid-block is investigated in **chapter 5** and **6**. The collagen-like block has been reported to form thermo-responsive triple helical nodes [33, 44], which result in the formation of physical gels from a symmetric triblock. The other functional end-block, when charged, forms complexes with oppositely charged homopolymers through electrostatic interaction. **Chapter 5** characterizes the gelation of physical gels by simultaneous triggering the collagen-like block and adding flexible homopolymer (PSS). The systems show interesting properties, illustrated by a micelle-to-network transition and a phase separation when the concentration is below the critical C*. The properties of the molecule are further analyzed through the charge-driven complex formation with a semi-flexible homopolymer (xanthan). These results are described in **chapter 6**. Although the gelation highly depends on the concentration of xanthan, the presence of the protein polymer and its interactions with xanthan have remarkable impacts on the network, indicated by both an increase in storage molulus and a change in shear-thinning properties. **Chapter 7** presents the third asymmetric triblock in which the asymmetry is introduced by modifying the symmetric collagen-like triblock telechelic [44]. The addition of one cysteine to the C-terminus of the symmetric triblock results in the formation of extra-molecular disulfide bonds. The effects of the disulfide bridge formation show up as changes in thermal stability: the appearance of a second melting temperature due to the stabilized

helices (which is higher than the melting temperature of the triple helices), and increased elastic modulus of the helical network. Finally, in **chapter 8**, we summarize and critically reflect on the findings reported in the thesis, and we suggest further research directions and possible applications.

References

1.   Wikipedia.

2.   F. Bordia, G. Paradossic, C. Rinaldic and B. Ruzickad, *Physica A*, 2002, **304**, 119- 128.

3.   L. Chen, G. E. Remondetto and M. Subirade, *Trends Food Sci. Technol.*, 2006, **17**, 272-283.

4.   T. Vermonden, R. Censi and W. E. Hennink, *Chem. Rev.*, 2012, **112**, 2853-2888.

5.   S. Rimmer, Woodhead, *Publishing Series in Biomaterials*, 2011.

6.   J. L. Drury and D. J. Mooney, *Biomaterials*, 2003, **24**, 4337-4351.

7.   K. Y. Lee and D. J. Mooney, *Chem. Rev.*, 2001, **101**, 1869.

8.   J. A. Hubbell, *Curr. Opin. Biotechnol.*, 2003, **14**, 551-558.

9.   N. M. Sangeetha and U. Maitra, *Chem. Soc. Rev.*, 2005, **34**, 821-836.

10.   S. k. Ahn, R. M. Kasi, S. C. Kim, N. Sharma and Y. Zhou, *Soft Matter*, 2008, **4**, 1151-1157.

11.   J. Rodrıguez-Hernandez, F. Checot, Y. Gnanou and S. Lecommandoux, *Prog. Polym. Sci.*, 2005, **30**, 691-724.

12.   L. M. Low, S. Seetharaman, K. Q. He and M. J. Madou, *Sensor. Actuat. B-Chem.*, 2000, **67**, 149-160.

13.   B. Jeong and A. Gutowska, *Trends Biotechnol.*, 2002, **20**, 305.

14.   B. Jeong, S. W. Kim and Y. H. Bae, *Adv. Drug Deliv. Rev.*, 2002, **54**, 37-51.

15.   P. Gupta, K. Vermani and S. Garg, *Drug Discov. Today*, 2002, **7**, 569.

16.   J. i. Kopecˇek, *Biomaterials*, 2007, **28**, 5185-5192.

17.   Y. Qiu and K. Park, *Adv. Drug Deliv. Rev.*, 2001, **53***, 321-339.

18.   M. R. Aguilar, C. Elvira, A. Gallardo, B. Vázquez and J. S. Román, *Topics in Tissue Engineering*, 2007, **3**.

19.   S. Arnott, A. Fulmer, W. E. Scott, I. C. M. Dea, R. Moorhouse and D. A. Rees, *J. Mol. Biol.*, 1974, **90**, 269-284.

20.   C. Tsitsilianis, *Soft Matter*, 2010, **6**, 2372-2388.

21.   D. Schmaljohann, *Adv. Drug Deliv. Rev.*, 2006, **58**, 1655-1670.

22.   A. M. Lowman , M. Morishita , M. Kajita , T. Nagai and N. A. Peppas, *J. Pharm. Sci.* , 1999, **88**, 933.

23.   X. Gao, C. He, C. Xiao, X. Zhuang and X. Chen, *Polymer*, 2013, **54** 1786-1793.

24.   D. Wang , T. Wu , X. Wan , X. Wang and S. Liu, *Langmuir*, 2007, **23**, 11866-11874.

25.   K. Yao, C. Tang, J. Zhang and C. Bunyard, *Polym. Chem.*, 2013, **4**, 528-535.

26.   M. A. Behrens, M. Lopez, A. L. Kjøniksen, K. Zhu , B. Nyström and J. S. Pedersen *Langmuir*, 2012, **28**, 1105-1114.

27. C. Chang, M. He, J. Zhou and L. Zhang, *Macromolecules*, 2011, **44**, 1642-1648.

28. H. Izawa and J. Kadokawa, *J. Mater. Chem.*, 2010, **20**, 5235-5241.

29. H. Lin, J. Zhou, C. Yingde and S. Gunasekaran, *J. Appl. Polym. Sci.*, 2010, **115**, 3161-3167.

30. S. M. Mithieux, J. E. Rasko and A. S. Weiss, *Biomaterials*, 2004, **25**, 4921-4927.

31. S. R. Bhatia and G. N. Tew, *ACS Symposium Series*, 2012, **1114**, 313-324.

32. M. Lemmers, J. Sprakel, I. K. Voets, J. van der Gucht and M. A. Cohen Stuart, *Angew. Chem. Int. Ed.*, 2010, **49**, 708-711.

33. P. J. Skrzeszewska, F. A. de Wolf, M. W. T. Werten, A. P. H. A. Moers, M. A. Cohen Stuart and J. van der Gucht, *Soft Matter*, 2009, **5**, 2057-2062.

34. A. A. Martens, G. Portale, M. W. T. Werten, R. J. de Vries, G. Eggink, M. A. Cohen Stuart and F. A. de Wolf, *Macromolecules*, 2009, **42**, 1002-1009.

35. H. Zhou, J. Woo, A. M. Cok, M. Wang, B. D. Olsen and J. A. Johnson, *PNAS*, 2012, **109**, 19119-19124.

36. P. J. Skrzeszewska, F. A. de Wolf, M. A. Cohen Stuart and J. van der Gucht, *Soft Matter*, 2010, **6**, 416-422.

37. C. Zhou, M. A. Hillmyer and T. P. Lodge, *J. Am. Chem. Soc.*, 2012, **134**, 10365-10368.

38. I. Koonar, C. Zhou, M. A. Hillmyer, T. P. Lodge and R. A. Siegel, *Langmuir*, 2012, **28**, 17785-17794.

39. C. Rufier, A. Collet, M. Viguier, J. Oberdisse and S. Mora, *Macromolecules*, 2008, **41**, 5854-5862.

40. J. P. Jung, J. Z. Gasiorowski and J. H. Collier, *Biopolymers*, 2010, **94**, 49-59.

41. D. W. P. M. Lowik, E. H. P. Leunissen, M. van den Heuvel, M. B. Hansen and J. C. M. van Hest, *Chem. Soc. Rev.*, 2010, **39**, 3394-3412.

42. W. Shen, K. Zhang, J. A. Kornfield and D. A. Tirrell, *Nature Materials*, 2006, **5**, 153 -158.

43. C. Xu, V. Breedveld and J. i. Kopecˇek, *Biomacromolecules*, 2005, **6**, 1739-1749.

44. M. W. T. Werten , H. Teles , A. P. H. A. Moers , E. J. H. Wolbert, J. Sprakel , G. Eggink and F. A. de Wolf, *Biomacromolecules*, 2009, **10**, 1106-1113.

45. M. Haidera, Z. Megeeda and H. Ghandehari, *J. Control. Release*, 2004, **95**, 1-26

46. R. L. DiMarco and S. C. Heilshorn, *Adv. Mater.*, 2012, **24**, 3923-3940.

Chapter 2

Design and production of bio-mimetic asymmetric triblock protein polymers

Abstract

This chapter focuses on the design, biosynthesis and purification of bio-inspired asymmetric triblock telechelic polypeptides. Various natural motifs including silk-like, collagen-like, elastin-like and poly-cationic sequences were combined into asymmetric triblock copolymeric proteins by genetic design. Expression of the designed, synthetic genes was carried out in the yeast *Pichia pastoris*. Not all of the encoded protein products were well-produced and/or easily purified from the extracellular medium, into which they were secreted. The failure in production of some proteins will be discussed.

2.1. Introduction

The protein polymers studied are essentially non-catalytic polyamino acids composed of a number of smaller polyamino acid stretches (modules) in tandem, designed to form certain secondary and supramolecular structures by interaction with modules in neighboring molecules. The polymers are produced biosynthetically as recombinant proteins and their entire amino acid sequence is fully determined by the design of the encoding synthetic genes. The modules are inspired by structural and bioactive domains from natural proteins, often animal extracellular matrix or other secreted proteins such as elastin, silk, collagen and, more recently, resilin. The study of such designed protein polymers and their material properties has recently gained tremendous momentum [1, 2]. The rapid development of genetic engineering techniques provided powerful tools for designing and producing this new type of biomaterials, essentially with tunable properties[3].

Stimuli-responsive and self-assembling materials are crucial for many biomedical applications such as drug delivery, tissue engineering and self-healing coating. While most chemosynthetic macromolecules lack biocompatibility, biodegradability and bio-functionality, these requirements are all naturally met by biosynthetic protein polymers. Responsive or "smart" materials can be made by incorporating temperature-, pH-, or ionic strength-sensitive modules. Examples are amino acid sequences that form secondary hydrogen-bonded or supramolecular structures melting above a certain temperature (collagen-like triple helices, coiled coils), moderately hydrophobic domains that phase-separate above a critical temperature (elastin-like coils), modules that fold into stack-forming beta sheets or –rolls (silk-like structures), or modules that carry a number of acidic or basic amino acids and self-assemble upon charge neutralization. Smart materials can be made in the way that they consist exclusively of such protein block copolymers. On the other hand, short stimulus-responsive peptides can be used to create hybrid chemosynthetic-peptide polymers with stimulus-responsive materials properties [4]. For several reasons, such as biotoxicity and difficulty of detection and purification, biosynthetic production of short peptides is often more challenging than that of longer polypeptide chains, while chemosynthetic production is often not feasible at relatively large (commercial) scale, because of the extremely high cost of chemosynthesis of

sequential peptides. This provides an advantage for materials consisting of (or containing) long, entirely biosynthetic protein polymers.

Although various microbial production systems are known for the successful production of recombinant proteins [5-8], *P. pastoris* is the system of preference for production of many protein polymers as secreted proteins [9, 10]. This host has a record of high-yield protein production, with various advantages such as high levels of mammalian recombinant proteins in the extracellular medium, a low-level endogenous protein secretion, and low protease activity in the medium [11]. Furthermore, product secretion into the medium facilitates product purification, thus reducing the cost of production. This yeast, as an eukaryotic organism, can handle the highly repetitive sequences of protein polymers virtually without gene recombination, and can provide further genetic stability by incorporation of the recombinant gene into the yeast's genome. It grows to very high cell densities on a cheap carbon source (methanol, which is also used as a powerful inducer of gene expression), and the *Pichia* fermentation process can be scaled up to industrial scale. Finally, it appears that many protein polymers can be isolated from the medium in one step by simple differential salt precipitation [12, 13].

2.2. Triblock copolymer composed of random coil, silk- and elastin-like blocks

Background

Since the first silk-/elastin-like protein polymers were reported by Capello [14], several studies have addressed combinations and variants of these two protein motifs [15-17]. Silk-like domains self-assemble into crystalline structures while elastin-like domains contribute to the flexibility and elasticity. A pH-responsive silk-like domain consisting of repeating $(GA)_3GE$ octapeptides folds into beta-sheets which then stack into crystallites upon charge neutralization at low pH [18, 19]. When such $((GA)_3GE)_n$ domains are fused with flanking randomly coiling domains that remain hydrophilic at low pH, the resulting protein polymer molecules self-assemble into supramolecular nanotapes that form pH-responsive hydrogels [20].

Elastin-like domains are typically composed of a number of VPGXG repeats, and undergo a thermoreversible phase transition. Below the so-called lower critical solution

temperature (LCST), elastin-like domains are soluble in aqueous solution, but when the temperature is raised above the LCST, they desolvate and form visible aggregates. In the VPGXG repeats, the amino acid at the X position can be freely chosen, and can be used to steer the properties of the elastin-like domains, especially their LCST. A variety of elastin-like protein polymers have been produced and characterized to date. Their LCST behavior can be used, among others, for purification by temperature cycling [21], and is also thought to be useful for application in tissue engineering [22] and drug delivery [22].

In the present work, we designed an asymmetric triblock protein composed of the afore-mentioned pH-responsive silk-like $((GA)_3GE)_n$ domain (further denoted as 'S_n'), a thermo-responsive elastin-like $(VPGXG)_m$ domain (denoted 'E_m') with an incidence of 30 mol-% Gly, 20 mol-% Ala and 50 mol-% Val at the X position, and a hydrophilic random coil domain 'C^P_4' that is not responsive to temperature or pH and consists of four identical 99 amino acid-long stretches with 22 mol-% proline and 33 mol-% glycine. The order of the blocks in the triblock polymer molecules is S_n-C^P_4-E_m, with the hydrophilic coil in the middle and with n = 12, 24, or 48, and m = 20, or 40. The C^P_4 mid-bock, which acts as a colloidal stabilizer, was already previously designed in our group [23], and was used for example in S_{24}-C^P_4-S_{24} and C^P_2-S_{48}-C^P_2 block copolymers [20] and telechelic polymers with trimer-forming collagen-like end blocks [24]. The final structures resulting from self-assembly of S_n-C^P_4-E_m, which is responsive to both temperature- and pH-stimuli, is likely dependent on the history of the ambient conditions as well as on the length of the S_n and E_m blocks.

Construction of the gene coding for S_n-C^P_4-E_m

The gene fragment encoding the S_n block (n being 12, 24, or 48) was constructed as described before [18] with a modification in the number of DNA monomer repeats. The gene fragment encoding the hydrophilic random-coiled C^P_4-block was obtained by digesting the adapter-modified version of vector pMTL23-P2 [20] with *Dra*III/*Van*91I and inserting the released ~0.6 kb C^P_4 fragment, previously denoted as P2, into the same vector digested with *Van91I* only.

The C^P_4 fragment was then released from the resulting vector by digestion with *Bsa*I/*Ban*I. The gene fragment encoding the elastin-like block E_m (m being 20 or 40) was constructed by multimerization of an E_{10} DNA monomer in vector pMTL23-aIII as

described previously [25]. The vector pMTL23-aIII-E_m so obtained was linearized with BsmBI and dephosphorylated, after which the BsaI/BanI-fragment coding for the C^P_4-block was inserted. The resulting vector was again linearized with BsmBI and dephosphorylated, and the BsaI/BanI- fragment coding for the S-block was then inserted to yield vector pMTL23-aIII-SCE. The DNA coding for each individual polymer domain and the final triblock constructs were checked by DNA sequencing.

Finally, the SCE fragments were cloned into expression vector pPIC9 (Invitrogen) using XhoI/EcoRI. This created a fusion with the *Saccharomyces cerevisiae* α-mating factor pre-pro sequence present in the vector. The plasmids were linearized with *Sal*I to promote homologous integration at the *his4* locus upon transformation of *P. pastoris* GS115 by electroporation [26].

Figure 2.1 Cloning scheme of $S_nC^P_4E_m$ construct.

For this SCE series, 6 gene constructs were made in *E. coli* by combination of varying different length of S and E block. However, five constructs were successfully transfected in to *P. pastoris* (Table 2.1). The construct which failed to be transfected is indicated with *. The reason is possibly due to the large size of the plasmid.

S block	S_{12}	S_{24}	S_{48}
E block			
E_{20}	$S_{12}C^P_4E_{20}$	$S_{24}C^P_4E_{20}$	$S_{48}C^P_4E_{20}$
E_{40}	$S_{12}C^P_4E_{40}$	$S_{24}C^P_4E_{40}$	$S_{48}C^P_4E_{40}$ (*)

Table 2.1 Produced set of $S_nC^P_4E_m$ construct.
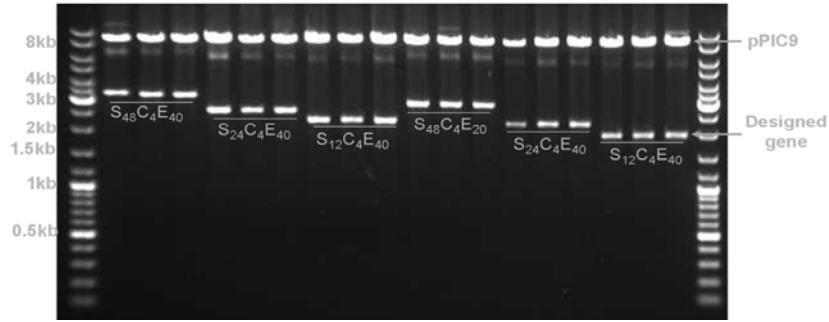
Figure 2.2 Representative image of DNA electrophoresis.

Fermentation, purification and characterization of S_n-C^P_4-E_m

The fed-batch fermentation of the transgenic *P. pastoris* was carried out in a 3-l Bioflo 3000 bioreactor (New Brunswick Scientific) at 30 °C and pH 5.5. The details of fermentation were previously reported [24].

All centrifugation steps were carried out in a Sorval centrifuge with a SLA-3000 or SLA-1500 rotor. Runs lasted 30 min and were carried out at 20000 xg. Resuspension of protein pellets was done in Milli-Q H_2O at 4 °C.

The pH was increased to 8 by slowly adding sodium hydroxide, which precipitated part of the medium salts. After centrifugation, dry ammonium sulfate was slowly added to the supernatant containing the recombinant protein product, to a final concentration of 45 % saturation. After overnight incubation at 4 °C, the collected protein pellets were resuspended in a three-fold smaller volume of Milli-Q H_2O and the precipitation procedure was repeated once more. Subsequently, NaCl was added to the re-solubilized protein to a

final concentration of 50 mM and subsequently, acetone was added to a final concentration of 40 % (v/v) in order to get rid of remaining *Pichia* proteins. After centrifugation, the acetone concentration in the supernatants was increased to 80 % v/v in order to precipitate the S_n-C^P_4-E_m polymer. After centrifugation, the pellets were air-dried overnight, resuspended in Milli-Q H_2O and lyophilized. The freeze-dried protein was stored until use.

Only two constructs from this series were produced by fermentation: $S_{12}C^P_4E_{40}$ and $S_{24}C^P_4E_{40}$. Others variants were not subjected to fermentation yet. The proteins were characterized by SDS-PAGE, Matrix Assisted Laser Desorption/Ionization Mass Spectroscopy (MALDI-TOF) and N-sequencing. Only $S_{12}C^P_4E_{40}$, which was supposed to a representative of this silk and elastin hybrid, was used for physico-chemical analysis, and the results are described in chapter 3 and 4.

2.3. Triblock copolymer composed of random coil, triple helix-forming and polycationic blocks

Background

Collagen is the most abundant protein in mammals. Together with elastin and other extracellular matrix components, collagen fibers determine the properties of connective tissue. Collagen has greater properties of strength than of elasticity. The collagen triple helix is subject to strict amino acid sequence constraints and requires a (large) number of consecutive (Gly-Xxx-Yyy) repeats with a high incidence of proline and 4-hydroxy proline at the Xxx- and Yyy- positions, respectively [27]. Previously, our group developed symmetric gel-forming triblock copolymers consisting of short, collagen-inspired $(PGP)_n$ end blocks and long, hydrophilic random coil middle blocks [24]. The end blocks, which will be further denoted 'T_n' were designed to form collagen-like triple helices with tunable helix melting temperature [28]. These telechelic polymers were capable of thermo-reversible gel formation, because the end blocks from neighboring molecules could form trimeric nodes holding the molecules in the network together [29, 30].

Just like hydrogen-bonding and hydrophobic interactions, electrostatic interactions are of prime importance to intermolecular interactions in nature. For example, the condensation of genetic materials (DNA) by histone proteins in chromatin is governed by electrostatic mechanism [31]. Charged amino acid residues that are buried in the interior of

proteins may have a significant impact on the stability of the folded state [32]. The electrostatic interaction between charged acidic and basic amino acids is dependent on (responsive to) the ambient pH and ionic strength.

In this work, we designed triblock copolymers that comprised the above-mentioned T_n block, a short block consisting of basic amino acids (denoted 'B'), and a variant of the afore-mentioned hydrophilic coil block C_4 with a scrambled (quasi randomized) amino acid sequence, which block is further denoted 'C^R_4'. The order of the blocks in the triblock molecules was, from N- to C-terminus: T_n-C^R_4-B. Different variants of the B block were used, containing for example six consecutive and twelve consecutive lysine residues or histidine residues. The asymmetric triblock molecules have one end-block that forms well-defined trimeric network nodes, and one end-block that forms charge-driven complexes with oppositely charged molecules.

Construction of the gene coding for T_9-C^R_4-B

Vector pMTL23-TR4 has been described by us previously [24]. The gene fragment contained in this plasmid encodes a fusion of (at the N-terminal side) the above-mentioned T_n block, with n=9, and (at the C-terminal side) the above-mentioned ~37 kDa hydrophilic random coil C^R_4 block, previously denoted as R4. To add the above-mentioned B block to the C-terminus of the encoded protein, the vector was digested with *Van*91I (3' to the TR4 gene) and a double-stranded *Dra*III/*Eco*RI adapter encoding the B block was inserted. This adapter was prepared by annealing of oligonucleotides:

 5'-GTGGTCATCACCATCATCATCACGGTTAAG-3′ and

5'-AATTCTTAACCGTGATGATGATGGTGATGACCACCGG-3.

Before ligation to the DNA segments coding for the other protein polymer domains, the DNA codes for individual polymer domains were checked by DNA sequencing, and the triblock constructs were also sequenced before transforming to yeast-expressing vector. The resulting T_n-C^R_4-B DNA was cloned into the *Pichia*-expressing vector pPIC9 (Invitrogen) using *Xho*I/*Eco*RI.
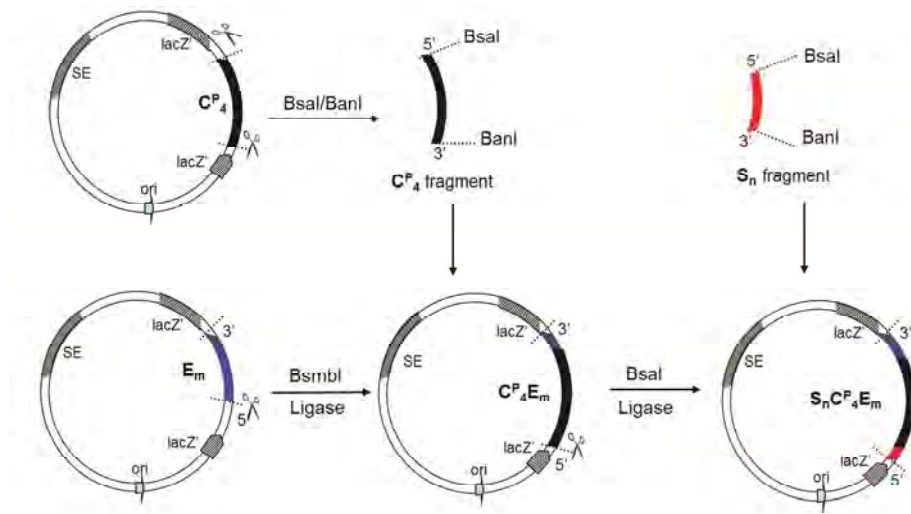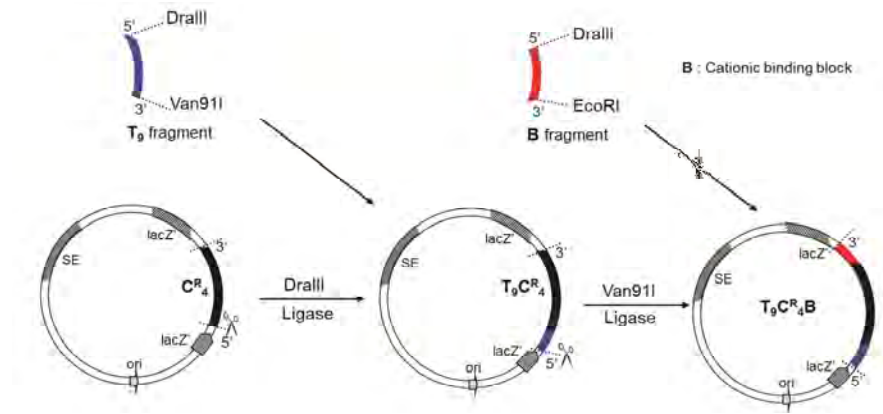
Figure 2.3 Cloning scheme of $T_9C^R_4B$ construct.

For this series, 4 gene constructs were made in *E. coli* by combination of varying different length of the cationic block (Histidine and Lysine), and were successfully transformed in to *P. pastoris* GS115 (Table 2.2).

T block	T_9
Cationic block	
H12	$T_9C^R_4B^{H12}$ (*)
H6	$T_9C^R_4B^{H6}$
K12	$T_9C^R_4B^{K12}$ (*)
K6	$T_9C^R_4B^{K6}$

Table 2.2 Produced set of $T_9C^R_4B$ construct.

Fermentation, purification and characterization of T_9-C^R_4-B

The fed-batch fermentation of the transgenic *P. pastoris* was carried out in a 3-l Bioflo 3000 bioreactor (New Brunswick Scientific) at 30 °C and pH 3. The details of fermentation were previously reported [24].

In this series, only two constructs with short cationic blocks came to successful expression. The products of other two constructs (indicated with *) were not detected in the fermentation supernatant (using SDS-PAGE for visualization of protein bands). In

25

agreement with this, no protein pellets were obtained after ammonium sulfate precipitation. Apparently, the two products marked with an asterisk were not produced.

All purification steps were carried out in a Sorval centrifuge with a SLA-3000 or SLA-1500 rotor. Runs lasted 30 min and were carried out at 20000 xg. Resuspension of protein pellets was done in warm Milli-Q H_2O at 50 °C.

The pH was increased to 8 by slowly adding sodium hydroxide, which precipitated part of the medium salts. After centrifugation, dry ammonium sulfate was slowly added to the supernatant containing the recombinant protein product, to a final concentration of 40 % saturation (for T_9-C^R_4-B^{H6}) and 45 % saturation (for for T_9-C^R_4-B^{K6}). After overnight incubation at 4 °C, the collected protein pellets were resuspended in a three-fold smaller volume of Milli-Q H_2O and the precipitation procedure was repeated once more. Other steps were the same as described above for S_n-C_4-E_m.

The proteins were characterized by SDS-PAGE and Matrix Assisted Laser Desorption/Ionization Mass Spectroscopy (MALDI-TOF). T_9-C^R_4-B^{H6} was used to study the electrostatic interaction with a flexible polyelectrolyte and the results are described in chapter 5. T_9-C^R_4-B^{K6} was used to study the electrostatic interaction with a semi-flexible polymer, and the results are described in chapter 6.

2.4. Triblock copolymer composed of a random coil middle block and two triple helix-forming end blocks, one of which carries a C-terminal cystein

Background

A previously-developed triblock copolymer consisting of the above-mentioned T_9 and C^R_4 blocks, T_9-C^R_4-T_9 [24], was modified so to create a new asymmetric network forming polymer. To achieve this, one cysteine amino acid was added to the end block at the C-terminus of the polypeptide. The cysteine residue can form a disulfide bond with another cysteine, thus linking two protein molecules together. This asymmetric triblock formed defined nodes, some of whose are stabilized with the disulfide bridges.

Construction of the gene coding for Trp-T_9-C^R_4-T_9-Cys

The T_9-C^R_4-T_9 [24] gene was modified so as to introduce a C-terminal Cys-Gly in the encoded protein, as well as an N-terminal Gly-Trp. First, a double-stranded DNA adapter was prepared by annealing of the following complementary oligonucleotides: 5'TCGAGAAAAGAGAGGCTGAAGCTGGTTGGGGTCCACCCGGTGCTCAGCTGCC AGCCGGTGGCTGTGGTTAATAG-3' and 5'-AATTCTATTAACCACAGCCACCGGCTGGCAGCTGAGCACCGGGTGGACCCC AACCAGCTTCAGCCTCTCTTTTC-3'.

The adapter was then ligated into an *Eco*RI/*Xho*I-digested vector pMTL23, to yield vector pMTL23-Trp-Cys. Vector pMTL23-TR4T was digested with *Dra*III/*Van*91I, after which the released T_9-C^R_4-T_9 gene fragment, previously denoted as 'TR4T' was ligated into the correspondingly digested and dephosphorylated vector pMTL23-Trp-Cys. The resulting vector pMTL23-Trp-TR4T-Cys was then digested with *Eco*RI/*Xho*I, and the obtained Trp-TR4T-Cys DNA fragment coding for Trp-T_9-C^R_4-T_9-Cys was subsequently cloned into expression vector pPIC9 using *Xho*I/*Eco*RI. Before ligation to the DNA segments coding for the other protein polymer domains, the DNA coding for each individual polymer domain was checked by DNA sequencing, and the triblock constructs were sequenced before transforming to the *Pichia*-expressing vector. The final vector was transfected into both GS115 *P. pastoris* and an *yps1* protease disruptant derived from GS115.

Fermentation, purification and characterization of T_9-C^R_4-T_9-Cys

The fed-batch fermentation of the transgenic *P. pastoris* was carried out in a 3-l Bioflo 3000 reactor (New Brunswick Scientific) at 30 °C and pH 3.

The purification of the protein from the cell-free broth was similar to the procedure we described previously [24]. The protein was characterized by SDS-PAGE and Matrix Assisted Laser Desorption/Ionization Mass Spectroscopy (MALDI-TOF). The discussion about this protein molecule is presented in chapter 7.
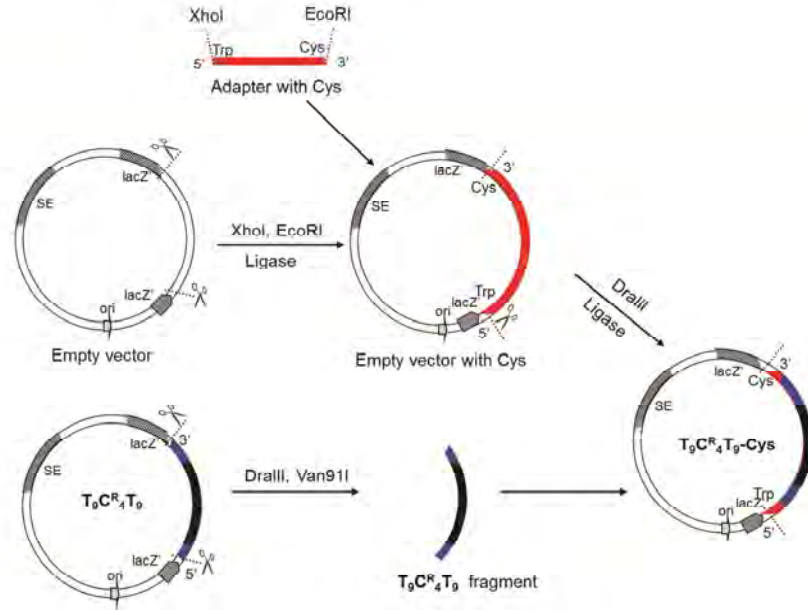
Figure 2.4 Cloning scheme of $T_9C^R_4T_9$-Cys construct.

2.5. Triblock copolymer composed of random coil, silk-like and triple helix-forming blocks

Background

As discussed above, the silk-like sequences $((GA)_3GE)_n$ and $((GA)_3GH)_n$ impart pH-responsive properties while collagen-like-triple helices introduce thermo-responsiveness. Another asymmetric design that we conceived is the combination of these silk-like and the triple helix-forming domains, viz. as the two end blocks of a triblock copolymer with a C^R_4 middle block. The resulting polymer is obviously responsive to two different stimuli, viz. pH and temperature.

Construction of the gene coding for S_n^X-C^R_4-T_9

Vector pMTL23-R4T has been designed and constructed in a way similar to the previously-described pMTL23-TR4 [24]. The C^R_4-T_9 block, previously denoted as R4T, was obtained by digestion of vector pMTL23-R4T with *Dra*III/*Van*91I, and was transferred to

pMTL23-AIII (containing *Bsa*I/*Ban*I) [20] linearized by *Dra*III. The resulted pMTL-AIII-R4T was linearized by *Bsa*I. The silk-like blocks were generated in a similar method as reported before [18, 20] to obtain pMTL23-S. The S_n^X blocks, which were obtained by digestion of pMTL23-S with *Bsa*I/*Ban*I, were ligated into the *Bsa*I -digested pMTL-AIII-R4T. Before ligation to the DNA segments coding for the other protein polymer domains, the DNA codes for all polymer domains were checked by DNA sequencing; and the triblock constructs were sequenced before transferring to the *Pichia*-expressing vector. The final construct pMTL-AIII-SR4T was then digested with *Xho*/*Eco*RI and the obtained DNA fragment SR4T, coding for S_n^X-C_4^R-T_9, was ligated into *Xho*/*Eco*RI-digested PIC 9. The final vector was transformed into GS115 *P. pastoris.*
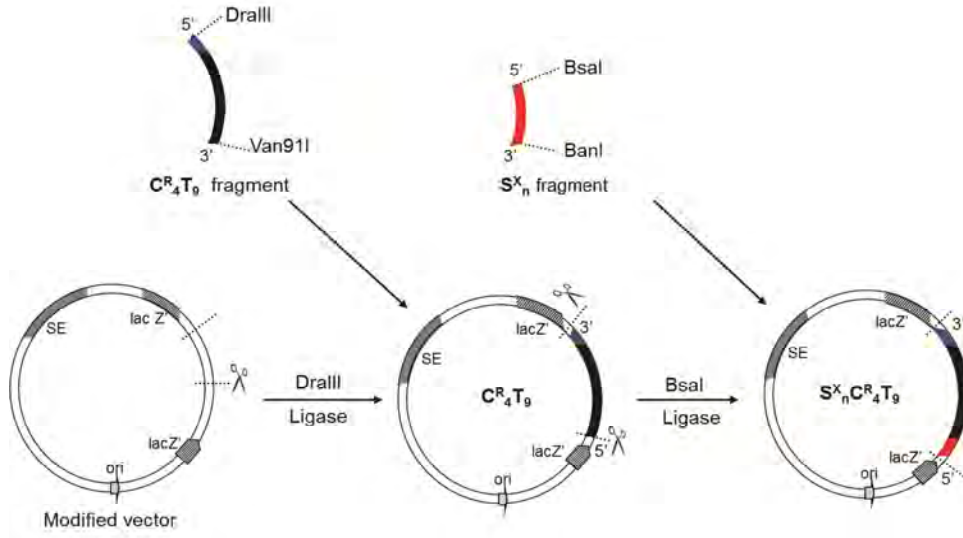
Figure 2.5 Cloning scheme of S_n^X-C_4^R-T_9 construct.

For this series, we used two types of silk-like sequence: $((GA)_3GE)_n$ (denoted as S_n^E) and $((GA)_3GH)_n$ (S_n^H). We varied the length of the S_n^X domain (i.e. the value of n), while the length of the T_m block was fixed at m = 9 (Table 2.3).

T block	T_9
Silk-like block	
S_6^E	S_6^E-C_4^R-T_9
S_8^E	S_8^E-C_4^R-T_9
S_6^H	S_6^H-C_4^R-T_9
S_8^H	S_8^H-C_4^R-T_9

Table 2.3 Produced set of $S_n^X C_4^R T_9$ construct.

Fermentation, purification and characterization of S_n^X-C_4^R-T_9

The fed-batch fermentation of the transgenic *P. pastoris* was carried out in a 3-l Bioflo 3000 bioreactor (New Brunswick Scientific) at 30 °C. Fermentation of the strains transformed with the S_n^E-C_4^R-T_9 genes did not result in any production of these triblock copolymers, even at pH 5, as appeared from SDS-PAGE and from the absence of ammonium sulfate-induced precipitate formation. The variants S_n^H-C_4^R-T_9 were not subjected to fermentation.

2.6. Conclusion

We exploited genetic engineering to make four different designs of constructs that encode four different combinations of asymmetric triblock protein polymers, and obtained the proteins by fermentation. Some of the artificial genes failed to result in protein production in fermentation; and some of them were not subjected to fermentation. The failure of production is likely due to protein expression or intracellular cleavage of the expressed protein or any unknown reasons. In summary, we obtained protein products in yeast fermentation for silk/random-coil/elastin (namely **SCE** in later chapters), collagen-like /random-coil/cationic block (namely **TR4H** or **TR4K** in later chapters) and collagen-like /random-coil/collagen-like modified with a cysteine (namely **TR4T-Cys** in later chapters).

References

1. L. Shen, N. Bao, Z. Zhou, P. E. Prevelige and A. Gupta, *J. Mater. Chem.* , 2011, **21**, 18868.

2. R. L. DiMarco and S. C. Heilshorn, *Adv. Mater.*, 2012, **24**, 3923-3940.

3. J. Kopecek, *Eur. J. Pharm. Sci.*, 2003, **20**, 1-16.

4. S. Banta, I. R. Wheeldon and M. Blenner, *Annu. Rev. Biomed. Eng.*, 2010, **12**, 167-186.

5. C. H. Shein, *Nature Biotech.*, 1989, **7**, 1141.

6. S. Hellwig, J. Drossard, R. M. Twyman and R. Fischer, *Nature Biotech.*, 2004, **22**, 1415.

7. D. C. Andersen and L. Krummen, *Curr. Opin. Biotechnol.*, 2002, **13**, 117-123.

8. C. P. Hollenberg and G. Gellissen, *Curr. Opin. Biotechnol.*, 1997, **6**, 554-560.

9. A. L. Demain and P. Vaishnav, *Biotechnol. Adv.*, 2009, **27**, 297-306.

10. J. Báez, D. Olsen and J. W. Polarek, *Appl. Microbiol. Biotechnol.*, 2005, **69**, 245-252.

11. R. Fischer, J. Drossard, N. Emans, U. Commandeur and S. Hellwig, *Biotechnol. Appl. Biochem.*, 1999, **30**, 117-120.

12. M. D. Golinska, T. T. H. Pham , M. W. T. Werten , F. A. de Wolf , M. A. Cohen Stuart and J. van der Gucht, *Biomacromolecules,* 2013, **14**, 48-55.

13. T. T. H. Pham, P. J. Skrzeszewska, M. W. T. Werten, W. H. Rombouts, M. A. Cohen Stuart, F. A. de Wolf and J. van der Gucht, *Soft Matter*, 2013, **9**, 6391-6397.

14. J. Cappello, J. Crissman, M. Dorman, M. Mikolajczak, G. Textor, M. Marquet and F. Ferrari, *Biotechnol. Prog.*, 1990, **6**, 198-202.

15. A. Nagarsekar, J. Crissman, M. Crissman, F. Ferrari, J. Cappello and H. Ghandehari, *Biomacromolecules,* 2003, **4**, 602-607.

16. J. Yao and T. Asakura, *J. Biochem.*, 2003, **133**, 147-154.

17. X. X. Xia, Q. Xu, X. Hu, G. Qin and D. L. Kaplan, *Biomacromolecules*, 2011, **12**, 3844-3850.

18. M. W. T. Werten, A. P. H. A. Moers, T. H. Vong, H. Zuilhof, J. C. M. van Hest and F. A. de Wolf, *Biomacromolecules,* 2008, **9**, 1705.

19. J. M. Smeenk, M. B. J. Otten, J. Thies, D. A. Tirrell, H. G. Stunnenberg and J. C. M. van Hest, *Angew. Chem. Int. Ed.* , 2005, **44**, 1968-1971.

20. A. A. Martens, G. Portale, M. W. T. Werten, R. J. de Vries, G. Eggink, M. A. Cohen Stuart and F. A. de Wolf, *Macromolecules,* 2009, **42**, 1002-1009.

21. D. E. Meyer and A. Chilkoti, *Nature Biotech.*, 1999, **17**, 1112.

22. D. L. Nettles, A. Chilkoti and L. A. Setton, *Adv. Drug Deliv. Rev.*, 2010, **62**, 1479-1485.

23. M. W. T. Werten, W. H. Wisselink, T. J. Jansen-van den Bosch, E. C. de Bruin and F. A. de Wolf, *Protein Eng.*, 2001, **14**, 447-454.

24. M. W. T. Werten, H. Teles, A. P. H. A. Moers, E. J. H. Wolbert, J. Sprakel, G. Eggink and F. A. de Wolf, *Biomacromolecules,* 2009, **10**, 1106-1113.

25. R. Schipperus, R. L. M. Teeuwen, M. W. T. Werten, G. Eggink and F. A. de Wolf, *Appl. Microbiol. Biotechnol.*, 2009, **85**, 293-301.

26. M. W. T. Werten, T. J. Van Den Bosch, R. D. Wind, H. Mooibroek and F. A. de Wolf, *Yeast*, 1999, **15**, 1087-1096

27. B. Brodsky and A. V. Ersikov, *Adv. Protein Chem.*, 2005, **70**, 301.

28. C. I. F. Silva, P. J. Skrzeszewska, M. D. Golinska, M. W. T. Werten, G. Eggink and F. A. de Wolf, *Biomacromolecules,* 2012, **13**, 1250-1258.

29. P. J. Skrzeszewska, F. A. de Wolf, M. W. T. Werten, A. P. H. A. Moers, M. A. Cohen Stuart and J. van der Gucht, *Soft Matter*, 2009, **5**, 2057-2062.

30. P. J. Skrzeszewska, F. A. de Wolf, M. A. Cohen Stuart and J. van der Gucht, *Soft Matter*, 2010, **6**, 416-422.

31. H. Schiessel, *J. Phys.: Condens. Matter,* 2003, **15**, R699-R774.

32. J. C. Williams, A. L. M. Haffa, J. L. McCulley, N. W. Woodbury and J. P. Allen, *Biochemistry*, 2001, **40** 15403-15407.

Chapter 3

Fibril formation by pH and temperature responsive silk-elastin block copolymers

Abstract

In this chapter, we study the self-assembly of silk/random-coil/elastin-like triblock $S_{12}C_4E_{40}$, in which the silk-like block (S) and elastin-like block (E) are separated by a random coil block (C_4) in comparison with a diblock $S_{24}E_{40}$. Upon lowering the pH, the acidic silk-like blocks fold and self-assemble into fibrils by a nucleation-and-growth process. While silk-like polymers without elastin-like blocks form fibrils by heterogeneous nucleation, leading to monodisperse populations, the elastin-like blocks allow for homogeneous nucleation, which gives rise to polydisperse length distributions, as well as a concentration-dependent fibril length. Moreover, the elastin-like blocks introduce temperature-sensitivity: at high temperature, the fibrils become sticky and tend to bundle and aggregate in an irreversible manner. At low pH, concentrated solutions of $S_{12}C_4E_{40}$ form weak gels that irreversibly lose elasticity in temperature cycling; this is also attributed to fibril aggregation.

3.1.   Introduction

Stimuli-responsive protein polymers are a very promising group of materials that have significant potential in many different applications, e.g., for regenerative medicine, tissue engineering, bioseparation, self-healing coatings, gene therapy or drug delivery [1-6]. Because of their interesting physicochemical properties and applicability these proteins are gaining more attention. Useful stimuli to which they reversibly respond can be pH, temperature or ionic strength. Genetic engineering provides the tool to design such protein-based polymers with precisely defined monomer sequences and molecular weights, thereby controlling physicochemical properties and biological fate, as needed for biomedical applications.

We focus in this study on the production and characterisation of two novel silk-elastin like protein polymers with pH- and temperature-responsive blocks, where stimuli can be separately addressed. We compare two proteins: 1) a 'diblock' polymer, labelled $S_{24}E_{40}$ which is composed of 24 silk-like (S) and 40 elastin-like (E) repeats, and 2) a 'triblock' polymer $S_{12}C_4E_{40}$ where 12 silk-like and 40 elastin-like sequences are connected by a random coil (C_4) block, that serves as an inert 'spacer' between silk-like and elastin-like blocks. The combination of sequences was designed to achieve distinct physical behaviours in one single hybrid molecule, in order to: 1) assess how they influence each other and 2) see whether qualitatively new behaviour would emerge. The presence of the C4 spacer may 'decouple' the silk-like and elastin-like blocks, so that only self-interactions of these blocks occur. Moreover, the C_4 block will probably affect the kinetics of self-assembly.

The random coil block (C_4) is composed of four identical, 99 amino acid long units that carry many uncharged and hydrophilic amino acids such as glutamine, asparagine and serine. These amino acids are inert to almost all stimuli, and therefore the C_4 block maintains a random coiled structure in a broad range of pH values and temperatures [7, 8]. The silk-like block (S) has been inspired by poly (GA) sequences found in natural silk as produced by the silkworm (*Bombyx mori*). It consists of repeats of the octapeptide GAGAGAGE [9], where glutamic acid imparts pH responsive properties [10]. It has been found that, upon lowering the pH, this block self-assembles into semi-flexible fibrils which feature a rather special secondary structure in water [8, 11], related to (but somewhat different from) the familiar ß-sheet [8, 11, 12]. The elastin-like block (E) is composed of a pentapeptide

repeat motif (VPGXG) where the X position is occupied by either valine, alanine, or glycine in a 5:3:2 ratio, respectively [13, 14]. Elastins with this kind of sequence are known to undergo a temperature-induced phase transition: above the transition temperature (lower critical solution temperature, LCST) the random-coiled structure changes into a so-called ß-spiral, thereby forming aggregates [15-17]. The transition temperature of these elastins depends on the hydrophobicity of the amino acid at the X position, the length of the block, the polymer concentration, and the nature and concentration of added salt [13].

Some silk-elastin like protein polymers have been described previously in literature and were reported to spun into fibers [18], self-assembly into micelle-like structure [19] or physically cross-linked networks [20]. They were used to develop protein-based tissue scaffolds [21] or systems for drug delivery and release [22]. Our group previously reported block copolymers, consisting of S_{24} and C_2 blocks, which spontaneously organize into stable nanofibers [23]. The present work is the first report in which doubly responsive behaviour (pH and temperature) is considered. We will compare the behaviors with singly-responsive counterparts such as the silk-random coil (S-C) combinations that have been described earlier [8, 24].

For the production of the heterologous proteins considered here we prefer the methylotrophic yeast *Pichia pastoris* because of its ability to excrete the product from the cell and to give very high yields of recombinant proteins. The purification of both proteins, which involves a precipitation with ammonium sulfate or a temperature cycle directly applied to the cell-free fermentation supernatant, is simple and very effective.

The physical properties and self-assembly into fibrils of $S_{24}E_{40}$ and $S_{12}C_4E_{40}$ were characterized by atomic force microscopy (AFM), light scattering and rheology. The properties were compared while changes of temperature and pH were applied either separately or simultaneously.

3.2.   Materials and Methods

Construction of vectors and strains

The gene encoding the $S_{12}C_4E_{40}$ triblock was prepared as follows. DNA encoding the silk-like S_{12}-block was created as illustrated before [10], with a modification in the number of DNA monomer repeats in such a way that the S_{12}-block encodes 12 repeats of the

GAGAGAGE octapeptide. DNA encoding the hydrophilic random-coiled C_4-block was obtained by digesting the adapter-modified version of vector pMTL23-P2 [8] with *Dra*III/*Van*91I and inserting the released ~0.6 kb fragment into the same vector via *Van*91I. The C_4 fragment was then released from the resulting vector by digestion with *Bsa*I/*Ban*I. The gene encoding the elastin-like block E_{40} was constructed by multimerization of an E_{10} DNA monomer in vector pMTL23-aIII as described previously [14], with the exception that only four monomers were concatenated. The E_{10} monomer encodes 10 repeats of the pentapeptide VPGXG, where the X positions are occupied by five valines, three alanines, and two glycines in quasi-random order. The vector pMTL23-aIII-E_{40} so obtained was linearized with *Bsm*BI and dephosphorylated, after which the *Bsa*I/*Ban*I-digested C_4-block was inserted. The resulting vector was again linearized with *Bsm*BI and dephosphorylated, and the *Bsa*I/*Ban*I-digested S_{12}-block was then inserted to yield vector pMTL23-aIII-$S_{12}C_4E_{40}$. The encoded triblock copolymer consists of ~700 amino acids with three distinct sequence types: $(GAGAGAGE)_{12}$-spacer-$(VPGXG)_{40}$, where the spacer (C_4) is

(GEPGNPGSPGNQGQPGNKGSPGNPGQPGNEGQPGQPGQNGQPGEPGSNGPQGSQ GNPGKNGQPGSPGSQGSPGNQGSPGQPGNPGQPGEQGKPGNQGPA)$_4$ (cloning - derived residues not indicated).

Construction of the diblock-bearing vector pMTL23-aIII-$S_{24}E_{40}$ was analogous to the above, except that no C_4-block was inserted, and that an S_{24}-block (encoding 24 repeats of the GAGAGAGE octapeptide) was used instead of the S_{12}-block. The encoded diblock copolymer consists of ~400 amino acids with two distinct sequence types: $(GAGAGAGE)_{24}$-$(VPGXG)_{40}$ (cloning-derived residues not indicated).

Finally, the $S_{12}C_4E_{40}$ and $S_{24}E_{40}$ fragments were cloned into expression vector pPIC9 (Invitrogen) via *Xho*I/*EcoR*I. This created a fusion with the *Saccharomyces cerevisiae* α-mating factor secretion signal present in the vector. The plasmids were linearized with *Sal*I to promote homologous integration at the *his4* locus upon transformation of *Pichia pastoris* GS115 by electroporation [25].

Fermentation of Pichia pastoris

The biopolymers were produced by methanol fed-batch fermentation of *P. pastoris* in 2.5 L Bioflo 3000 bioreactors (New Brunswick Scientific) as described previously [26]. The pH was maintained at 5.5 for $S_{12}C_4E_{40}$ and at 6.0 for $S_{24}E_{40}$, and the growth temperature

was 30 °C. The methanol level in the broth during the induction phase was kept constant at ~0.2 % (w/v) by means of a gas sensor-controller.

Biopolymer purification

The purification of the $S_{12}C_4E_{40}$ triblock from the cell-free broth was similar to the procedure we described previously for related elastin-free $S_{24}C_4S_{24}$ triblocks [23], with the exception that 40 % of ammonium sulfate saturation was used for protein precipitation and that Milli-Q H_2O was used instead of 10 mM ammonia in all steps.

The diblock $S_{24}E_{40}$ was purified from the cell-free broth by twice-repeated Inverse Transition Cycling (ITC) [14] in the presence of 2 M NaCl. In this procedure, the elastin-like protein is precipitated by centrifugation after heating to 65 °C ("hot spin"). After resuspending the pellet and cooling to 4 °C the elastin-like protein re-dissolves, whereas heat-denatured host-derived proteins remain insoluble and precipitate upon centrifugation ("cold spin").

Both proteins were dialyzed using Spectra/Por 7 tubing (Spectrum Labs) with a 1 kDa molecular weight cut-off. The desalted proteins were freeze-dried for storage until use.

Product characterization

Electrophoresis (SDS-PAGE) was performed using the NuPAGE Novex system (Invitrogen) with 10% Bis-Tris gels (Invitrogen), MES-SDS running buffer (Invitrogen) and SeeBlue Plus2 (Invitrogen) prestained molecular mass markers. Gels were stained with Coomassie SimplyBlue SafeStain (Invitrogen). N-terminal sequencing was done by Midwest Analytical (St. Louis, MO), either on the main band in SDS-PAGE after blotting onto PVDF membrane ($S_{24}E_{40}$), or on the purified protein in solution ($S_{12}C_4E_{40}$).

The molecular mass distribution of the product was analysed by matrix-assisted laser desorption/ionization time-of-flight mass spectroscopy (MALDI-TOF MS). The analyses were performed using an Ultraflex mass spectrometer (Bruker), on a 600 µm AnchorChip target (Bruker) and with 2,5-dihydroxyacetophenone (Sigma-Aldrich) as matrix. Samples were prepared and measured as described previously [26].

Atomic Force Microscopy (AFM)

Stock solutions of $S_{12}C_4E_{40}$ and $S_{24}E_{40}$ were prepared by dissolving pure, lyophilized products to a concentration of approximately 10 g/L in 10 mM NaOH (Merk, Germany). They were kept at 4 °C for 20 min, occasionally vortexed to allow complete dissolution of the protein. Then products were acidified with 10 mM HCl (Merk, Germany) and diluted with 10 mM sodium phosphate buffer at pH 2 to a final concentration of 5 g/L for $S_{24}E_{40}$. For $S_{12}C_4E_{40}$, final protein solutions made by diluting the stock solutions with Milli-Q H_2O to concentration of 5 g/L were titrated to pH 2 with 1M HCl. The samples were incubated at five different temperatures (4 °C, 25 °C, 35 °C, 45 °C and 55 °C) to allow supramolecular assembly to occur. To prevent biological contamination, all tubes were sterilized with ethanol and all solutions were filtered before experiments. At each time point samples were taken and diluted with Milli-Q H_2O to a final product concentration of 0.1 g/L for AFM imaging. A drop (50 µl) of each sample was deposited onto a clean hydrophilic silica wafer (Siltronic Corp.) and left for 2 min. The wafer was then washed with 500 μl of Milli-Q H_2O to remove salts, and dried under a stream of nitrogen. The dry samples were analyzed using a Nanoscope V in Scan Asyst™ imaging mode, using non-conductive silicon nitride probes (Veeco, NY, USA) with a spring constant of 0.32 N/m. Images were recorded between 0.200-0.990 Hz and further processed with NanoScope Analysis 1.20 software (Veeco Instruments Inc. 2010, USA).

Dynamic Light Scattering (DLS)

A 5 g/L stock solution was prepared by dissolving pure, lyophilized proteins in 10 mM NaOH. To analyze the kinetics of fibril growth, samples were prepared by diluting the stocks with 10 mM sodium phosphate buffer at pH 2 to a final concentration of 0.2 g/L for the diblock. For the triblock, the working solutions with concentration of 1 g/L made by diluting the stock solution with Milli-Q H_2O were titrated to pH 2 to study the growth kinetics. All solutions were sterilized using 0.2 μm filters (Milipore) to prevent contamination and remove dust before measurement. Light scattering was performed using an ALV dynamic light scattering instrument with a Cobolt Samba- 300 DPSS laser (300 mW) operating at a wavelength of 532 nm and an ALV-5000/60X0 multiple τ digital correlator. A refractive index matching bath of filtered cis-decalin surrounded the

cylindrical scattering cell. All measurements were undertaken at a fixed angle θ of 90 °, corresponding to a scattering vector $q = \dfrac{4\pi n}{\lambda}\sin\dfrac{\theta}{2} \sim 0.02$ nm^{-1}, where n is the refractive index of the solvent (water). The temperature was varied between 15 °C and 60 °C using a Haake F3-K thermostat.

Rheology

Experiments were carried out on an Anton Paar MCR501 Rheometer equipped with a C10/TI Couette geometry, with bob and cup diameter of 9.991 and 10.840 mm, respectively. Freeze-dried protein was first dissolved in water at pH 10 and then 1 M HCl was added until the pH was 2 and the final protein concentration was 50 g/L. The solutions were loaded immediately into the rheometer. A thin layer of oil was used to minimize evaporation. Gel formation was monitored by applying a 1 Hz sinusoidal deformation of 1 % to the system. The storage modulus (G') and loss modulus (G'') were obtained while different temperature ramps were introduced during gel formation. The temperature was controlled by a Peltier system which allows fast heating and cooling. The temperature-cycles were applied as 5 °C - 15 °C - 25 °C - 35 °C - 25 °C- 15 °C - 5 °C.

3.3. Results and Discussion

Polymer biosynthesis and product characterization

The two protein polymers, $S_{12}C_4E_{40}$ and $S_{24}E_{40}$, were biosynthesized in *P. pastoris*. The recovery of purified dry product per litre of cell-free broth was above 500 mg. The purified proteins were characterized by SDS-PAGE, MALDI-TOF and N-terminal sequencing. The SDS-PAGE of $S_{12}C_4E_{40}$ (Appendix, Figure A3.1a) and $S_{24}E_{40}$ (Appendix, Figure A3.1b) showed that both proteins appear to be pure and intact. Both proteins migrated at an apparent molecular weight much higher than their true molecular weight. Whereas the standard protein markers in SDS-PAGE are always relatively hydrophobic, our products are composed of atypical and relatively polar amino acids. As a consequence, they bind less SDS [7, 10]. This strongly reduces their migration velocity, and leads to a high apparent molecular mass [14, 27, 28]. N-terminal sequencing of the two protein polymers confirmed their identity. For both proteins, roughly one-fourth of the molecules appeared N-terminally

extended with a single Glu-Ala repeat, which commonly occurs because of partial processing of the α-factor prepro secretory signal by the *P. pastoris* dipeptidylaminopeptidase [7]. The molecular mass of $S_{12}C_4E_{40}$ and $S_{24}E_{40}$ was verified by MALDI-TOF, which shows monodisperse products with a mass close to the theoretical values of 60134 Da and 30008 Da, respectively (Appendix, Figure A3.2).

Fibril formation

Fibril formation was first studied in dilute solutions with concentration of 5 g/L. The preparation of the sample plays an important role, as the proteins need to be well dissolved. After the solutions were acidified to pH 2, they were incubated at different temperatures and sampled at different times for AFM analysis. The supramolecular structures formed were adsorbed, from the solution, onto a clean piece of oxidized silicon wafer. The high pH conditions were also studied by AFM, however no fibrils were observed.

Figure 3.1 (for $S_{12}C_4E_{40}$) and Figure 3.2 (for $S_{24}E_{40}$) provide clear evidence that both proteins form thin fibrils which grow longer in the course of time. At high magnification, the fibrils of the triblock seem to have periodic morphology (Appendix, Figure A3.3). Periodicity, if any, can be only faintly noticed. Such periodicity may result from a twist in a ribbon-like structure; several natural proteins form fibrils which have this feature. The ribbon-like fibrils were previously found in a polymer with only S and C blocks [8, 12].

The length of the fibrils (Figure 3.3) was calculated by averaging the length of at least 50 well-defined individual fibrils in AFM images, and plotted as a function of incubation time. The filaments of both proteins appeared to be rather polydisperse. If the growth rate is homogeneous in the sample, new nuclei are formed in the course of experiment, from which fibrils grow: in other words, the concentration of nuclei is not constant in time, but increases. This contrasts with our findings for elastin-free $S_{24}C_4S_{24}$, which does not form new nuclei in the course of the experiment and thus forms monodisperse fibrils [24]. Clearly, in the present case of $S_{12}C_4E_{40}$ and $S_{24}E_{40}$, homogeneous nucleation is possible, causing poly-dispersity. The growth rate of both polymers is temperature dependent, $S_{12}C_4E_{40}$ growing faster than $S_{24}E_{40}$. The temperature dependence is probably caused by the elastin blocks. $S_{12}C_4E_{40}$ fibrils grew equally fast at different temperatures until 8 h (when a length of about 300 nm was reached), but after that time, the growth rate increased with increasing temperatures up to 35 °C. After 24 h, the fibril length often exceeded the

maximum AFM frame size (10 μm). The filaments of the diblock, which grew much more slowly, did not display such multiphasic growth and their length did not exceed 1 μm, even after one week.

The elastin-free triblock $S_{24}C_4S_{24}$ [8, 10, 24, 29] grows much faster than both $S_{12}C_4E_{40}$ and $S_{24}E_{40}$: after 1 h at room temperature, filaments can grow up to 1.5 μm. However, as the elastin-free triblock has more silk-like octapeptides, it is at this stage not possible to discern whether this difference in growth speed is caused by the presence of the elastin-like block in $S_{12}C_4E_{40}$ and $S_{24}E_{40}$.

After 48 h at 35 °C, the length of $S_{24}E_{40}$ fibrils, as measured by AFM, seems to decrease. The same was observed for $S_{12}C_4E_{40}$ but after 24 h at 45 °C and 55 °C (Figure 3.3). There may be several explanations for this observation. First, fibrils might become weaker at high temperature and then be susceptible to breaking. Thermally activated breaking implies very weak bonds (~10 kT) which are very unlikely since this would also imply fast breaking under mechanical shear, which is not observed. Secondly, the change in length may be apparent due to some other effects. For example, if longer fibrils are unstable with respect to aggregation, and aggregates are not captured by the sampling method adopted here, one expects that long fibrils would become progressively underrepresented in the AFM sample. Hence, this observation may also be a first indication that the fibrils have a tendency to aggregate. Below we discuss evidence for aggregation, so this may indeed explain the apparent decrease in length, as well as the clusters observed in AFM images.

The morphology of $S_{24}E_{40}$ fibrils (after 6 h of incubation) does not seem to significantly depend on temperature (Figure 3.2A, B, C). After a long incubation time (7 days, Figure 3.2D, E, F), the fibrils of $S_{24}E_{40}$ had a less well-defined structure; we mainly visualized many short rod-shaped particles. In contrast, the fibrils from $S_{12}C_4E_{40}$ (Figure 3.1) were longer and more homogenous.

41
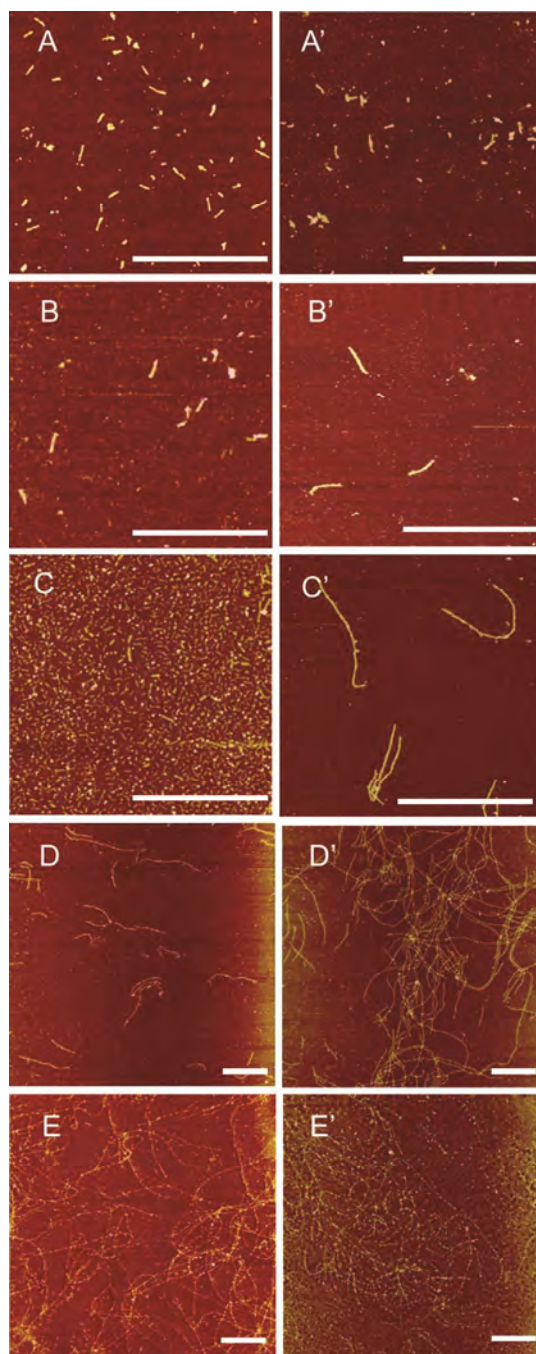
Figure 3.1 Representative AFM images of fibrils by low-pH induction of $S_{12}C_4E_{40}$ at 4 °C (left column) and 35 °C (right column) after (A, A') 1 h, (B, B') 3 h, (C, C') 7 h, (D, D') 24 h and (E, E') 48 h, respectively. All the scale bars correspond to 1.5 μm.

42
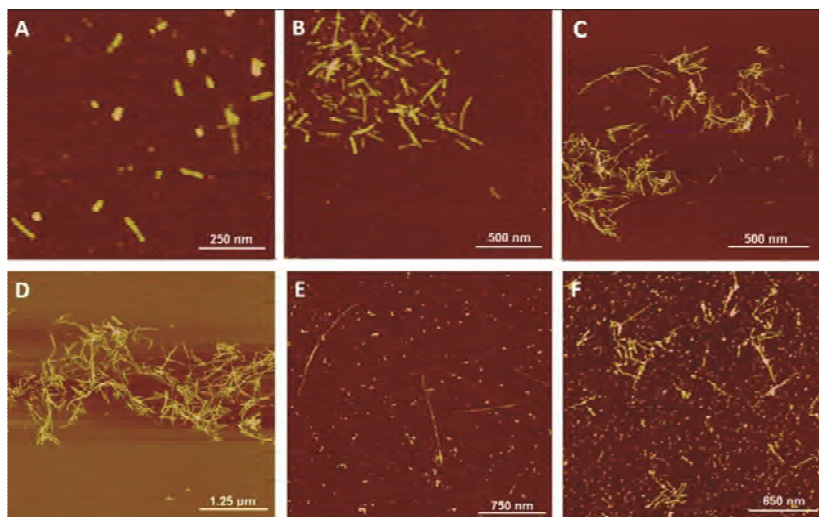
Figure 3.2 Representative AFM images of fibrils by low-pH induction of $S_{24}E_{40}$ (A) at 4 °C after 6 h, (B) at 25 °C after 6 h, (C) at 35 °C after 6 h, (D) at 4 °C after 7 days, (E) at 25 °C after 7 days, (F) at 35 °C after 7 days.
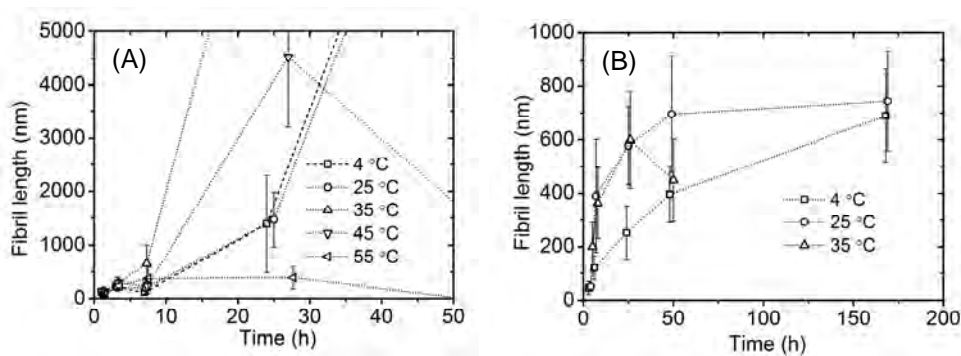
Figure 3.3 Fibril growth as a function of time elapsed after the onset of growth of (A) $S_{12}C_4E_{40}$ and (B) $S_{24}E_{40}$, as induced by pH. Fibril length was determined as the average of 50 individual fibrils imaged by AFM at different time and temperature.

Light scattering: growth followed by sedimentation

Figure 3.4 shows light scattering intensity data as a function of time after acidification for dilute samples at various temperatures. In Figure 3.4A ($S_{12}C_4E_{40}$), we observe a fast initial increase, followed by a slower increase for 15 °C and 20 °C, and a slow decrease for 35 °C. In Figure 3.4B ($S_{24}E_{40}$), in all three cases (25 °C, 35 °C and 45 °C), there is an initial increase, followed by a decrease to very low intensity; this happens on time scales

from 1 h to 4 h, being faster at higher temperatures. The intensity in Figure 3.4B fluctuates considerably between individual readings. All the features in Figure 3.4B indicate that fibril growth is followed by sedimentation during the experiment, most likely caused by aggregation of the fibrils into larger objects. In our earlier study on elastin-free $S_{24}C_4S_{24}$ polymers [24] where non-aggregated fibrils were found, no such intensity decays were seen implying absence of any sedimentation. The driving force for aggregation is probably temperature-enhanced hydrophobic attraction between the elastin-like units. In fact, $S_{12}C_4E_{40}$ show irreversible thermo-responsive aggregates upon heating at neutral pH, when the self-assembly of the S block is not triggered (Appendix, Figure A3.4). This also explains the increasing rate of sedimentation with temperature in Figure 3.4B. The highly hydrophilic C_4 block [7] in $S_{12}C_4E_{40}$ has a stabilizing influence, so that only at 35 °C the triblock aggregates sufficiently to show clear sedimentation. At 15 °C and 20 °C, there is a trade-off between growth and sedimentation but the overall trend is still an increase in scattering. Fused proteins were reported to have an effect on the transition temperature of a responsive elastin-like polypeptide, in which surface hydrophobicity in molecular proximity to the elastin-like polypeptide depresses the transition temperature [30].
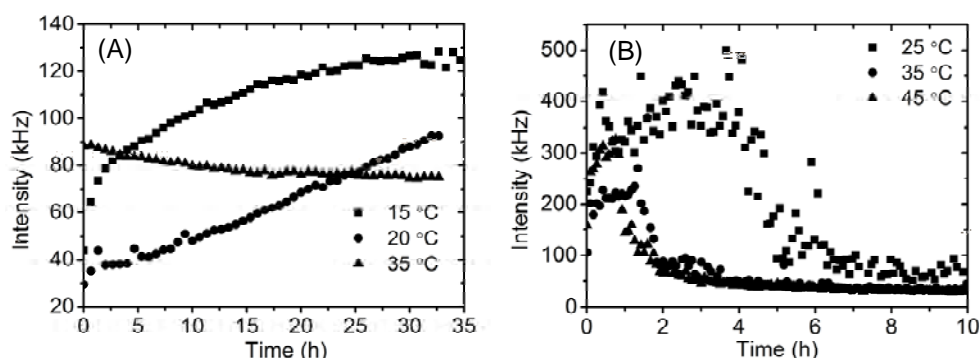
Figure 3.4 Growth kinetics as a function of time followed by measuring the intensity of scattered light of (A) 1 g/L $S_{12}C_4E_{40}$, (B) 0.2 g/L $S_{24}E_{40}$ at different temperature.

Fibril bundling at high temperature

The indication from Figure 3.4 that aggregation may occur, particularly at higher temperatures, is further supported by an AFM image of filaments formed by the triblock $S_{12}C_4E_{40}$ prepared at 55 °C, 24 h (Figure 3.5B). Indeed, a comparison between fibrils

grown during one month at 4 °C (Figure 3.5A) and at 55 °C (Figure 3.5C) clearly shows that bundling is induced by temperature likely higher than transition temperature, i.e. when individual fibrils become 'sticky'.
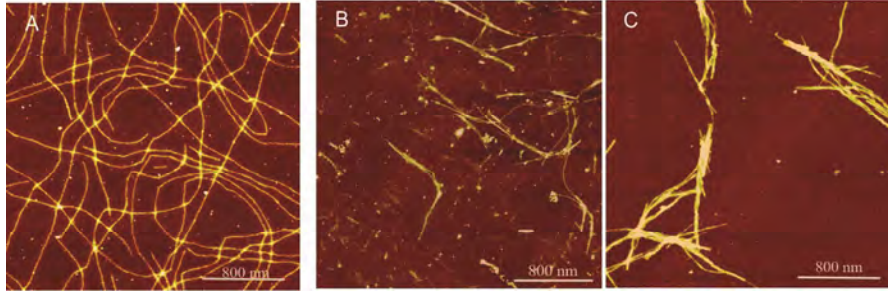
Figure 3.5 AFM images of $S_{12}C_4E_{40}$ fibril bundles formed at low pH and high temperature: (A) 4 °C after one month, (B) 55 °C after 24 h, (C) 55 °C after one month.

The effect of concentration and temperature on filament length
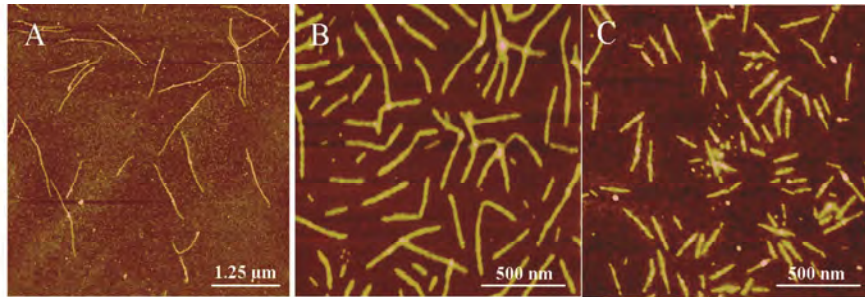
Figure 3.6 AFM images of fibrils made at (A) low concentration, no pre-heating, (B) high concentration and no-preheating, (C) low concentration (same as in A) but with pre-heating.

When fibrils are formed at a higher polymer concentration, their length is much smaller. An example is given for $S_{12}C_4E_{40}$ (Figure 3.6B). Since the length is determined by the ratio between the concentration of protein and the concentration of nuclei, this implies that the concentration of nuclei increases relatively more than the total polymer concentration. This supports our earlier conclusion that homogeneous nucleation occurs in these polymers, in contrast to elastin-free silk-like polymers [24]. Apparently, the elastin-like block enhances not only aggregation and sedimentation but also nucleation. Probably, the hydrophobic attraction brings protein molecules together in dense clusters, thereby facilitating folding and nucleation of a fibril. If this is indeed the case, then it is to be

45

expected that the rate of nucleation should increase with increasing temperature, as the elastin-like block has a stronger tendency to cluster at higher temperature. To test this, we heated a sample for 15 min at 45 °C before quenching to low pH. The resulting fibrils were indeed much shorter than fibrils in samples that had not been pre-heated (Figures 3.6C and A, respectively). This indicates that heating indeed increases the number of nuclei.

Gel formation

At concentrations of 35 g/L and higher, gels are formed by $S_{12}C_4E_{40}$ at pH 2. For example, with protein concentration of 50 g/L, gelation occurred after 6 h of incubation at 4 °C. Figure 3.7 shows the storage moduli of gels made at 50 g/L and 90 g/L, respectively, as a function of time, when cycling the temperature between 5 °C and 35 °C. The fresh gels at 5 °C are rather weak, having moduli of 39 Pa and 420 Pa, respectively. In contrast, gels formed by the elastin-free $S_{24}C_4S_{24}$ prominently display a high modulus (~10000 Pa) at protein concentrations as low as 1 g/L [8, 29]. The difference may be well explained by the much smaller length of $S_{12}C_4E_{40}$ fibrils at higher concentrations, as discussed in the previous section (Figure 3.6).

To investigate the temperature response of the $S_{12}C_4E_{40}$ gels, the modulus was measured over two temperature cycles, where heating and cooling between 5 °C and 35 °C was performed discontinuously in steps of 10 °C. Figure 3.7 shows that the modulus decreases upon heating from 5 °C to 35 °C, but the gel is not capable of full recovery upon cooling from 35 °C to 5 °C. This suggests that irreversible aggregation of fibrils occurs over the heating cycle, which very likely hampers the recovery of the initially formed network. The irreversible character of the triblock is probably due to the silk-like block as the gel formation was triggered by pH. The elastin-like block makes the system temperature-sensitive, but the thermo-responsive reversibility may be lost because the elastin-like block is connected to the silk-like fibrils rather than free in solution. As a result, bundled fibrils may not be able to separate upon cooling. Possibly, we are observing the combined effects of interaction between elastin-like and silk-like blocks. Literature reports of comparable tandem silk-elastin like copolymers [31, 32] also describe hydrogels at concentrations of the order of 100 g/L, but these did not display significant environmental post-gelation temperature sensitivity [31] due to irreversible crystallization of the silk-like blocks which prevent the elastin-like block from reversible folding.
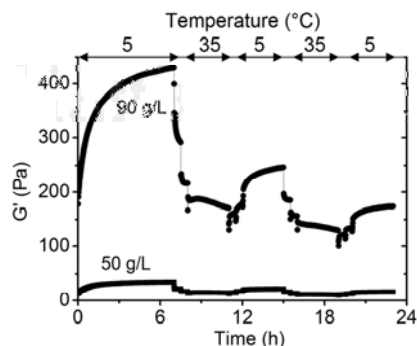
Figure 3.7 Storage modulus as a function of time during gelation of $S_{12}C_4E_{40}$ when the solutions are quenched to low pH at 5 °C with concentrations of 90 g/L and 50 g/L. After forming the gel, the temperature was cycled between 5 °C and 35 °C as indicated.

3.4.   Conclusion

In this chapter, we reported the production and investigation on fibril formation of two biosynthetic silk/elastin protein block copolymers (a diblock and a triblock) which both contain silk-like (S) and elastin-like (E) sequences; one of the two also contains a hydrophilic random coil sequence (C). Both the diblock ($S_{24}E_{40}$) and the triblock ($S_{12}C_4E_{40}$) are capable of pH-triggered, slow self-assembly into fibrils. This behavior, which is also known for elastin-free silk-like block copolymers, must clearly be attributed to the silk-like block. The elastin-like block introduces temperature sensitivity, due to its nature as an LCST polymer. This has two consequences: (a) it allows homogeneous fibril nucleation to occur, which introduces fibril poly-dispersity and a concentration dependence of fibril length; (b) it leads to 'sticky' fibrils, which undergo temperature-dependent bundling, aggregation and sedimentation. The latter effects are most prominent for $S_{24}E_{40}$ which lacks the hydrophilic C block in $S_{12}C_4E_{40}$. Weak gels are formed in $S_{12}C_4E_{40}$ solutions when they are quenched to low pH at concentrations higher than about 40 g/L. These gels respond to temperature in an irreversible manner, which we also ascribe to fibril aggregation.

47

References

1. D. A. Tirrell, M. J. Fournier and T. L. Mason, *Curr. Opin. Struct. Biol.*, 1991, **1**, 638-641.

2. D. E. Meyer, K. Trabbic-Carlson and A. Chilkoti, *Biotechnol. Progress*, 2001, **17, (**720-728.

3. S. Zhang, *Nat. Biotechnol.*, 2003, **21**, 1171-1178.

4. J. Huang, C. Wong Po Foo and D. L. Kaplan, *Polym. Rev. (Philadelphia, PA, U. S.)*, 2007, **47**, 29-62.

5. R. Dandu, H. Ghandehari and J. Cappello, *J. Bioact. Compat. Polym.*, 2008, **23**, 5-19.

6. D. L. Nettles, A. Chilkoti and L. A. Setton, *Adv. Drug Delivery Rev.*, 2010, **62**, 1479-1485.

7. M. W. T. Werten, W. H. Wisselink, T. J. Jansen-van den Bosch, E. C. de Bruin and F. A. de Wolf, *Protein Eng.*, 2001, **14**, 447-454.

8. M. Schor, A. A. Martens, F. A. deWolf, M. A. Cohen Stuart and P. G. Bolhuis, *Soft Matter,* 2009, **5**, 2658-2665.

9. M. Krejchi, E. Atkins, A. Waddon, M. Fournier, T. Mason and D. Tirrell, *Science*, 1994, **265**, 1427-1432.

10. M. W. T. Werten, A. P. H. A. Moers, T. Vong, H. Zuilhof, J. C. M. van Hest and F. A. de Wolf, *Biomacromolecules*, 2008, **9**, 1705-1711.

11. E. J. Cantor, E. D. T. Atkins, S. J. Cooper, M. J. Fournier, T. L. Mason and D. A. Tirrell, *J. Biochem.*, 1997, **122**, 217-225.

12. M. Schor, A. A. Martens, F. A. deWolf, M. A. Cohen Stuart and P. G. Bolhuis, *Soft Matter*, 2009, **5**, 2658-2665.

13. D. E. Meyer and A. Chilkoti, *Biomacromolecules*, 2004, **5**, 846-851.

14. R. Schipperus, R. Teeuwen, M. Werten, G. Eggink and F. de Wolf, *Appl. Microbiol. Biotechnol.*, 2009, **85**, 293-301.

15. R. Langer, L. G. Cima, J. A. Tamada and E. Wintermantel, *Biomaterials*, 1990, **11**, 738-745.

16. D. W. Urry, *Angew. Chem., Int. Ed. Engl.*, 1993, **32**, 819-841.

17. D. W. Urry, *J. Phys. Chem. B*, 1997, **101**, 11007-11028.

18. W. Qiu, W. Teng, J. Cappello and X. Wu, *Biomacromolecules*, 2009, **10**, 602.

19. X.-X. Xia, Q. Xu, X. Hu, G. Qin and D. L. Kaplan, *Biomacromolecules*, 2011, **12**, 3844-3850.

20. A. A. Dinerman, J. Cappello, H. Ghandehari and S. W. Hoag, *J. Controlled Release*, 2002, **82**, 277-287.

21. W. Qiu, Y. Huang, W. Teng, C. M. Cohn, J. Cappello and X. Wu, *Biomacromolecules*, 2010, **11**, 3219-3227.

22. J. Cappello, J. W. Crissman, M. Crissman, F. A. Ferrari, G. Textor, O. Wallis, J. R. Whitledge, X. Zhou, D. Burman, L. Aukerman and E. R. Stedronsky, *J. Controlled Release*, 1998, **53**, 105-117.

23. A. A. Martens, J. van der Gucht, G. Eggink, F. A. de Wolf and M. A. Cohen Stuart, *Soft Matter*, 2009, **5**, 4191-4197.

24. L. H. Beun, X. J. Beaudoux, J. M. Kleijn, F. A. de Wolf and M. A. Cohen Stuart, *ACS Nano*, 2011, **6**, 133-140.

25. M. W. T. Werten, T. J. van den Bosch, R. D. Wind, H. Mooibroek and F. A. de Wolf, *Yeast*, 1999, **15**, 1087-1096.

26. M. W. T. Werten, H. Teles, A. P. H. A. Moers, E. J. H. Wolbert, J. Sprakel, G. Eggink and F. A. de Wolf, *Biomacromolecules*, 2009, **10**, 1106-1113.

27. D. T. McPherson, J. Xu and D. W. Urry, *Protein Expression Purif.*, 1996, **7**, 51-57.

28. D. E. Meyer and A. Chilkoti, *Biomacromolecules*, 2002, **3**, 357-367.

29. A. A. Martens, J. van der Gucht, G. Eggink, F. A. de Wolf and M. A. Cohen Stuart, *Soft Matter*, 2009, **5**, 4191-4197.

30. K. Trabbic‑Carlson, D. E. Meyer, L. Liu, R. Piervincenzi, N. Nath, T. LaBean and A. Chilkoti, *Protein Eng., Des. Sel.*, 2004, **17**, 57-66.

31. A. A. Dinerman, J. Cappello, H. Ghandehari and S. W. Hoag, *Biomaterials*, 2002, **23**, 4203-4210.

32. M. Haider, V. Leung, F. Ferrari, J. Crissman, J. Powell, J. Cappello and H. Ghandehari, *Mol. Pharmaceutics*, 2005, **2**, 139-150.

Appendix
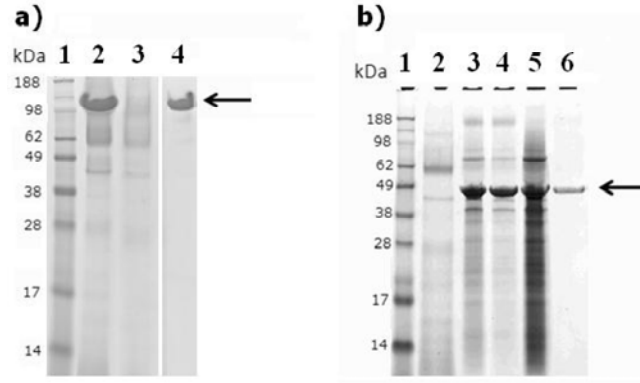
Figure A3.1   SDS PAGE of a) $S_{12}C_4E_{40}$ purified by ammonium sulfate precipitation: Lane 1: molecular mass marker, Lane 2: fermentation supernatant, Lane 3: supernatant after precipitation with ammonium sulfate at 40% saturation (host-derived proteins), Lane 4: pellet after precipitation with ammonium sulfate at 40% saturation (product); b) $S_{24}E_{40}$ purified by ITC method with 2M NaCl; Lane 1: molecular mass marker; Lane 2: supernatant after hot spin; Lane 3: pellet with protein after hot spin; Lane 4: supernatant with protein after cold spin; Lane 5: pellet after second hot spin; Lane 6: supernatant after second cold spin (purified protein). The arrows point to the product bands.
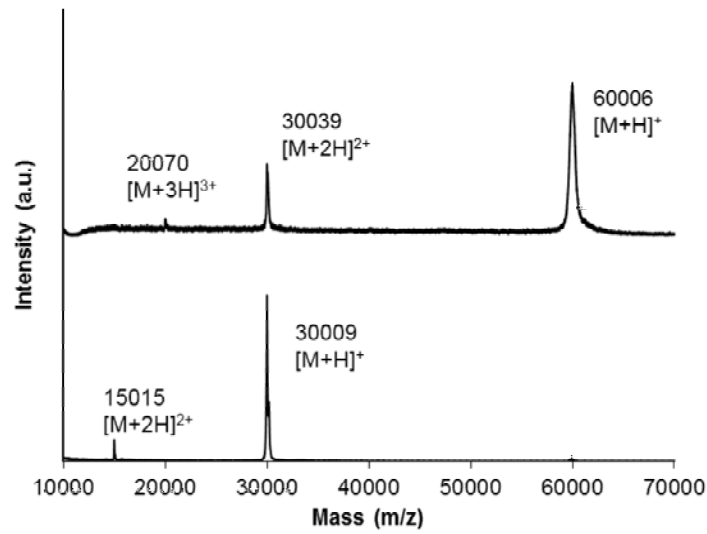
Figure A3.2 MALDI-TOF of (top) purified $S_{12}C_4E_{40}$ and (bottom) purified $S_{24}E_{40}$. The various charged- molecular ions are indicated.
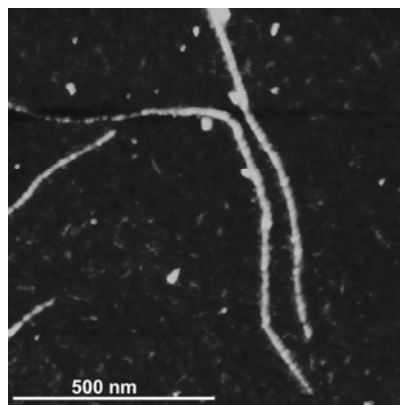
Figure A3.3 Fibril morphology obtained by AFM of single fibril formed by pH-triggered self-assembly of $S_{12}C_4E_{40}$ in 20 h at 4 °C.
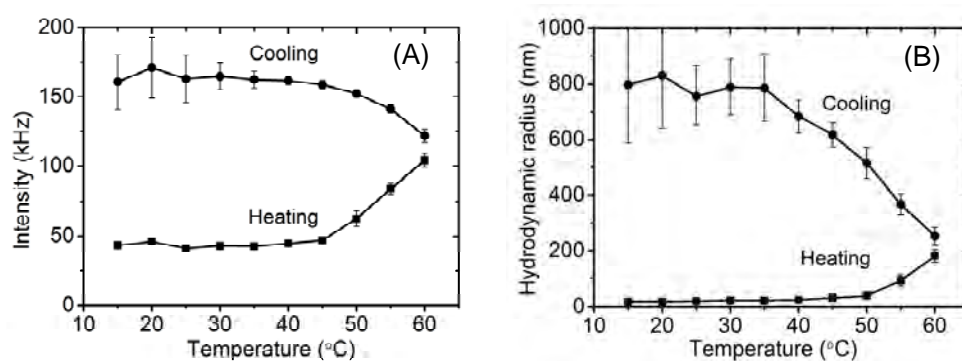
Figure A3.4 Irreversible thermo-responsive aggregates of $S_{12}C_4E_{40}$ upon heating at neutral pH, when the self-assembly of the S block is not triggered: (A) scattering intensity and (B) hydrodynamic radius.

Chapter 4

Pathway-dependent properties of a multi-stimuli sensitive biosynthetic hybrid network

Abstract

In this chapter, we study the self-assembly of an asymmetric triblock copolymer consisting of an elastin-like and a silk-like block bridged by a hydrophilic spacer. The elastin-like block aggregates at high temperature, leading to thermo-reversible micellization. The silk-like block self-assembles at low pH, and forms long fibrils, which dissociate again at high pH. The self-assembly of both blocks is strongly enhanced by increasing the salt concentration. When two blocks are sequentially triggered to self-assemble, the reversibility is lost; the final morphology and mechanical properties depend on the pathway that is chosen. A micellar solution formed at high temperature transforms into a gel network of sticky fibrils when the pH is lowered. Heating a solution of fibrils, formed at low pH, leads to the irreversible formation of bundles and large aggregates.

4.1.   Introduction

With the increasing demand for innovative multi-functional biomaterials for medical applications, there is a need to combine different functionalities within one system. Advanced bioengineering offers the possibility to combine and incorporate distinctive properties from various natural proteins into a single new molecule. For example, silk-elastin-like copolymer proteins have been synthesized [1, 2] and fabricated into scaffolds, nanofibers, nanoparticles and hydrogels [3-7]. Properties of these copolymers highly depend on the arrangement of the amino acids and the arrangement of different domains [4]. Ideally, the newly designed molecules have to possess all desired properties of each of the domains. However, the combination of different self-assembly domains within one system also introduces additional complexity. For example, the different domains will often have a tendency to self-assemble into different shapes that may not be mutually compatible. One structure (e.g., spherical micelles) might have to transform into another (e.g., filaments), which may imply kinetic barriers. Such kinetic barriers can make the result of the assembly process dependent on the precise history of the sample. When self-assembling blocks are used that can be triggered independently of each other, we obtain novel hybrid materials with properties that depend on the order in which triggers are applied, e.g. on the self-assembly pathway.

To study self-assembly in such hybrid systems in a systematic way, control of the self-assembly pathway is needed. This can be achieved by using responsive self-assembly blocks, which can be triggered independently of each other. Recently, we reported a biosynthetic, dual-responsive triblock copolymer, in which a silk-like and an elastin-like block are separated by a long hydrophilic spacer [8]. This latter block has no propensity to fold and simply forms a random coil in a wide range of temperature and pH. The silk-like block is inspired by poly (GA) sequences found in natural silk, and consists of 12 repeats of the octapeptide (GAGAGAGE) where the glutamic acid imparts pH responsive properties. Upon lowering the pH to below 4, these blocks self-assemble into β-rolls (β-sheet-like structures) with hydrophobic faces; the combination with the hydrophilic random coils has been investigated extensively and it is known that the β-rolls in this molecule stack to form long fibrils [9, 10]. The elastin-like blocks are comprised of 40 repeats of the pentapeptide motif (VPGXG) where the X position is occupied by either valine, alanine, or

54

glycine in a 5:3:2 ratio, respectively. This block has a lower critical solution temperature (LCST) and aggregates at a temperature higher than the LCST [11]. Like the silk-like block, the aggregation of the elastin-like block is influenced by the attached hydrophilic block which tends to suppress aggregation. Previously, we showed that the combination of silk and elastin-like block with an inert spacer leads to fibril formation at low pH in a way dependent on temperature [8]. However, due to the presence of the hydrophilic block, the elastin-like block itself could not induce a thermo-reversible micellar state in salt-free solution, even at temperatures up to 70 °C, but goes into irreversible coacervate aggregation. Hence, in order to better exploit the reversible self-assembling properties of the elastin-like block in the conjugate, we have to change conditions.

In this chapter, we first show how salt enhances the self-assembly of the elastin-like blocks, leading to a lowering of the LCST so that temperature-triggered micellization becomes possible. We then study the self-assembly of the dual (pH- and temperature)-responsive block copolymer along different kinetic pathways.

Since pH and temperature (T) constitute virtually independent triggers, we can present kinetic pathways as curves connecting a starting point and an end point in the pH, T plane, as illustrated in Figure 4.1A. Of course, there are many such curves; for the sake of illustration, we discuss here only limiting cases of large parameter changes (pH and T) and we simply change the order in which they are applied. Our starting point is always a simple molecular solution at low T (where the elastin-like block tends to dissolve) and high pH (where the silk-like block is fully deprotonated and dissolved as well). We first explore changes along one axis (T or pH), where we expect formation of micelles or fibrils, respectively. Finally, we explore pathways to a high T, low pH end point along pathway c (first increase T and then lower pH) and d (first lower pH, then increase T). A schematic picture of expected structures formed in different conditions is presented in Figure 4.1B

It may be important to realize at this point that reversibility is not simply an intrinsic property of the material, e.g. if the self-assembly is T-reversible at high pH, it is not necessarily also T-reversible at low pH because the global structure may be very different in both cases.
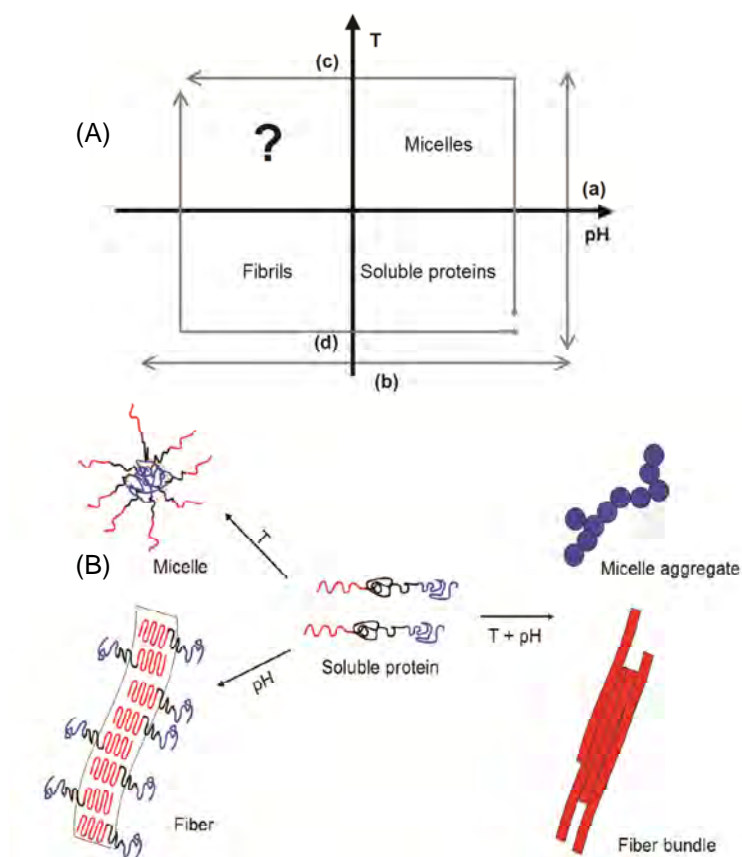
Figure 4.1 (A) Several self-assembly pathways in the (pH, T) plane for a silk-hydrophilic random coil-elastin based conjugate polymer. The elastin-like blocks drive aggregation into micelles at high temperature, while the silk-like blocks tend to stack into fibrils at low pH. The final structure of the hybrid system depends on the order in which these stimuli are applied. (B) Schematic picture of structures expected to form upon applying pH, temperature or both.

4.2. Materials and Methods

Design, production and purification of proteins

Three polymers are discussed in this study. The triblock copolymer $S_{12}C_4E_{40}$ which was designed as reported in a previous paper [8] was purified by ammonium sulfate precipitation. The product has a purity of >95 %, as confirmed by SDS-PAGE and matrix-assisted laser desorption/ionization time-of-flight mass spectroscopy (MALDI-TOF). The silk-like block S_{12} consists of 12 (GAGAGAGE) repeats which (in water) adopts a β-roll conformation

upon lowering the pH < 4 [9]. The middle block C_4 consists of four identical 99 amino acid long units that carry many uncharged and hydrophilic amino acids; it assumes a random coil configuration at any temperature and pH [12]. This is not to say this random coiled block has no effects on the self-assembly. In any self-assembled object, the spacer blocks will interact repulsively, thereby balancing the driving force for the self-assembly. The pH-triggered fibril formation was reported in the case of triblock $C_2S_{48}C_2$ [9], which forms strong pH-triggered fibrils due to the stacking of β-roll. The elastin-like block E_{40} is composed of 40 (VPGXG) pentapeptide repeats having 50 % valines, 30 % alanines, and 20 % glycines in quasi-random order at the X position [13]. The diblock C_4E_{40} was also genetically designed, by ligating the C_4 block to the E_{40} block in the same way as for $S_{12}C_4E_{40}$. The gene template C_4E_{40} was cloned into the expression vector pPIC9 (Invitrogen) using *XhoI/EcoRI*. This creates a fusion with the *Sacchromyces cerevisiae* α-mating factor secretion signal present in vector pPIC9 [14]. The DNA plasmids were linearized with *SalI* to promote homologous integration at the his4 locus upon transformation of *Pichia pastroris* GS115 by electroporation [15].

The biopolymers were produced by fermentation of *P. pastoris* in 2.5 L Bioflo 3000 bioreactors (New Brunswick Scientific) as reported before [16]. The pH was maintained at 5.5 through fermentation and the methanol concentration was maintained at 0.2 % (v/v) during the induction phase. The purification was carried out as reported before [8, 9] with ammonium sulfate at 40 % saturation. The purification method with ammonium sulfate precipitation which has been used in our various reports gives high protein purity [8, 9, 16]. The proteins were dialyzed using Spectra/Por 7 tubing (Spectrum Labs) with a 1 kDa molecular weight cut-off. The desalted proteins were freeze-dried for storage until use.

The molecular mass distribution of the product was analyzed by MALDI-TOF. The analyses were performed using an Ultraflex mass spectrometer (Bruker), on a 600 µm AnchorChip target (Bruker) and with 2,5-dihydroxyacetophenone (Sigma-Aldrich) as matrix. Samples were prepared and measured as described previously [16]. The molecular weight of the triblock $S_{12}C_4E_{40}$ and the diblock C_4E_{40} are 60058 dalton and 53249 dalton, respectively (Appendix, Figure A4.1). The obtained values are the same as the theoretical molecular weights of these proteins as 59997 dalton and 53150 dalton, respectively.

Atomic force microscopy (AFM)

Stock solutions at a concentration of 5 g/L were prepared by solubilizing freeze-dried $S_{12}C_4E_{40}$ in Milli-Q H_2O at pH 11 on ice. Then 5 M NaCl (Sigma) was added to obtain a final concentration of 2.5 M. The pH was lowered to 2 by adding 1 M HCl (Merk, Germany) to the solutions. Supramolecular assembly occurred at room temperature or in a water bath with controlled temperature. In parallel experiments, protein solutions were adjusted to pH 2 without the presence of NaCl. All tubes were precleaned with ethanol, and solutions were micro- filtrated (0.2 µm pore size) to prevent biological contamination. To observe fibril bundles, protein solutions of 5 g/L were quenched to pH 2 with or without the presence of 2.5 M NaCl, and fibrils were grown overnight at 20 °C. The pH-triggered fibril solutions with NaCl incubated overnight at 30 °C were heated at 60 °C for 3 h and cooled back to 20 °C to induce fibril bundles. To observe micelles formed by $S_{12}C_4E_{40}$ in 2.5 M NaCl at pH 11, a protein solution (1 g/L) was heated at 60 °C in 30 min.

To prepare samples for imaging, a drop of 30 µl of each sample was deposited onto a clean hydrophilic silica wafer, incubated for two minutes and then washed with Milli-Q H_2O and dried under a mild stream of nitrogen. The dry samples were analyzed using a Nanoscope V in Scan Asyst™ imaging mode, using non-conductive silicon nitride probes (Veeco, NY, USA) with a spring constant of 0.32 N/m (air-scanning mode). Images were recorded between 0.200-0.990 Hz and further processed with NanoScope Analysis 1.20 software (Veeco Instruments Inc. 2010, USA).

Dynamic Light Scattering (DLS)

Protein stock solutions were prepared as above. Working solutions were made by diluting the stock solutions in 5 mM phosphate buffer at pH 7.4 or Milli-Q H_2O pH 11, and NaCl was added to a final concentration of 2.5 M. In other experiments, NaCl was added and adjusted to different concentrations of 1 M, 1.5 M, 2 M and 2.5 M. All solutions were sterilized using 0.2 µm filters (Milipore) to prevent contamination and remove dust before measurement. Light scattering was performed using an ALV dynamic light scattering instrument with a Cobolt Samba- 300 DPSS laser (300 mW) operating at a wavelength of 532 nm and an ALV-5000/60X0 multiple τ digital correlator. A refractive index matching bath of filtered cis-decalin surrounded the cylindrical scattering cell. All measurements

were taken at a fixed angle θ of 90 °, corresponding to a scattering vector $q = \frac{4\pi n}{\lambda} \sin\frac{\theta}{2}$ ~ 0.023 nm^{-1}, where n is the refractive index of the solvent (water). The temperature was varied between 15 °C and 60 °C using a Haake F3-K thermostat. A temperature-ramp was performed by cycling from 20 °C to 60 °C with maximal deviation of 0.2 °C.

Rheology

Experiments were carried out using a rheometer (Physica MCR 301) with Couette CC10/TI geometry and a bob and cup diameter of 9.991 and 10.840 mm, respectively. The protein $S_{12}C_4E_{40}$ solutions were prepared as above to the final protein concentration was fixed at 50 g/L. The solutions were quickly loaded into the rheometer. A solvent trap (Anton Paar) with oil was used to minimize evaporation. Gel formation was monitored by applying a sinusoidal deformation to the system (f = 1 Hz and γ=1 %) until a constant modulus was reached. The temperature was controlled by a connected Peltier system. In temperature-ramps, the system was monitored by applying a sinusoidal deformation for 3 h at each temperature.

4.3.   Results and Discussion

Salt-dependent self-assembly of the elastin-like block

We have previously reported the fibril growth kinetics of the triblock $S_{12}C_4E_{40}$ in salt-free solutions [8]. Although the elastin-like block did have an effect on the self-assembly of the silk-like block, the elastin-like block by itself (e.g. at high pH where the silk-like block is not self-assebling) was not significantly reversibly responsive to temperature under these conditions. Many previous studies [17, 18] showed that NaCl enhances the self-assembly of elastin-based polypeptides, leading to a decrease of the transition temperature (T_t). It has been argued that this decrease in T_t by NaCl is related to polarization of water molecules in the first dehydration shell, which weakens hydrogen bonding between water and the polynmer [18]. We therefore decided to study the salt-dependence of our elastin block for a diblock copolymer C_4E_{40}, which lacks the silk-like block.

We use light scattering to study micelle formation of C_4E_{40} upon heating from 20 °C to 60 °C at different NaCl concentrations (Figure 4.2A). For NaCl concentrations below 1.5

M, no increase in scattering intensity is observed within this temperature range. However, in the presence of 2 M NaCl, the scattering intensity increases when the temperature reaches 60 °C, indicating the formation of micelles. At 2.5 M NaCl, micelle formation starts already at 50 °C. Moreover, cooling back to 20 °C results in a decrease in scattering intensity, indicating a reversible thermo-responsive property. Hence, the presence of NaCl clearly enhances the attraction between elastin-like blocks, leading to a decrease of the T_t. We note that the protein polymers show high T_t even in the presence of high concentration of NaCl, probably due to the hydrophilicity of the C_4 block.
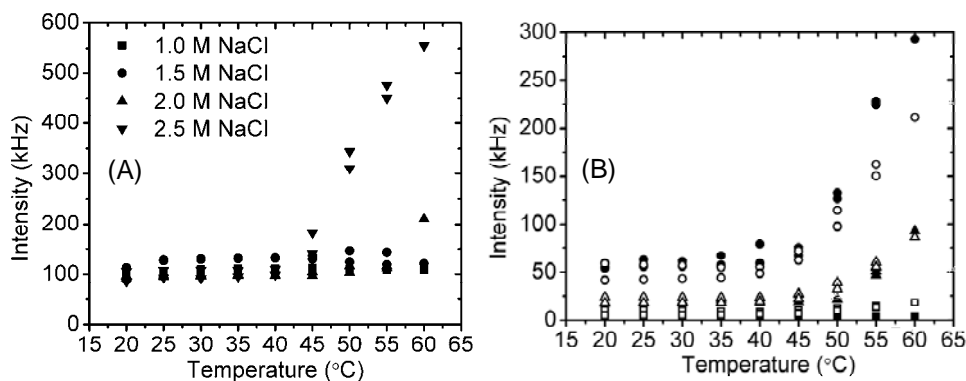
Figure 4.2 Thermo-responsive micellization of $S_{12}C_4E_{40}$ and C_4E_{40}, (A) The effects of salt on T_t for C_4E_{40} at a concentration of 2 g/L at pH 7.4, (B) The effects of concentration on T_t (at pH 11) for $S_{12}C_4E_{40}$ (open symbols) and C_4E_{40} (filled symbols) in the presence of 2.5 M NaCl (squares: 0.1 g/L; triangles: 0.5 g/L; circles: 1 g/L).

Reversible micelle formation of $S_{12}C_4E_{40}$ at high pH (pathway a)

Next, we study the temperature-responsiveness of the triblock $S_{12}C_4E_{40}$ in the presence of 2.5 M NaCl and at high pH, where the silk-like block does not self-assemble (pathway a in Figure 4.1A). Figure 4.2B shows the scattering intensity as a function of the temperature; for comparison we include the corresponding data for diblock C_4E_{40} at 2.5 M NaCl (at neutral pH) for various protein concentrations. In all cases, the scattering intensity increases when the temperature is increased above a critical value. At low T, the scattering is low; in fact is too low to have well-defined values for hydrodynamic size (diffusion coefficient). It is important to note that the change of the scattering intensity is fully reversible for both triblock and dibock polymers: upon cooling, the scattering intensity

decreases again. The hydrodynamic radius of the aggregates above the T_t is 30 ± 2 nm in all cases, which corresponds well to the size expected for a micellar object. The representative AFM images of these micelles are shown in Appendix, Figure A4.2. There is no significant difference in behavior between the triblock and the diblock, showing that the silk-like blocks likely have no effect on the micellization caused by the aggregating elastin-like blocks at high pH. Indeed, AFM shows the absence of any fibrillar structures under these conditions (at pH 7 and pH 11). In Figure 4.2B, the reversible formation of micelles is more noticeable at higher protein concentration than at low concentration.
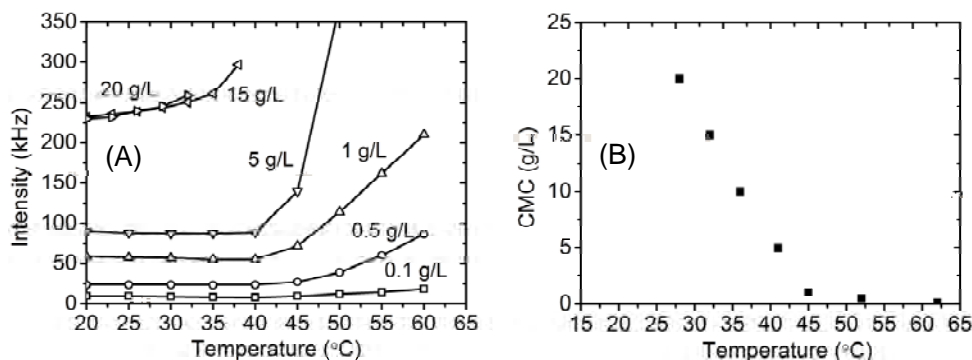
Figure 4.3 (A) Scattering intensity as a function of temperature for various concentrations (at high pH in NaCl), (B) Critical micelle concentration (CMC) of $S_{12}C_4E_{40}$ as a function of temperature at high pH (11) and in 2.5 M NaCl.

The temperature at which the scattering objects are formed decreases with increasing concentration. This implies that for each temperature there is a different critical micelle concentration (CMC) (Figure 4.3A). In other words, there is a dependence of CMC on the temperature. The temperature at each CMC is determined from the intersection of lines representing the horizontal part (below T_t) and the rising part (above the T_t) of the scattering intensity in Figure 4.3A. We collected the CMC values from scattering experiments over a concentration range of 0.1 to 20 g/L (Figure 4.3B). At higher temperature, the driving force for aggregation of the elastin-like blocks becomes stronger, leading to a lowering of the CMC. Similar effects have been observed elsewhere [19][20]. The CMC (T) curves should, of course, have asymptotes on both ends, as CMC cannot get negative and is fully suppressed (CMC → ∞) at very low T. However, there is no a priori,

generally accepted function for the T-dependence. We therefore refrain from fitting a simple function through the data.

Fibril formation at low temperature (pathway b)

Next, we study the behavior of the triblock copolymer at low pH and low temperature, where only the silk-like block self-assembles. As shown previously, the protein forms fibrils at low pH, due to the stacking of proteins that have folded into β-sheet like structures after charge neutralization [8, 9]. To study the effect of NaCl on such pH-induced fibril formation, we used AFM to visualize filaments after a 4 h-incubation at 20 ℃. Representative AFM images for samples in the presence and in the absence of NaCl are displayed in Figure 4.4A and 4.4B (respectively). Fibrils formed in the presence of NaCl (Figure 4.4C) are longer and more polydisperse than fibrils formed in salt-free solution (Figure 4.4D). The average length of fibrils grown in the presence of 2.5 M NaCl (Figure 4.4A) is 290.7 ± 119.6 nm; without NaCl (Figure 4.4B) this is 111.2 ± 38 nm. In terms of the fibrillar structure, height analysis shows no significant difference between these two conditions (Figure 4.4E and 4.4F). We notice that the width of the fibrils appears slightly bigger in the presence of NaCl but we cannot report a precise quantitative result with the current method.

To study the fibril growth with and without NaCl in more detail, we used light scattering (Figure 4.5). In the absence of salt, fibril formation is slow, in agreement with our previous finding that filaments of 1 µm in length were only observed after more than a day [8]. As shown in Figure 4.5, $S_{12}C_4E_{40}$ solutions with 2.5 M NaCl show a significant enhancement in both hydrodynamic radius (Figure 4.5A) and scattering intensity (Figure 4.5B) as compared to those without NaCl. This indicates that NaCl accelerates fibril growth of the silk-elastin-like triblock copolymer: it likely leads to more and longer filaments. This is probably due to the aggregation of elastin-like block facilitate the nucleation of the fibrillar self-assembly. Previously, we have reported that the sticky elastin block facilitates nucleation of the fibrillar self-assembly of the silk-like blocks, leading to polydisperse fibrils [8]. Probably, this effect is enhanced even further by salt, because salt increases the attractive interactions between the elastin-like blocks. This enhanced attraction likley also increases the growth rate of the fibrils.

To investigate the reversibility of the fibril formation, we carried out cycles in which the pH of a 5 g/L $S_{12}C_4E_{40}$ solution at 20 °C is repeatedly decreased and increased. As shown in Figure 4.6, both scattering intensity and hydrodynamic radius increase when the pH is lowered from pH 11 to pH 2, as a result of fibril formation. Upon raising the pH back to 11, the scattering intensity and hydrodynamic radius decrease again, indicating that the fibrils dissociate. Also in subsequent cycles, fibril formation and dissociation are fully pH-reversible. This agrees with findings reported for a symmetric silk-based triblock $C_2S_{48}C_2$, which also showed complete pH-reversibility [21]. Apparently, the elastin-like blocks do not influence the pH-reversibility of the silk-like blocks at this temperature.
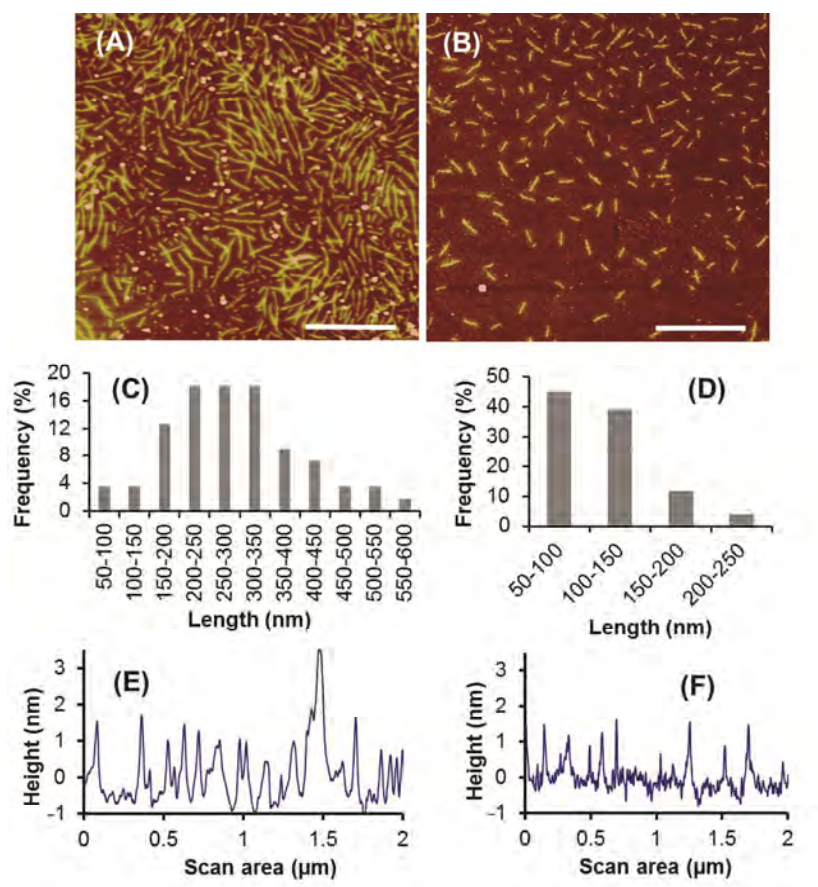
Figure 4.4 Effect of salt on pH-triggered fibrils (at pH 2) analyzed by AFM: (A, C, E) in the presence of NaCl, and (B, D, F) in the absence of NaCl. (A) and (B): Representative AFM images of the fibrils

after 4- h incubation; (C) and (D): Length distribution of the fibrils; (E) and (F): height analysis of the fibils. Scale bars correspond to 500 nm.
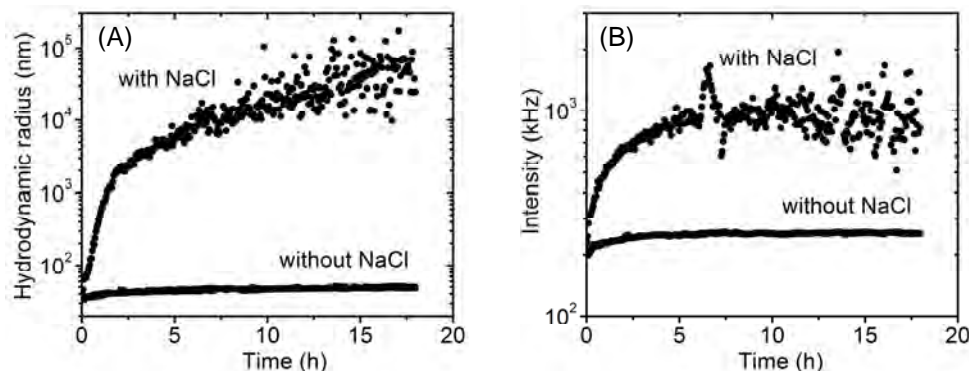
Figure 4.5 Light scattering data for pH-triggered (pH 2) fibril growth at 20 °C at a concentration of 5 g/L in the presence and in the absence of 2.5 M NaCl: (A) hydrodynamic radius and (B) scattering intensity in the course of time.
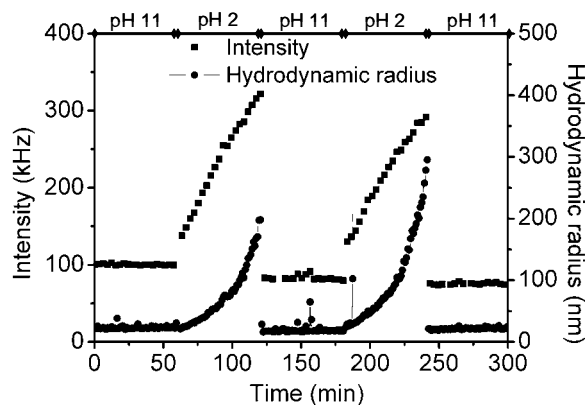
Figure 4.6 pH-reversibility of fibril formation of 5g/L $S_{12}C_4E_{40}$ solution at 2.5 M NaCl at 20 °C (below T_t).

Fibril growth at high temperature (pathway c)

Above, we studied the behaviors of the triblock copolymer under conditions where only one of the two blocks self-assembles. Next, we consider the stepwise assembly, in which the two blocks are triggered one after the other. In this section, we describe the case when the temperature is increased first, followed by a lowering of the pH (pathway c in Figure

4.1A). At high temperature and high pH, the protein polymers are present as micelles and we monitor by light scattering what happens upon a quench to pH 2 (Figure 4.7A). The scattering intensity significantly increases upon lowering the pH to 2, which indicates fibril growth. However, the objects are too big to reliably determine their size. Therefore, we have no data for the hydrodynamic radius. The intensity is much higher than those at low temperature (Figure 4.6), suggesting that large and more massive objects form; we speculate that these are fibril bundles. There is a lot of scatter for the diffusion radius, which could be due to the sedimentation of these big objects or the fact that the relaxation of such objects is longer than the autocorrelation measurements. Upon increasing the pH back to 11, the scattering intensity decreases again, indicating that the process is pH-reversible and that the system goes back to a micellar solution.
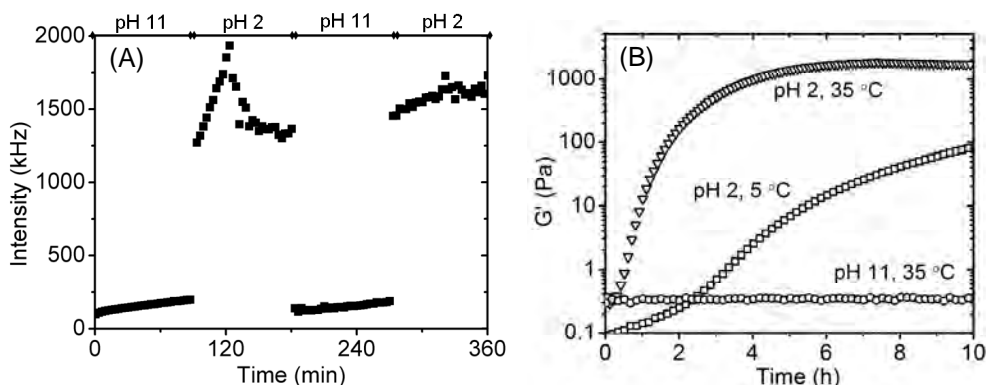
Figure 4.7 (A) pH-reversibility of fibril formation of 5 g/L $S_{12}C_4E_{40}$ solutions in 2.5 M NaCl and at 45 °C (above T_t), (B) Storage modulus of 50 g/L $S_{12}C_4E_{40}$ in the presence of 2.5 M NaCl as a function of time at different temperature at both high pH (11) and low pH (2).

At higher concentrations (50 g/L), the block copolymers form gels [8] along both pathway a and c in Figure 4.1B. We investigated this gelation by rheology using oscillatory measurement at low shear rate (strain 1%, frequency 1Hz) so that we can avoid any effect of shear on the fibrillar gels. Figure 4.7B shows the time dependence of elastic modulus of $S_{12}C_4E_{40}$ solutions of 50 g/L in the presence of NaCl, after a pH quench from 11 to 2 for temperatures both below (5 °C) and above (35 °C) the T_t of the elastin-like block. Clearly, the modulus increases much more strongly upon pH-induced fibril formation when the temperature is higher. At 35 °C, which is above the T_t, the modulus increases to

approximately 1000 Pa, while below the T_t (at 5 °C) the modulus reaches only about 100 Pa. Solutions without pH-triggered fibrils, at pH 11, do not show any gelation although the temperature was above the T_t (35 °C) (Appendix, Figure A4.3). Hence, we conclude that pH-triggered self-assembly of silk-like fibrils is crucial for the network formation.

Temperature-induced association of fibrils at low pH (pathway d)
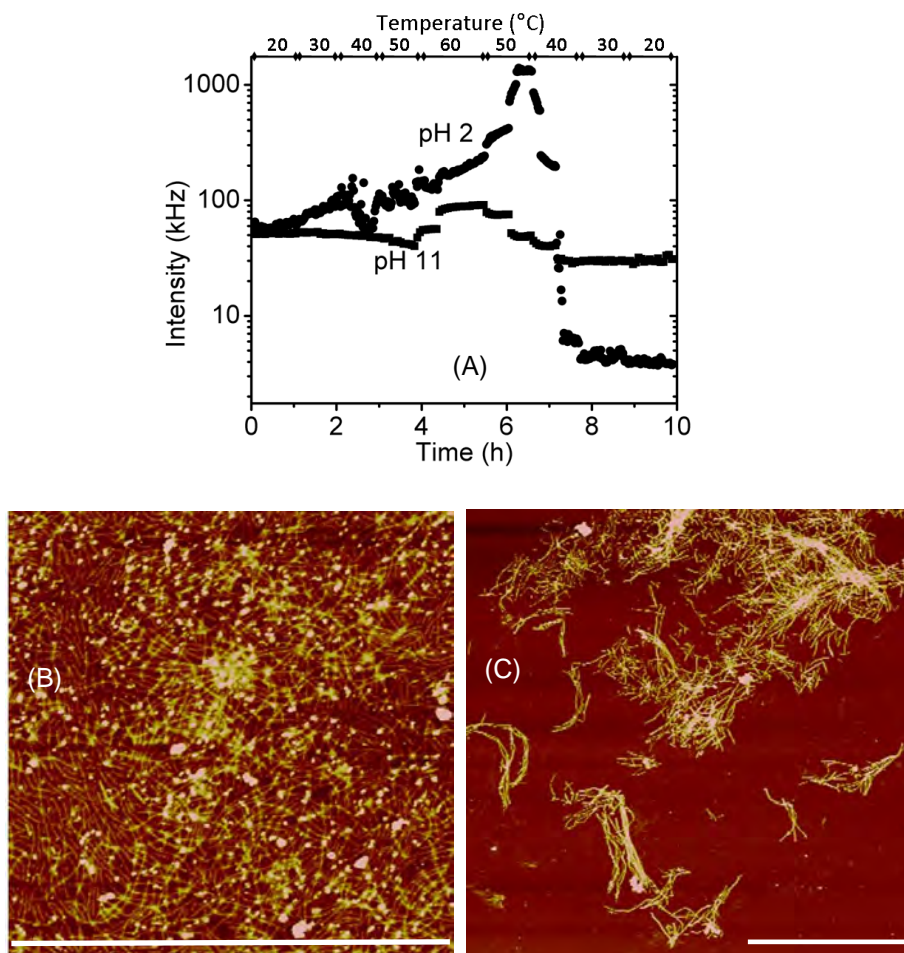
Figure 4.8 (A) Light scattering intensity during a temperature ramp of 5 g/L $S_{12}C_4E_{40}$ solutions in the presence of 2.5 M NaCl at pH 2 and 11, (B) Representative AFM image of pH-triggered fibril grown at low temperature (30 °C) for 20 h, (C) Fibril bundles formed after 3 h-heating at 60 °C, and subsequent cooling at room temperature of the pH-triggered fibril solution shown in B. Scale bars correspond to 3 µm.

Finally, we consider the case where the fibrils are first allowed to grow at low pH (2) and low temperature before the temperature is raised above the T_t of the elastin-like blocks.

To study the effect of temperature on solutions of $S_{12}C_4E_{40}$ fibrils, light scattering with a temperature-ramp from 20 °C to 60 °C was carried out on dilute protein solutions of 5 g/L in 2.5 M NaCl at pH 2. As shown in Figure 4.8A, the scattering intensity increases strongly when the temperature is raised. This probably indicates that fibrils aggregate as a result of the decreased solubility of the elastin-like blocks at high temperature. Cooling back to room temperature initially leads to a further increase of the scattering intensity, followed by a sharp decrease in the scattering intensity. The latter is caused by sedimentation of fibril aggregates as could be seen by visual inspection of the samples. On another hand, heating the protein solution at pH 11 results in only the micellization, and cooling helps the micelles completely dissociate.

Similarly, we analyzed the changes of fibril morphology/structure by AFM by first letting the fibril grow at low temperature (30 °C) for 20 h and then sequentially heating at 60 °C for 3h and cooling the fibril solution at RT. The representative AFM image shows separate fibrils grown in the presence of NaCl at low pH, low T (Figure 4.8B). As expected, fibril bundles formed after sequential heating-cooling the fibril solution (Figure 4.8C). Hence, at low pH, the fibril dispersions aggregate irreversibly upon heating and they are no longer thermo-reversible, i.e., they cannot be redispersed by simply cooling down. This suggests that the interaction between filaments at low T is still attractive at a short distance, but also repulsive at longer distances. In other words, there is an activation barrier keeping them separated at low T.

We also analyzed the reversibility of the $S_{12}C_4E_{40}$ hybrid network at higher concentrations (50 g/L), by monitoring the elastic modulus of the gels during a temperature cycle. Figure 4.9 displays how the modulus of the gels prepared at different temperature changes over the temperature-ramp. The gel prepared at low temperature (Figure 4.9A) shows a continuous growth boost when temperature is increased. The storage modulus reaches 8000 Pa at 35 °C, the highest temperature of the cycle. Cooling results in a decrease in storage modulus, this is probably due to sedimentation. This indicates that the heating induces fibril aggregates or bundles and cooling releases these aggregates. The next temperature cycle shows an increase in storage modulus; however the modulus is lower than that at the same temperature in the first temperature cycle, indicating an

irreversible thermo-response. This irreversible thermo-response was also reported in a previous paper where a gel of the same protein was prepared in the absence of NaCl [8]. In contrast, the gel prepared at high temperature (Figure 4.9B) shows a fast increase of elastic modulus. Cooling also results in a decrease in storage modulus. The thermo-responsive behavior of this gel during temperature cycles is more complex (Figure 4.9B).
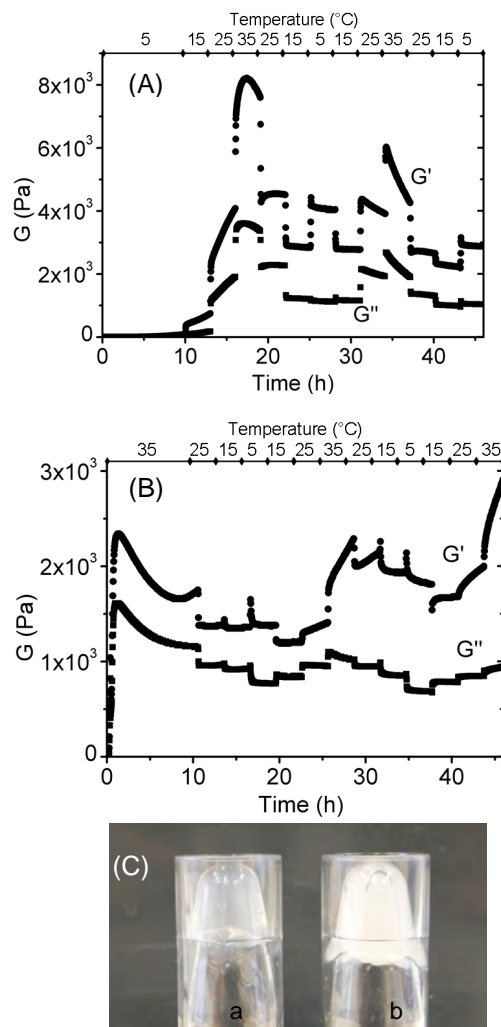
Figure 4.9 (A) Modulus changes of concentrated $S_{12}C_4E_{40}$ (50 g/L) solutions prepared at low temperature, (B) Modulus changes of concentrated $S_{12}C_4E_{40}$ (50 g/L) solutions prepared at high temperature during a temperature variation experiment, (C) Morphology of gels: C-a shows the gel after the temperature cycle in Figure A; C-b shows the gel after the temperature cycle in Figure B.

Figure 4.9C shows that the gels not only have different mechanical properties as illustrated in Figure 4.9A and B but also a significant different morphology. The gel obtained (after the described temperature cycles) at low gelation temperature is transparent, indicating a homogeneous gel with thin strands (Figure 4.9Ca). In contrast, the gel obtained after the described temperature cycles at high gelation temperature is milky, indicating a heterogeneous gel with large objects (Figure 4.9Cb). More observations are needed to get insights of gel structure. Nevertheless, we observed a remarkable influence of the gelation temperature on the gel properties: (i) when fibril growth is pH- triggered at low temperature where the elastin-like blocks are not active, the gel is homogenous with most likely fibrils, and the gel is irreversibly responsive to temperature; (ii) when fibril growth is pH-triggered at high temperature where the elastin-like blocks are active, the gel is clearly inhomogeneous and the properties are too complex to be precisely determined.

We note that the elastin-like blocks are quite dynamic and individually weak, hence, easy to slide and reorganize while the silk-like blocks organizes in a stable way, therefore, can be kinetically directed towards different paths and structures. This substantial difference of the two self-assembling blocks used likely plays a key role in the resulted structure.

4.4.   Conclusion

This chapter reports the observations on bio-inspired hybrid networks formed in the presence of 2.5 M NaCl by a polymer that is composed of: (1) a reversibly pH-responsive silk-like block and (2) a thermo-responsive elastin-like block, bridged by (3) a random coil hydrophilic middle block. When only one of the triggers (pH, temperature) is applied, the self-assemble properties of both end blocks are fully reversible.

Above the T_t, when the elastin-like blocks are organized in micelles, pH-triggered self-assembly of the silk-like blocks results in aggregates, likely due to sticky fibers. It is not possible to conclude whether fibers are formed by stacking of micelles which are surrounded by β-roll domains, or whether the fibrils grow from free β-rolls, although the enhanced rate of fibril formation at high temperature suggests the former scenario. Additionally, below the pH at which silk-like blocks assemble into filaments, heating accelerates not only the filament formation process but also aggregation of fibrils into bundles. Cooling did not reverse this process, but rather led to further irreversible

69

aggregation. Rheological data show pathway-dependent network formation: the gel prepared at low temperature is homogenous with a clear irreversible thermo-response while the gel prepared at high temperature is inhomogeneous with a sophisticated thermo-response.

We note that in this system, high concentration of NaCl was used to trigger the reversible thermo-response of the elastin-like block. In order to reduce such extreme triggering condition, design improvements in elastin-like sequence and the length of the spacer are considered. Other types of charged amino acids can be used in silk-like blocks so that the fiber formation can be triggered at a pH close to physiological conditions. More observations are needed to figure out how the dominant influence of silk-like block would affect the kinetic differences, and whether the kinetic difference is just a transient state since the dynamic elastin-like blocks likely reorganize towards thermodynamic stability. Nevertheless, the present system clearly illustrates the complexity that can arise in hybrid self-assembling systems, where non-equilibrium self-assembly processes make the supramolecular structure highly dependent on the triggering order.

References

1.   A. Nagarsekar, J. Crissman, M. Crissman, F. Ferrari, J. Cappello, H. Ghandehari, *Biomacromolecules,* 2003, **4** (3), 602-607.

2.   J. A. Gustafson, H. Ghandehari, *Adv. Drug Delivery Rev.,* 2010, **62** (15), 1509-1523.

3.   A. A. Dinerman, J. Cappello, H. Ghandehari, *Biomaterials,* 2002, **23** (21), 4203-4210.

4.   R. Danhu, A. Von Cresce, R. Briber, P. Dowell, J. Cappello, H. Ghandehari, *Polymer,* 2009, **50**, (2), 336-374.

5.   W. Qiu, W. Teng, J. Cappello, X. Wu, *Biomacromolecules,* 2009, **10** (3), 602-608.

6.   X. X. Xia, Q. Xu, X. Hu, G. Qin, D. L. Kaplan, *Biomacromolecules,* 2011, **11** (12), 3844-3850.

7.   W. Hwang, B. H. Kim, R. Dandu, J. Cappello, H. Ghandehari, J. Seog, *Langmuir,* 2009, **25** (21), 12682-12686.

8.   M. D. Golinska, T. T. H. Pham, M. W. T. Werten, F. A. de Wolf, M. A. Cohen Stuart and J. van der er Gucht, *Biomacromolecules,* 2012, **14**, (1), 48-55.

9.   A. A. Martens, G. Portale, M. W. T. Werten, R. J. de Vries, G. Eggink, M. A. Cohen Stuart, F. A. de Wolf, *Macromolecules,* 2009, **42** (4), 1002-1009.

10. J. M. Smeenk, M. B. J. Otten, J. Thies, D. A. Tirrell, H. G. Stunnenberg, J. C. M. van Hest, *Angew. Chem., Int. Ed. Engl.*, 2005, **117** (13), 2004-2007.

11. D. W. Urry , *J. Phys. Chem. B,* 1997, **101** (51), 11007-11028.

12. M. W. Werten, W. H. Wisselink, J. T. J. van den Bosch, E. C. de Bruin, F. A. de Wolf, *Protein Eng.,* 2001, **14** (6), 447-54.

13. R. Schipperus, R. L. M. Teuwen, M. W. Werten, G. Eggink, F. A. De Wolf, *Appl. Microbiol. Biotechnol.,* 2009, **85** (2), 293-301.

14. M. W. T. Werten, T. J. van den Bosch, R. D. Wind, H. Mooibroek, F. A. de Wolf, *Yeast* 1999, **15** (11), 1087-1096.

15. M. W. T. Werten, F. A. de Wolf, *Appl. Environ. Microbiol.,* 2005, **71** (5), 2310-2317.

16. M. W. T. Werten, H. Teles, A. P. H. A. Moers, E. J. H. Wolbert, J. Sprakel, G. Eggink, F. A. de Wolf, *Biomacromolecules,* 2009, **10** (5), 1106-1113.

17. C. H. Luan, T. M. Parker, K. U. Prasad, D. W. Urry, *Biopolymers,* 1991, **31** (5), 465-475.

18. J. Reguera, D. W. Urry, T. M. M. Parker, D. T. McPherson, J. C. Rodríguez-Cabello, *Biomacromolecules,* 2007, **8** (2), 354-358.

19. R. L. M. Teeuwen, S. S. van Berkel, T. H. H. van Dulmen, S. Schoffelen, S. A. Meeuwissen, H. Zuilhof, F. A. de Wolf, J. C. M. van Hest, *Chem. Comm.*, 2009, **27**, 4022-4024.

20. K. T. Carlson, D. E. Meyer, L. Liu, R. Piervincenzi, N. Nath, T. LaBean, A. Chilkoti, *Protein Eng., Des. Sel.,* 2004, **17** (1), 57-66.

21. L. H. Beun, X. J. Beaudoux, J. M. Kleijn, F. A. de Wolf, M. A. Cohen Stuart, *ACS Nano*, 2012, **6** (1), 133-140.

Appendix
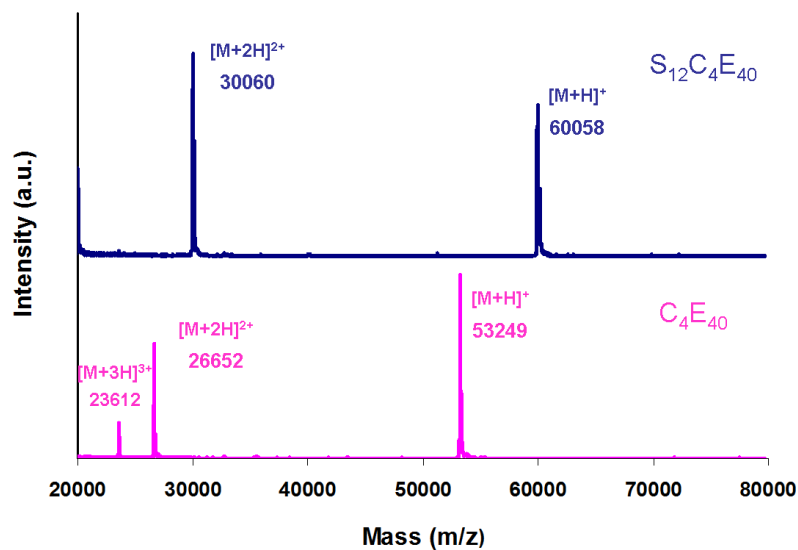
Figure A4.1 MALDI-TOF of $S_{12}C_4E_{40}$ and C_4E_{40}. Various molecular ions are indicated.
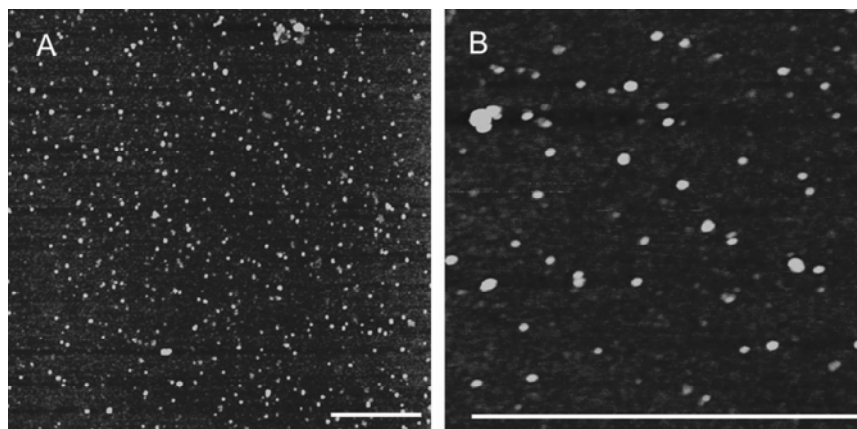
Figure A4.2 Micelles formed by $S_{12}C_4E_{40}$ in 2.5 M NaCl at pH 11 after 30 min-heating at 60 °C (B is a zoomed-in area of A). The size of the objects is ~30 nm. Scale bars correspond to 1 µm.
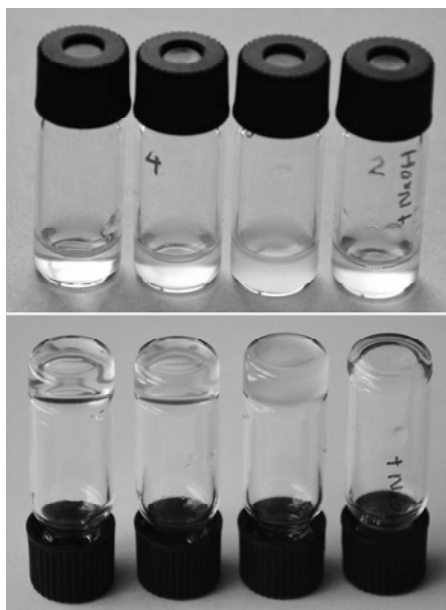
Figure A4.3 Gel of $S_{12}C_4E_{40}$ formed at pH 2 overnight at different conditions. (Top figure from left to right): transparent gel formed at 35 °C without NaCl, gel with NaCl formed at 20 °C, milky gel with NaCl formed at 35 °C, gel with NaCl formed at 35 °C is disrupted after 1M NaOH is added; (Bottom figure) upside down vials with the same order.

Chapter 5

Multi-responsive physical gels formed by a biosynthetic triblock protein polymer and a polyanion

Abstract

In this chapter, we report the design and production of a biosynthetic asymmetric triblock copolymer which consists of one collagen-like and one cationic block spaced by a hydrophilic random coiled block. The polymer associates into micelles when a polyanion is added due to the electrostatic interaction between the cationic block and the polyanion. The collagen-like block self-assembles into thermo-responsive triple helices upon cooling. When both end blocks are induced to self-assemble, a physical gel is formed via thermo-responsive association of the charge-driven micelles. The self-assembly of both end blocks, and the effects of salt and temperature thereon were characterized by light scattering and rheology.

5.1. Introduction

Polymer hydrogels are appealing materials with a wide range of applications. The gels consist of a three-dimensional network that spans the volume of a liquid medium. This internal network structure may result from physical bonds (physical gels) or chemical bonds (chemical gels). When the gels are formed by strong chemical bonds, they cannot be re-dissolved and are thermally irreversible, whereas gels formed by weak noncovalent interactions (physical entanglements, hydrophobic or charge-driven force, hydrogen-bond) are reversible [1, 2]. In physical gels, depending on the nature of the bonds, the junction formation can be reversibly controlled, thereby changing the shape and mechanical properties of the gels. Such responsive properties of physical gels widen the application of the materials [2-5].

A well-known class of network formers is that of telechelic polymers with an ABA triblock structure, where A is the sticky end block connected by the middle block B [6-16]. A symmetric telechelic polymer with collagen-like end-blocks and a random coil middle block was studied in our group recently. The functionality of the nodes in networks formed by these polymers is exactly three, because the end blocks, consisting of 9 (Pro-Gly-Pro) repeats, associate by exclusively forming triple helices [7, 17].

Another example of physical gels formed by symmetric ABA triblocks is one where both A blocks are charged. Upon adding an oppositely charged homopolymer, a multi-responsive gel is formed in which the micellar nodes are polyelectrolyte complexes [11, 18]. These gels respond not only to changes in temperature and concentration but also to ionic strength, cationic/anionic composition and pH.

The mechanical and rheological properties of physical networks are determined by the number of active bridges. In networks formed by symmetric triblock copolymers, however, the connectors can return to the same node, leading to the formation of a loop. Such a loop can be considered as a molecular mechanical imperfection, which has a critical impact on the properties of polymer networks built on an end-linked architecture [7 19, 20]. One strategy to reduce the number of loops is to use an asymmetric ABC type triblock copolymer, where the two associating end blocks are different [21 22, 23]. If each end block can only form nodes with itself, unimolecular loop formation is prevented. Further, loops that can form will have to be longer, which reduces their probability to occur by a factor. The end blocks

can be chosen so that they are responsive to different physicochemical triggers. In summary, the resulting physical gels are expected to be stronger and to possess tunable properties due to the selectively triggered assembly of the two end blocks.
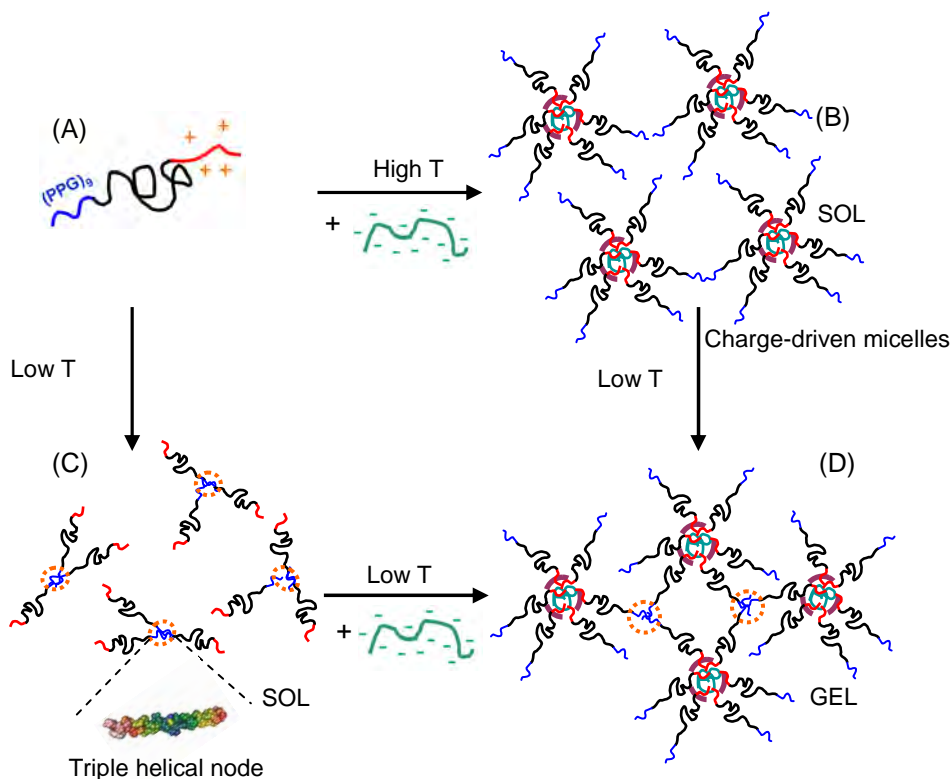
Figure 5.1 Scheme of the self-assembly of asymmetric triblock protein polymer TR4H. (A) The single triblock consisting of one collagen-like block T and one charged block H, connected by a hydrophilic random coil-like mid-block R4. (B) Charge-driven micellization of the triblock with an oppositely charged homopolymer at high temperature. (C) Formation of thermo-responsive triple helical nodes upon cooling. (D) Gel formation due to the formation of triple helical nodes among the charge-driven micelles.

In this study, we designed and biosynthesized a multi-responsive asymmetric protein polymer by combining an N-terminal triple-helical forming end block T (consisting of 9 (Pro -Gly-Pro) repeats) with a C-terminal charged end block H (consisting of 6 histidine amino acids), connected by a hydrophilic random-coiled R4 mid-block (Figure 5.1A). This polymer can form networks along essentially two pathways. Upon adding an oppositely charged homopolymer to a solution of TR4H at high temperature (where the T blocks do

not associate), micelles are formed with nodes consisting of polyelectrolyte complex. A gel can form upon subsequent cooling, which allows triple helical nodes to appear (A→B→D). Alternately, when the solution is first cooled to trigger trimer formation, upon adding the charged homopolymer, the network is formed (A→C→D). The T block self-assembles into triple helical nodes upon cooling (Figure 5.1C). When polyanion is added and the temperature is lowered simultaneously, a physical gel is formed (Figure 5.1D). We use a combination of light scattering and rheology to characterize the self-assembly of this asymmetric triblock and its micellization with a polyelectrolyte.

5.2. Materials and methods

Polymer biosynthesis

Vector pMTL23-TR4 has been described by us previously [17]. The TR4 gene contained in this plasmid encodes an N-terminal $(Pro-Gly-Pro)_9$ triple-helix-forming end block 'T' and an ~37 kDa hydrophilic random-coiled block 'R4'. To add a $(His)_6$ cationic tail to the C-terminus of the encoded protein, the vector was digested with *Van91I* (3' to the TR4 gene) and a double-stranded *DraIII/EcoRI* adapter 'H' encoding the 6 His residues was inserted. This adapter was prepared by annealing of oligonucleotides:
 5'-GTGGTCATCACCATCATCATCACGGTTAAG-3' and
5'-AATTCTTAACCGTGATGATGATGGTGATGACCACCGG-3'.
The resulting TR4H gene was cloned into *Pichia pastoris* expression vector pPIC9 (Invitrogen) via *XhoI/EcoRI*. Transformation of *P. pastoris* was as described previously [17].

The yeast was grown in a 2.5 L bioreactor as described previously [17]. Purification of the secreted protein was similar as before [17, 24, 25], with the exception that 40 % of ammonium sulfate saturation was used. The purified protein was dialyzed using 1kDa Spectra/Por 7 tubing (Spectrum Labs) and freeze-dried for storage until use. The protein is referred to as TR4H.

Product characterization

Electrophoresis (SDS-PAGE) was performed using the NuPAGE Novex system (Invitrogen) with 10% Bis-Tris gels, MES-SDS running buffer and SeeBlue Plus2

prestained molecular mass markers. Gels were stained with Coomassie SimplyBlue SafeStain.

The molecular mass distribution of the product was analysed by matrix-assisted laser desorption/ionization time-of-flight mass spectroscopy (MALDI-TOF MS). The analyses were performed using an Ultraflex mass spectrometer (Bruker), on a 600 µm AnchorChip target (Bruker) and with 2,5-dihydroxyacetophenone as matrix. Samples were prepared and measured as described previously [17, 25].

Sample preparation

Protein solutions were prepared by solubilising freeze-dried TR4H in 10 mM phosphate buffer pH 7.4 at different concentrations and then heated at 55 °C for 30 min to melt any triple helical structures. Samples studied at different temperatures were always equilibrated for a period of 4 h. To study the aggregation of TR4H with a polyanion, TR4H was first solubilized in 10 mM phosphate buffer pH 3 at 60 °C, and then sodium polystyrene sulfonate (PSS, Mw=63000 g/mol, Polymer Source) was added.

Static scattering

Light scattering at a detection angle of 90 ° (for triple helical micelization) was performed with an ALV light scattering apparatus, equipped with a 400 mW argon ion laser operating at a wavelength of 532.0 nm. The temperature was controlled by a Haake F3-K thermostat. In other experiments, the measurements were performed with a Zetasizer (Malvern) at an angle of 173 °. The light scattering intensity is expressed as the excess Rayleigh ratio R_θ divided by the polymer concentration as described previously [26].

The Rayleigh ratio (R_θ) is used as an absolute measure for the scattered light intensity:

$$R_\theta = \frac{I_{sample} - I_{solvent}}{I_{toluene}} \times R_{toluene} \times \frac{n^2_{solvent}}{n^2_{toluene}} \qquad \text{(Eq.5.1)}$$

where I_{sample}, $I_{solvent}$, and $I_{toluene}$ are the scattered intensity of the sample, the solvent, and the reference (toluene), respectively, and where $R_{toluene}$ is the known Rayleigh ratio of toluene at the angle used [26, 27], and where $n_{solvent}$ and $n_{toluene}$ are the refractive indices of the solvent and of toluene, respectively.

The Rayleigh ratio can be linked to the concentration and mass of the scattering objects:

$$\frac{K_R C}{R_\theta} = \frac{1}{M} \times \frac{1}{P(qR)} \times \frac{1}{S(q)}$$ (Eq.5.2)

where C is the weight concentration of the polymer, M is the molecular mass and R is the radius of the objects that contribute to the scattered light. $P(qR)$ and $S(q)$ are the form factor and the structure factor, respectively. K_R is an optical constant defined as:

$$K = \frac{4n_m^2 \pi^2}{\lambda^4 N_{Av}} \times \left(\frac{dn}{dc}\right)^2$$ (Eq.5.3)

where n_m is the reflective index of water, dn/dc is the refractive index increment of protein, estimated to be 0.00018 m^3/kg [28], λ is the wavelength of the light source (532.0 nm), and N_{Av} is Avogadro's number.

In our experiments, the scattering vector $q=(4\pi n/\lambda)\sin(\theta/2)$ is approximately 2.22 x10^{-11} m^{-1} so that qR is small for the micelles (which have a radius in the order of 10 nm). We therefore assume that $P(qR)=1$. Furthermore, at low concentrations, the structure factor can be approximated as

$$\frac{1}{S(q)} = 1 + 2B_2 \frac{C}{M}$$ (Eq.5.4)

Substitution into equation 2, gives:

$$\frac{K_R C}{R_\theta} = \frac{1}{M} + 2B_2 \frac{C}{M^2}$$ (Eq.5.5)

By plotting $K_R C/R_\theta$ versus C, we can obtain the molar mass of the micelles from the intercept and the second virial coefficient B_2 from the slope.

Dynamic light scattering

Dynamic light scattering at an angle of 90 ° was performed with an ALV light scattering apparatus, equipped with a 400 mW argon ion laser operating at a wavelength of 532.0 nm and an ALV-5000 multiple τ digital correlator and a Photo Multiplier Tube (PMT) detector.

We obtain the mean hydrodynamic radius (R_h) of the scattering objects from the measured autocorrelation function using the cumulants method [29], as given by the standard ALV software. Furthermore, the CONTIN method [29] is used to analyze the distribution of

particle radii. The data are analyzed with the program AfterALV (AfterALV 1.0d, Dullware), which provides $\Gamma_i W_i$ as default output for each size fraction i, with Γ_i, the autocorrelation decay rate corresponding to fraction i, and W_i, the intensity weighted contribution (this is called the 'equal-area representation' and we refer to $\Gamma_i W_i$ as the probability of fraction i) [29]. The absolute values of $\Gamma_i W_i$ vary strongly between different samples, which makes it difficult to compare results directly. We therefore normalized $\Gamma_i W_i$ with the highest value of $\Gamma_i W_i$ for each sample.

Titration

The titrations were carried out at 60 °C in 10 mM phosphate buffer pH 3 by adding solutions of 1.092 g/L PSS solution into 1 g/L TR4H solution. After every dosage, the laser light-scattering intensity and the correlation function were recorded.

The R_h and the scattered intensity are studied as a function of the mole fraction of positive charge ratio, *f-*, which is defined as follows:

$$f- = \frac{[-]}{[+]+[-]} \qquad\qquad (Eq.5.6)$$

where *[-]* and *[+]* are the molar charge concentration of charged monomers of each polymer chain. The effect of salt on the micelles is studied by titrating 5 M NaCl into the micellar solution.

Rheology

Two different protein concentrations, 100 g/L and 150 g/L, were tested. A given amount of protein was dissolved in 10 mM phosphate buffer pH 3 and then heated to 60 °C for 30 min to disrupt the triple helix formed. PSS (Mw=63 000 g/mol) was added to get the charge ratio *f-*=0.61. The solutions were heated to 60 °C for 10 min more to form the charge-driven micelles of TR4H/PSS. Subsequently, the solutions were cooled to 4 °C overnight to trigger the gel formation due to the formation of triple helical nodes among the charge-driven micelles. The measurements were carried out on a stress-controlled DHR3 rheometer (TA instruments) equipped with a Peltier temperature control system. To enable measurements on small sample quantities, it was necessary to use an 8 mm parallel plate as geometry. Consequently, and due to the relatively weakness of the gels, the rheological measurements were always performed at the edge of the sensitivity of the

rheometer. About 60 µl of the gels was deposited on the Peltier-controlled bottom plate, after which the top plate was lowered and the sample squeezed in between the plates. A thin layer of tetradecane was used to cover the sample and prevent evaporation. The linear dynamic oscillatory properties of the gels were measured at different temperatures over a frequency range between 0.1 and 100 rad/s, and at a low strain of 1 %. The stability of the gel was checked at each temperature by performing consecutive oscillatory measurements.

5.3.   Results and Discussion

Polymer biosynthesis and product characterization

The triblock polymer TR4H was produced by recombinant *P. pastoris* in methanol fed-batch fermentations. The recovery of purified dry product was above 500 mg per liter of cell-free broth. The purified protein was analyzed by SDS-PAGE and MALDI-TOF. The SDS-PAGE (Appendix, Figure A5.1) shows that the protein is intact and pure. The protein migrates at an apparent molecular weight much higher than its true molecular weight. This aberrant mobility is typical for this class of protein polymers and is due to the amino acid composition of the middle block, which is composed of atypical and relatively polar amino acids, resulting in low binding to SDS [17, 24, 25]. The molecular mass of TR4H was verified by MALDI-TOF, which shows a monodisperse product with a mass very close to the theoretical value of 40159 Da (Appendix, Figure A5.2), and thus indicated the product to be intact and pure.

The formation of trimeric clusters by association of the T blocks

We first study the thermo-responsive formation of triple helices in the absence of polyanion (Figure 5.2A). The formation of triple helical clusters due to the T blocks was investigated by light scattering.

In order to confirm the thermo-responsive properties of the triple helix formation, we measured the scattered intensity of TR4H solutions at different temperatures. As shown in Figure 5.2B, the scattered intensity gradually decreases upon increasing the temperature. This can be ascribed to melting of the triple helices, so that trimers dissociate into monomers. The helices melt around a temperature of 30 °C at the concentration used, in agreement with previously found values [7].

To obtain the apparent mass of the clusters formed at temperatures below the melting point, we obtain the Rayleigh ratio R_θ for different concentrations and plot $K_R C/R_\theta$ as a function of protein concentration (Figure 5.2B). According to equation 5, this plot should give a straight line, where the intercept can be used to obtain the average mass of the clusters. When the temperature is 40 °C, where no triple helices are expected to form, the apparent mass of the scattering objects is 38.5 kg/mol, which is close to the theoretical value of the free polymer (40 kg/mol). This indicates that the telechelics exist as monomers at this temperature (Figure 5.2C). At low temperature, the scattering intensity increases, which indicates cluster formation. At 20 °C the obtained apparent mass is 84.7 kg/mol. This means that the average aggregation number is n=84.7/38.5=2.2. This is below the expected value if all molecules would be present in trimers, n=3. Our explanation is that the experimental temperature at which the triple helical micelles are formed is too close to the melting temperature to achieve complete triple helix formation. As shown in Figure 5.2B, the low temperature plateau has not been reached (in particularly for 5 g/L sample), meaning that trimerization is incomplete.
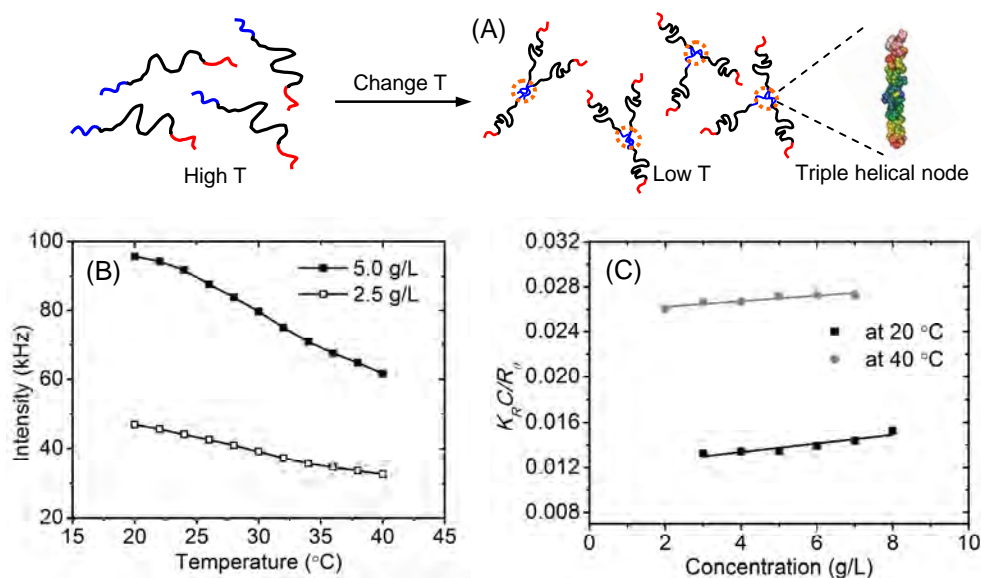
Figure 5.2 Formation of thermo-responsive triple helical nodes: (A) General scheme of the triple helix formation; (B) Change in scattering intensity as a function of temperature due to the melting of triple helical nodes at two different protein concentrations; (C) $K_R C/R_\theta$ at angle 90 ° as a function of protein concentration.

Unfortunately, in our experimental set up, the measurements could not be carried out below 20 °C. Nevertheless, we conclude that triple helix formation leads to the reversible formation of small clusters at low temperature.

Formation of charge-driven micelles upon adding a polyanion

Next, we study cluster formation of TRH with a polyanion at temperatures where the T blocks do not self-assemble.

The H block consists of 6 histidine residues, which are positively charged when the pH of the solution is below the pI of histidine (6.5). The charge level is dependent on the pH. The telechelic protein was solubilized in 10 mM phosphate buffer pH 3 so that the H block was completely charged. Adding oppositely charged homopolymer (PSS) at high temperature is, therefore, expected to lead to the formation of charge-driven micelles, due to the electrostatic interaction between the positively charged H blocks and the negatively charged PSS (Figure 5.3A).

Figure 5.3B displays the scattered intensity as a function of the mixing ratio f- (defined in equation 6). At f-=0, the intensity is very low, but it increases immediately after the first addition of PSS, indicating the formation of micelles. The intensity increases gradually upon adding the polyanion and shows a maximum at f-=0.61 with a corresponding hydrodynamic radius of 25 nm. The maximum corresponds to the preferred micellar composition where the charge stoichiometry, which theoretically is 0.5, is achieved. In this system, the polyanion has to be overdosed slightly to achieve the preferred composition. Probably, non-electrostatic forces play minimal roles [30]. Surprisingly, there is another high peak occurring at f-=0.85, which disappears again after more addition of the polyanion. The changes in particle size and polydispersity, as analyzed by the CONTIN method, are shown in Figure 5.3C. The micelles at f-=0.61 have a size of 25 nm and a narrow size distribution, indicating that there is only one sort of particles in solution. The large objects of around 500 nm at f-=0.85 indicate aggregation. The solution is also slightly turbid at this composition (Appendix, Figure A5.3). These large clusters could be due the depletion effect of PSS molecules between different dissociating micelles, leading to larger, multimicellar aggregates [27, 31]. In the remainder of this paper, we will only consider solutions at the preferred micellar composition of f-=0.61, where stable micelles are formed.
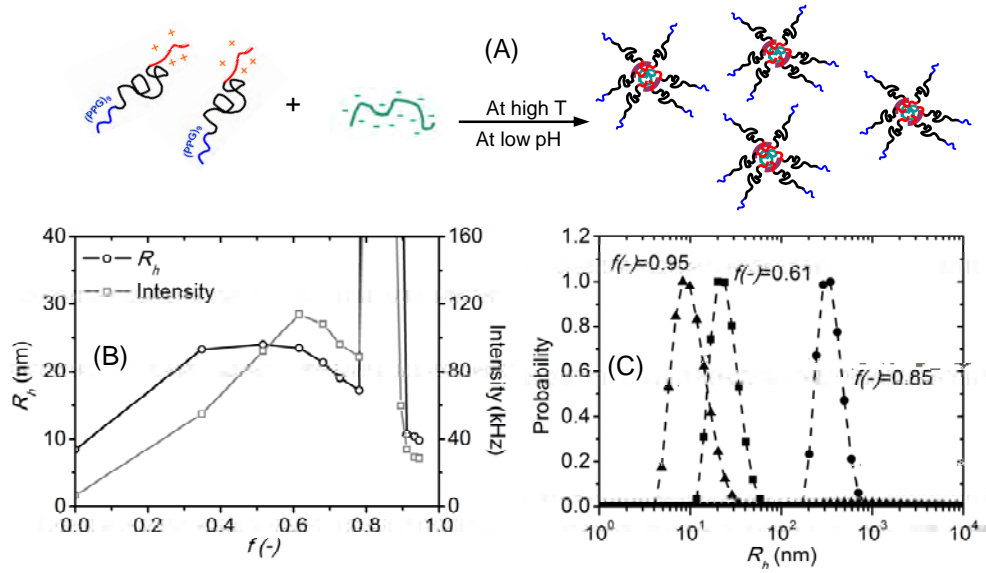
Figure 5.3 Charge-driven complex formation of TR4H with PSS at high temperature: (A) The general scheme of charge-driven TR4H/PSS micelles; (B) Light scattering titration of charged TR4H with PSS solutions showing the scattered intensity and the hydrodynamic radius as a function of the charge ratio f-; (C) CONTIN analysis of TR4H/PSS micelles at different f-.

Determining the micellar aggregation number
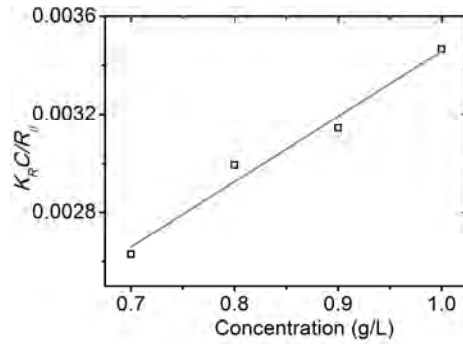
Figure 5.4 $K_R C/R_\theta$ at an angle of 173 ° as a function of protein concentration for TR4H/PSS micelle solutions.

To obtain an estimate for the aggregation number of TR4H/PSS micelles at f-=0.61 and at high temperature (60 °C), we plot $K_R C/R_\theta$ as a function of protein concentration (Figure 4). The apparent mass of TR4H/PSS micelles ($M^{micelle}$) obtained from the intercept of this line (equation 5) is 1258.2 kg/mol. Since a PSS molecule has many more charged units

(307 units) than a TR4H molecule (6 units), and the total charge of the micelle $f-=0.61$, we have:

$$f- = 0.61 = \frac{N_{PSS} \times 307}{N_{PSS} \times 307 + N_{TR4H} \times 6}$$

where N_{PSS} and N_{TR4H} are the number of PSS molecules and protein molecules in a micelle, respectively. The apparent mass of TR4H (M_{TR4H}) is measured in a previous section (38.5 kg/mol) and the mass of PSS (M_{PSS}) is 63 kg/mol, so we obtain:

$$N_{PSS} \times 63 + N_{TR4H} \times 38.5 = 1258.2$$

From the calculation, we get $N_{PSS} = 0.95\sim1$ and $N_{TR4H} = 31$. Therefore, one charge-driven micelle is composed of 1 PSS molecule and 31 TR4H molecules.

Effects of ionic strength on the charge-driven TR4H/PSS micelles
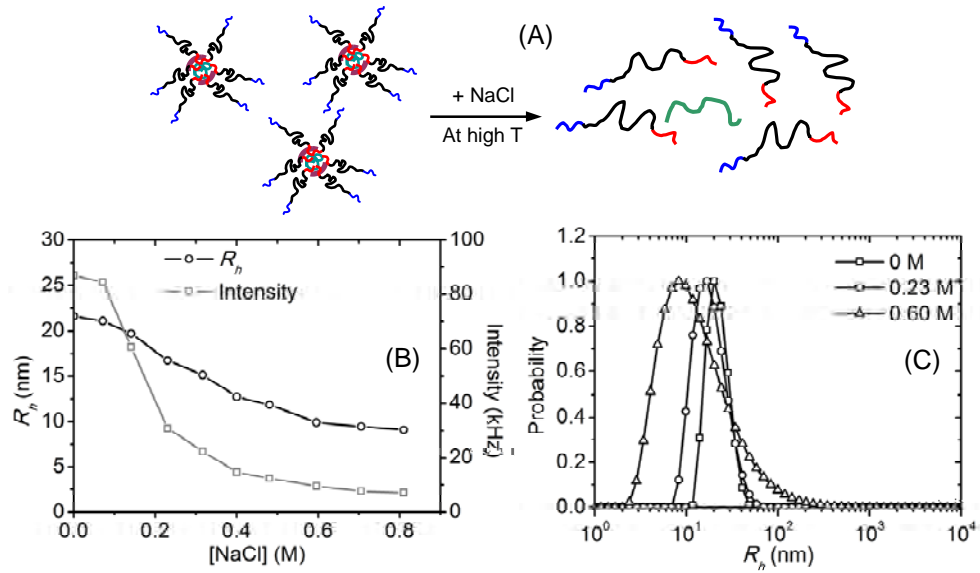
Figure 5.5 Effect of ionic strength on charge-driven TR4H/PSS micelles: (A) General scheme of TR4H/PSS micelle dissociation due to NaCl; (B) Light scattering titration of charge driven TR4H/PSS micelles by NaCl at 60 °C; (C) CONTIN analysis of charge-driven TR4H/PSS micelles at different ionic strength.

It is well-known that charge-driven coacervate core micelles are sensitive to ionic strength and dissociate above a critical salt concentration (Figure 5.5A) [32, 33]. To examine the salt dependence of our micelles, TR4H/PSS micellar solutions at $f-=0.61$ at a protein

concentration of 1 g/L were titrated with 5M NaCl solution. The experiments were carried out at high temperature (60 °C) so that the T blocks did not form triple helical nodes.

Indeed, we find that both the scattered intensity and the hydrodynamic radius decrease upon an increase of the salt concentration (Figure 5.5B). The dissociation begins around 0.1 M NaCl and completes above 0.6 M NaCl. CONTIN analysis (Figure 5.5C) indicates that the micelle solutions have a narrow size distribution at low salt concentration. Upon addition of NaCl, the micelle size becomes smaller and more polydisperse. A similar salt-induced dissociation of electrostatic complex micelles was observed previously [11, 27]. The increase in salt concentration diminishes the electrostatic interaction between oppositely charged components, resulting in both a decrease in the aggregation number and a decrease in the number of micelles caused by an increase of the critical micelle concentration [27].

Effect of temperature on charge-driven TR4H/PSS micelles: micelle-to-network transition

Above, we have considered conditions where only one of the two end blocks of the polymer can self-assemble. Now, we will focus on conditions where both blocks associate. We do this by changing the temperature in micellar TR4H/PSS solutions, so that the T blocks can also self-assemble. At low concentrations, this is expected to lead to multi-micellar clusters, while at higher concentrations gels may be formed (Figure 5.6A).

The charge-driven micelle solutions at a protein concentration of 1 g/L formed at high temperature (60 °C) were step-wise cooled to 40 °C and 20 °C (Figure 5.6B). The scattering intensity and hydrodynamic radius increase slightly at 40 °C, followed by a more significant, slow increase upon cooling to 20 °C. This can be ascribed to the association of T blocks into triple helical knots, leading to the connection of the charge-driven micelles into bigger aggregates. To confirm the reversibility of this aggregation, the solutions were kept at 20 °C for an hour, during which the scattering intensity increased from 400 to 470 kHz. Note that at 20 °C, the scattering intensity and hydrodynamic radius are still increasing after one hour, which is probably because the formation of triple helices is rather slow [7]; then the temperature was increased again in steps to 40 and 60 °C (Figure 5.6C). Upon heating again to 40 °C (Figure 5.6C), there is a fast decrease in both scattering intensity and hydrodynamic radius, indicating dissociation of the triple helical connections among the charge-driven micelles. At 60 °C, both scattering intensity and hydrodynamic

radius decrease to values similar to those at the starting condition at 60 °C shown in Figure 5.6B, indicating the complete melting of triple helical connections between the charge-driven micelles. We therefore conclude that the temperature-induced association of micelles by triple helical connections is fully reversible.
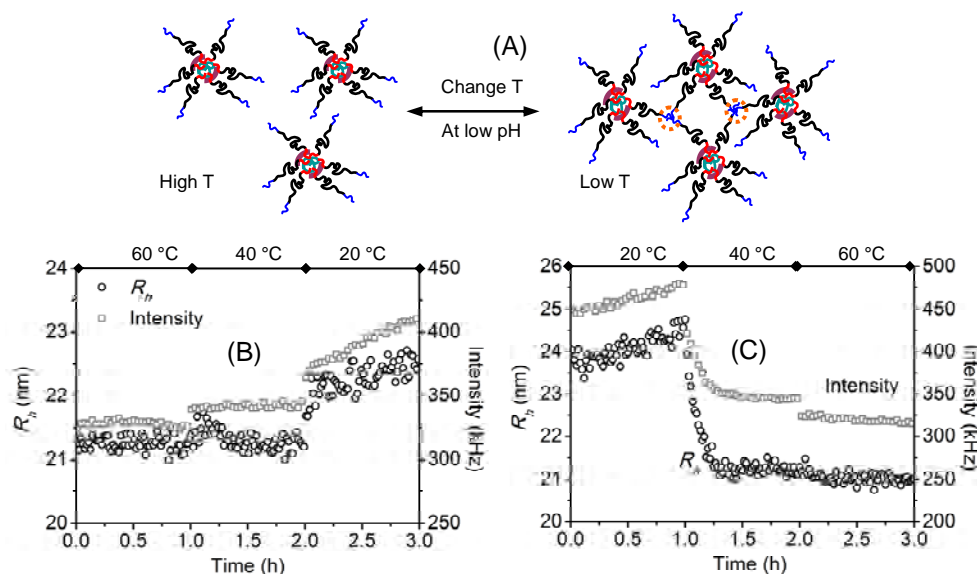
Figure 5.6 Thermo-responsive properties of the charge-driven TR4H/PSS complex: (A) General scheme of association of charge-driven TR4H/PSS micelles upon cooling; (B) Increase in both scattering intensity and hydrodynamic radius upon cooling due to the formation of triple helical nodes among the micelles; (C) Decrease in both scattering intensity and hydrodynamic radius upon heating due to the melting of the triple helical nodes.

Formation of a physical gel due to thermo-triggered association of charge-driven TR4H/PSS micelles

At the low protein concentration above, we have confirmed the formation of triple helical connections between the charge-driven TR4H/PSS micelles. We also investigated the formation of these connections at higher protein concentrations (from 100 g/L) by rheology. Indeed, we find that a solution of charge-driven TR4H/PSS micelles forms a visco-elastic physical gel upon cooling. As shown in Figure 5.7A, the gels are of a dynamic nature with a crossover frequency (i.e. frequency where $G'=G''$) around 20 rad/s or, equivalently, a relaxation time of about 0.05 s. This time is much smaller than that of the triple helical network [7], indicating that the triple helices are not responsible for the

relaxation. The breaking and reforming of the micelles is most likely responsible for the relaxation. Similar relaxation times were for example observed for charge-driven networks of symmetric triblock copolymers [18]. Figure 5.7A shows that the storage and loss moduli of the hydrogels formed at low temperature (10 °C) are relatively strongly dependent on concentration. This dependence is similar to the physical gels formed by the symmetric telechelic which consists of two identical T blocks [7].
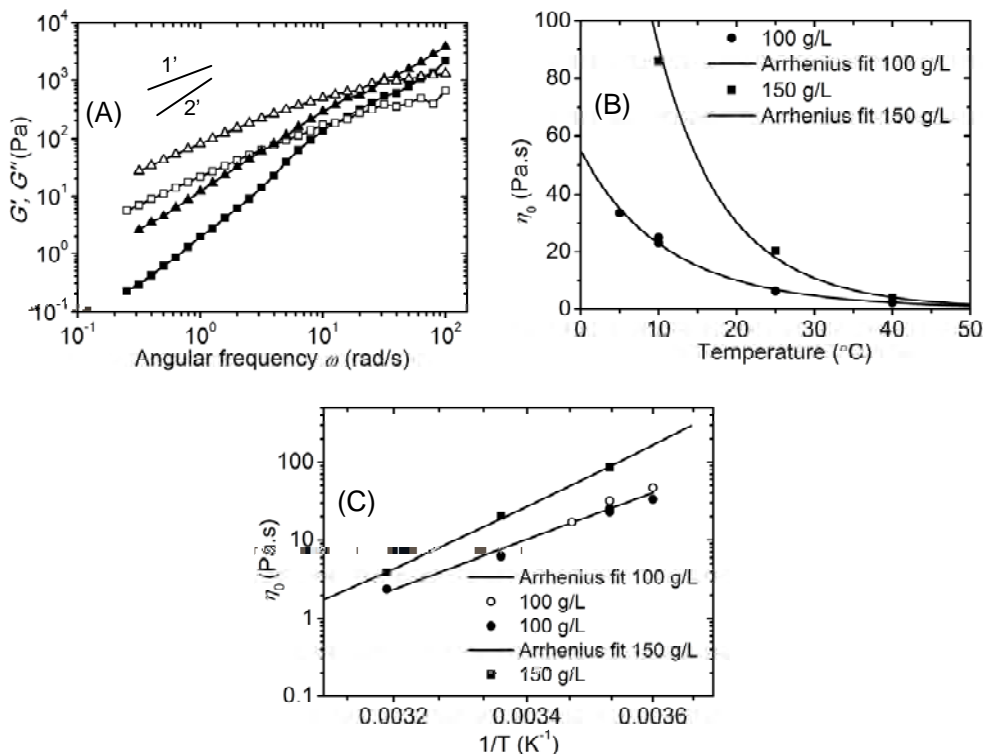
Figure 5.7 Network formation of TR4H/PSS micelles upon cooling. (A) Loss G'' (open symbols) and storage G' (closed symbols) moduli as function of angular frequency for the TR4H/PSS micelle gels at a protein concentration of 100 g/L w/v (squares) and 150 g/L (up-pointing tri-angles) at 10 °C, (B) Zero-shear viscosity η_0 as function of temperature T for the TR4H/PSS micelle gels for both protein concentrations (100 g/L w/v in black and 150 g/L in red), (C) Arrhenius plot of zero-shear viscosity for the same concentrations as in Fig. B. The lines in B and C are fits of the data to the Arrhenius equation. The closed symbols in figure C correspond to gelation pathway A→B→D of Figure 5.1, while the open symbols correspond to gelation pathway A→C→D.

Although the terminal low-frequency slope of 2 for the elastic modulus is not entirely reached in the measurements (which is most likely an experimental artifact as we are close

to the limit of the sensitivity of the rheometer), we did reach the terminal low-frequency slope of 1 for the loss modulus [34], enabling us to calculate the zero-shear viscosity:

$$\eta_0 = \lim_{\omega \to 0} \frac{G''}{\omega} \qquad \text{(Eq.5.7)}$$

The temperature-dependence of the zero-shear viscosity is shown in Figure 5.7B for different protein concentrations. As expected, the viscosity shows a strong dependence on temperature. This dependence can be fitted with an Arrhenius equation (Figure 5.7C)

$$\eta_0 = A.\exp(\frac{-E_a}{RT}) \qquad \text{(Eq.5.8)}$$

with R being the ideal gas constant and T being the absolute temperature in K.

The fitting yields A=5.4 10^{-10} Pa.s and E_a= -56.3 kJ/mol for the 100 g/L and A=9.20 10^{-13} Pa.s and E_a= -75.9 kJ/mol for the 150 g/L sample. This indicates that the dissociation of the charge-driven complex is an activated process, just like the physical gels formed by symmetric telechelics with two identical T blocks [7]. Our observation that the activation energy depends on concentration is probably because the structure of the network also affects the relaxation rate, as discussed previously [11]. We also tested whether the gelation pathway has an effect on the gel properties. The open symbols in Figure 5.7C correspond to an experiment in which the temperature was decreased before adding the polyanion (pathway A→C→D in Figure 5.1). It can be seen that the viscosities are more or less along the two pathways, suggesting that the system reaches an equilibrium state. However, more experiments on the kinetics of the gelation process along different pathways are needed to confirm this.

Multi-responsive gels and phase stability

Because the gels that we study require the presence of two kinds of cross-links, our gels should be responsive to both temperature and salt. This is shown visually in Figure 5.8A for a gel of 10 g/L. Both heating to 60 °C (Figure 5.8Aa) and adding salt to a concentration of 0.4 M (Figure 5.8Ac) turn the gel into a liquid.
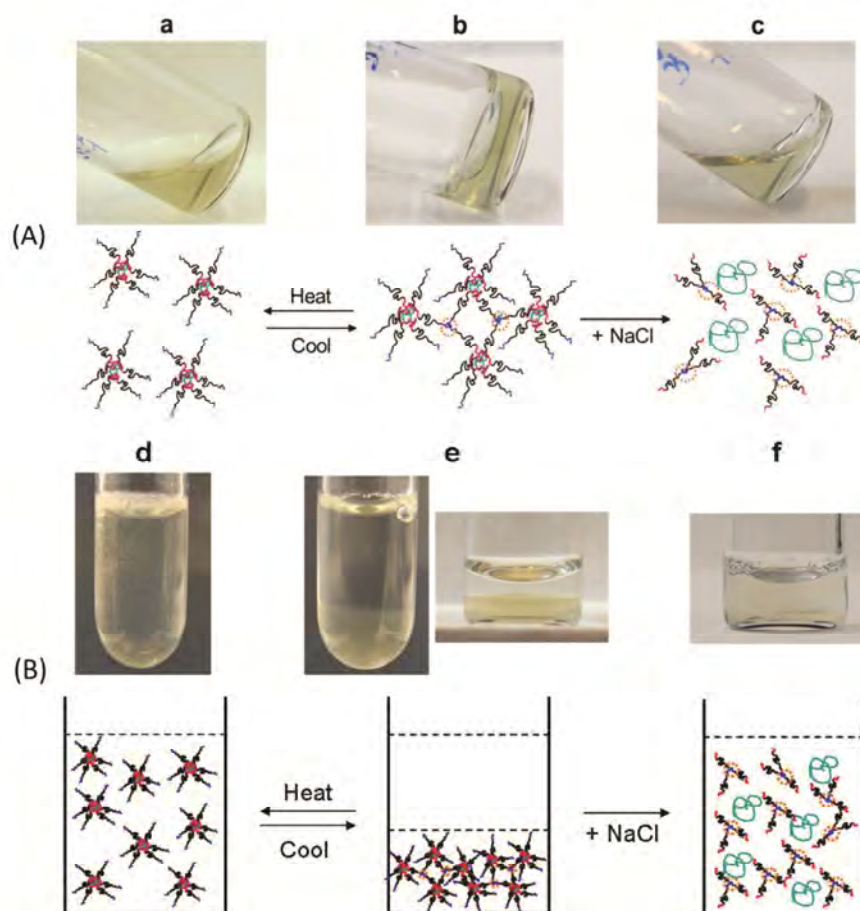
Figure 5.8 (A) Responsive behaviors of 100 g/L gel to physical triggers: (a) aqueous solution of charge-driven TR4H/PSS micelles at high temperature (60 °C) and low salt, (b) gelation of charge-driven TR4H/PSS micelles upon cooling to 4 °C in 10 h, (c) disrupted gel (at 4 °C) due to addition of NaCl to a final concentration 0.4 M. (B) Phase separation when the protein concentration is below the critical concentration and the effects of heating or increased ionic strength thereon: (d) disrupted phase separation due to melting the triple helical nodes among the micelles, (e) associative charge-driven TR4H/PSS micelles at 4 °C results in a viscous condensed phase dropped to the vial bottom, (f) disrupted phase separation (at 4 °C) due to an addition of NaCl to 0.2 M.

When the concentration is lower than the gelation point, triggering the self-assembly of both end blocks does not lead to gelation, but in some cases to a liquid-liquid phase separation, as shown in Figure 5.8B. We find this phase separation in a concentration range of 100 g/L to 80 g/L (below 10 g/L was not tested). The phase separation occurs due to the high attraction between the micelles upon cooling, induced by the triple-helix formation.

The representative phase separated solutions for different overall concentrations are shown in Appendix, Figure A5.4. The bottom phase, which contains most of the polymer is highly viscous and presumably consists of a visco-elastic gel network (Figure 5.8Be). Pham et al [35] reported a similar phase behavior of associative polymers, poly(ethylene oxide) chains fully end-capped with C16 and C18 hydrophobes. When the bridging between micelles is favorable, the micelles tend to form multiplets (or aggregates of multiple micelles), which eventually can lead to macroscopic phase separation when the concentration is below the percolation threshold concentration. The transition from a phase separated system to a single gel-phase occurs around 90 g/L in our case. This probably means that the density of the condensed viscous phase is 90 g/L.

As shown in Figure 5.8B, the phase separation disappears completely when either of the two kinds of nodes is melted. Heating a phase-separated system to 60 °C leads to melting of the triple helices, so that the system goes back to a single-phase system of micellar aggregates (Figure 5.8Bd). Likewise, adding 0.2 M salt to a phase-separated system leads to dissociation of the polyelectrolyte complexes that form the micellar cores, so that the system goes to a solution of trimeric clusters (Figure 5.8Bf).

5.4. Conclusion

We reported an asymmetric triblock protein polymer ABC with different functional endblocks, which was genetically designed and biosynthesized. The triblock represents a new design of biosynthetic multi-responsive network former. The desired responsive properties of each end block impart the gel features: one block forms triple helical nodes below the melting temperature and the other, charged block forms micelles with oppositely charged polyelectrolytes. Our approach shows that by selectively combining different blocks together into an asymmetric triblock polymer, novel types of responsive hydrogels are achievable.

References

1. N. M. Sangeetha and U. Maitra, *Chem. Soc. Rev.*, 2005, **34**, 821-836.

2. K. Ahn, R. M. Kasi, S. C. Kim, N. Sharma and Y. Zhou, *Soft Matter*, 2008, **4**, 1151-1157.

3. L. M. Low, S. Seetharaman, K. Q. He and M. J. Madou, *Sensors and Actuators B*, 2000, **67**, 149-160.

4. B. Jeong and A. Gutowska, *TRENDS in Biotechnology*, 2002, **20**, 305-311.

5. T. Vermonden, R. Censi and W. E. Hennink, *Chem. Rev.*, 2012 **112**, 2853-2888.

6. W. Shen, J. A. Kornfield and D. A. Tirrell, *Macromolecules*, 2007, **40**, 689-692.

7. P. J. Skrzeszewska, F. A. de Wolf, M. W. T. Werten, A. P. H. A. Moers, M. A. Cohen Stuart and J. van der Gucht, *Soft Matter,* 2009, **5**, 2057-2062.

8. R. A. Hule, R. P. Nagarkar, B. Hammouda, J. P. Schneider and D. J. Pochan, *Macromolecules,* 2009, 42, 7137-7145.

9. S. Ganesh, S. Prakash and R. Jayakumar, *Biopolymers*, 2003, **70**, 346-354

10. W. Wu, J. Shen, P. Banerjee and S. Zhou, *Biomaterials,* 2010, **31**, 8371-8381.

11. M. Lemmers, J. Sprakel, I. K. Voets, J. van der Gucht and M. A. Cohen Stuart, *Angew. Chem. Int. Ed.*, 2010, **49**, 708-711.

12. G. R. Mahdavinia, A. Pourjavadi, H. Hosseinzadeh and M. J. Zohuriaan, *Eur. Polym. J.*, 2004, **40**, 1399-1407.

13. B. Guo, A. Elgsaeter, B. E. Christensen and B. T. Stokke, *Polymer Gels and Networks,* 1998, **6**, 471-492.

14. Y. Ma, Y. Tang, N. C. Billingham and S. P. Armes, *Biomacromolecules*, 2003, **4**, 864-868.

15. W. D. Lim and T. G. Park, *J. Appl. Polym. Sci.*, 2000, **75**, 1615-1623.

16. H. S. Choi, T. Ooya, S. Sasaki and N. Yui, *Macromolecules*, 2003, **36**, 9313-9318.

17. M. W. T. Werten, H. Teles, A. P. H. A. Moers, E. J. H. Wolbert, J. Sprakel, G. Eggink and F. A. de Wolf, *Biomacromolecules,* 2009, **10**, 1106-1113.

18. M. Lemmers, E. Spruijt, L. Beun, R. Fokkink, F. Leermakers, G. Portale, M. A. Cohen Stuart and J. van der Gucht *Soft Matter*, 2011, **8**, 104-117.

19. P. J. Skrzeszewska, F. A. de Wolf, M. A. Cohen Stuart and J. van der Gucht, *Soft Matter*, 2010, **6**, 416-422.

20. H. Zhou, J. Woo, A. M. Cok, M. Wang, B. D. Olsen and J. A. Johnson, *PNAS* 2012, **109**, 19119-19124.

21. C. Zhou, M. A. Hillmyer and T. P. Lodge, *J. Am. Chem. Soc.*, 2012, **134**, 10365-10368.

22. I. Koonar, C. Zhou, M. A. Hillmyer, T. P. Lodge and R. A. Siegel, *Langmuir,* 2012, **28**, 17785-17794.

23. C. Rufier, A. Collet, M. Viguier, J. Oberdisse and S. Mora, *Macromolecules,* 2008, **41**, 5854-5862.

24. A. A. Martens, G. Portale, M. W. T. Werten, R. J. de Vries, G. Eggink, M. A. Cohen Stuart and F. A. de Wolf, *Macromolecules,* 2009, **42**, 1002-1009.

25. M. D. Golinska, T. T. H. Pham, M. W. T. Werten, F. A. de Wolf, M. A. Cohen Stuart and J. van der Gucht, *Biomacromolecules,* 2013, **14**, 48-55.

26. J. Wang, M. A. Cohen Stuart, A. T. M. Marcelis, M. Colomb-Delsuc, S. Otto and J. van der Gucht, *Macromolecules*, 2012, **45**, 7179-7185.

27. J. Wang, A. de Keizer, R. Fokkink, Y. Yan, M. A. Cohen Stuart and J. van der Gucht, *J. Phys. Chem. B,* 2010, **114**, 8313-8319.

28. H. Zhao, P. H. Brown and P. Schuck, *Biophys. J.*, 2011, **100**, 2309-2317.

29. P. Stepanek, *Brown, W., Ed.; Clarendon Press: Oxford, U.K.*, 1993, **Chapter 4**, 177.

30. C. L. Cooper, P. L. Dubin, A. B. Kayitmazer and S. Turksen, *Curr. Opin. Colloid Interface Sci.,* 2005, **10**, 52-78.

31. Y. Yan, N. A. M. Besseling, A. de Keizer, M. Drechsler, R. Fokkink and M. A. Cohen Stuart, *J. Phys. Chem. B,* 2007, **111**, 11662-11669.

32. A. V. Kabanov, T. K. Bronich, V. A. Kabanov, K. Yu and A. Eisenberg, *Macromolecules,* 1996, **29**, 6797-6802.

33. Xiaofei Yuan, Atsushi Harada, Yuichi Yamasaki and and Kazunori Kataoka, *Langmuir,* 2005, **21**, 2668-2674.

34. C. W. Macosko, *Wiley-VCH, NY*, 1994.

35. Q. T. Pham and W. B. Russel, *Macromolecules,* 1999, **32**, 2996-3005.

Appendix
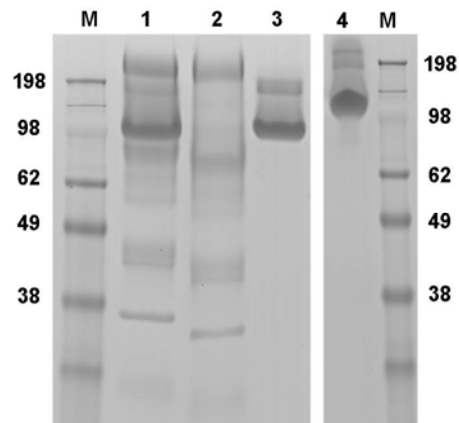
Figure A5.1 SDS-PAGE of TR4H during purification process (M) Protein marker, (lane 1) cell-free fermentation broth, (lane 2) Supernatant of 40 % ammonium sulfate saturation 1x, (lane 3) Protein precipitation with 40 % ammonium sulfate saturation 1x , (lane 4) Purified TR4H by precipitation with 40 % ammonium sulfate saturation twice.
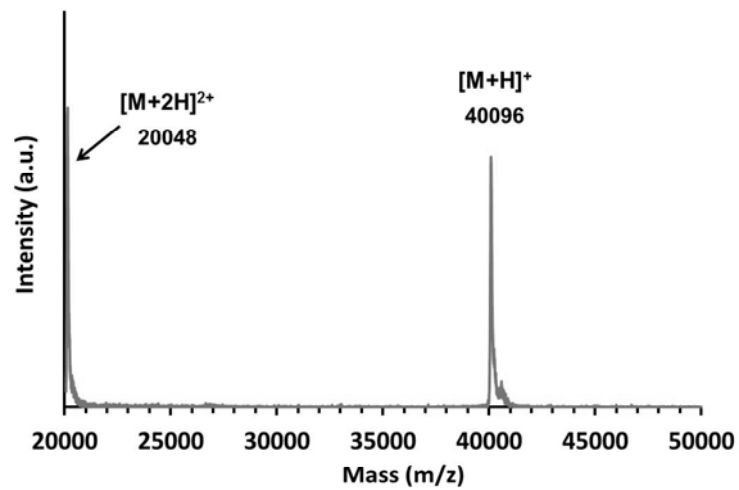
Figure A5.2 MALDI-TOF of purified TR4H. Singly and doubly charged molecular ions are indicated.
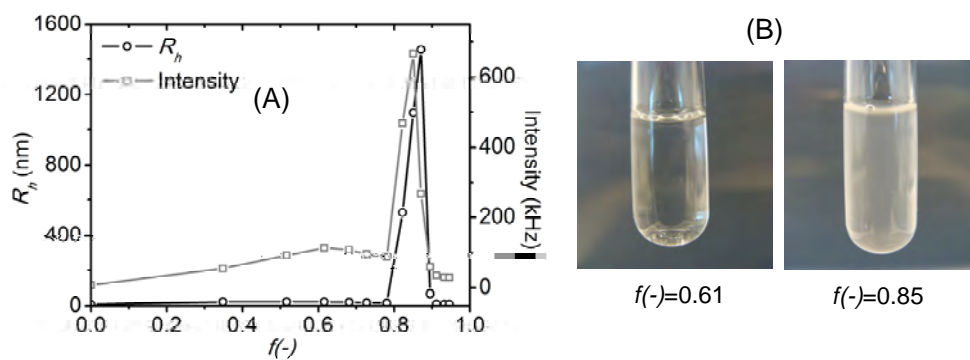
FigureA5.3 (A) Light scattering titration of charged TR4H with PSS in 10 mM phosphate buffer at pH 3 , (B) Clear sample at the stoichiometric peak (f-=0.61) and visible large aggregates at the second peak at f-=0.85.
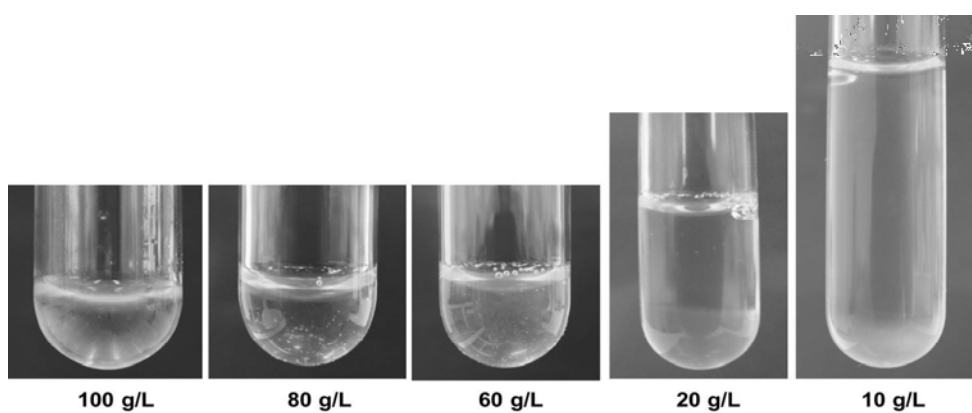
Figure A5.4 Phase separation of temperature-induced charge-driven TR4H/PSS micelle solutions at different protein concentrations.

Chapter 6

Enhanced properties of xanthan hydrogels through electrostatic crosslinking with a biosynthetic triblock protein polymer

Abstract

In this chapter, we study the electrostatic complexation of an asymmetric triblock protein polymer with a semi-flexible polyelectrolyte (xanthan). The protein polymer has one 'reactive' poly-lysine end-block which can bind to xanthan by electrostatic interactions, and another 'reactive' end-block which can self-assemble into thermo-sensitive triple helices; the end-blocks are connected by a neutral, hydrophilic, mostly inert spacer that forms a random coil in water. The complexation of the protein with xanthan depends on both temperature and pH. The triblock protein modifies the properties of the xanthan hydrogels in three ways: (1) a significant increase in storage modulus, (2) thermo-sensitivity and (3) a two-step strain softening, where the first step is probably due to forced unbinding of the proteins from the xanthan backbones.

6.1.　Introduction

Polysaccharide gums, which are naturally occurring components found in plants and some microorganisms, are cheap and very abundant. They have diverse applications as thickeners, emulsifiers, lubricants, sweeteners, and drug release modifiers. Indeed, they have very attractive properties such as biodegradability, non-toxicity and the ability to sequester a large amount of water. However, most gums require relatively high concentration or modification for functional applications [1].

Among the polysaccharide gums, xanthan gum is produced at industrial scale, and has been well studied [2]. Xanthan is widely used as a food additive due to its physical (high viscosity, pseudo-plasticity) and chemical (water soluble, pH stability) properties. This polysaccharide consists of a (1-4)-β-D-glucose backbone with a charged trisaccharide side chain at every second glucose residue [3]. The glucuronic acid and pyruvic acid groups on the side chains give xanthan gum its negative charge. Its pseudo-plasticity is due to its high molecular weight and its ability to form complex aggregates through hydrogen bonds and polymer entanglement [2]. The chain-chain association in xanthan gels is modulated by salt content and temperature [4]. The shear thinning pseudo-plasticity of xanthan gum results from disaggregation of the network and the alignment of individual molecules in the direction of shear [2].

Polyelectrolyte complexes of xanthan with other polyelectrolytes in aqueous milieu are known to exhibit many interesting physico-chemical properties. For example, the ionic interactions between the carboxyl group of xanthan and the amino group of chitosan lead to pH-sensitive swelling behavior, which enables the controlled release of entrapped agents [5, 6]. In many hydrogel applications, the crosslinks density is an important factor determining the stability and pH-swelling characteristics, as well as the mechanical properties [7]. Xanthan gum hydrogels cross-linked by β-lactoglobulin show a high dependence of gelation kinetics on the mixing ratio and the junction zones involves these two molecules [8, 9]. Polyelectrolyte-protein conjugates offer new opportunities to obtain control over the architecture and properties of xanthan networks [10]. By cross-linking xanthan polymers in a controlled way, we might obtain networks with properties that resemble those of the cytoskeleton polymer network, in which the molecular structure of the crosslinker determines the macroscopic properties [11].

In this study, we explore the making of xanthan-based hydrogels with new properties. In particular, we investigate the electrostatic complexation of xanthan with a biosynthetic triblock protein polymer in both dilute and concentrated solutions. The protein consists of two different short end-blocks (a thermo-responsive collagen-like block and a poly-lysine block) spaced by a much longer inert random-coiled block. When charged, the poly-lysine block interacts with xanthan while the collagen-like block can self-assemble at low temperature, thus establishing physical crosslinks between xanthan molecules in hydrogels (see Figure 6.1). Light scattering is used to study the complexation of xanthan and the protein at high dilution, where xanthan likely behaves like a polyelectrolyte. The effects of crosslinks induced by the protein at high concentration of xanthan are studied by rheology.
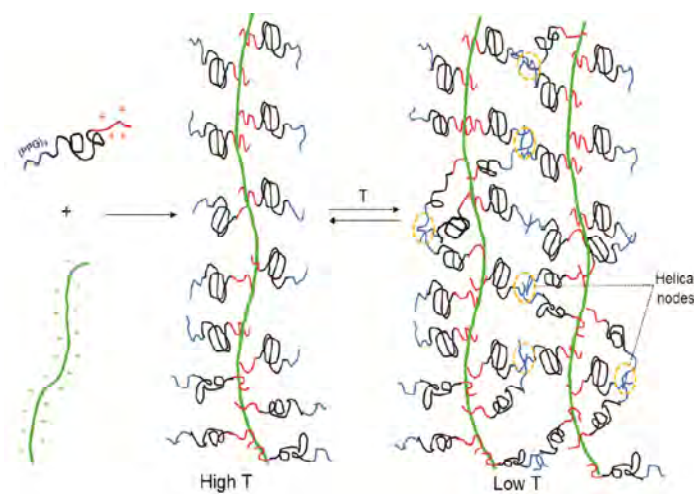
Figure 6.1 Scheme of electrostatic complexation of xanthan and the asymmetric triblock protein at high and low temperature (T). The triblock protein polymer has one end-block binding with xanthan molecules by electrostatic interaction and the other end-block self-assembling into thermo-sensitive triple helices.

6.2.   Materials and Methods

Protein polymer synthesis

The protein is designed by genetic engineering and produced by fermentation in the same way as the triblock protein reported in chapter 5. Briefly, a $(Lys)_6$ cationic tail (K) was added to the C-terminus of a TR4 sequence featuring an N-terminal $(Pro-Gly-Pro)_9$

triple-helix-forming end block 'T' and an ~37 kDa hydrophilic random-coiled block 'R4'. The resulting TR4K gene was cloned into *Pichia pastoris* expression vector pPIC9 (Invitrogen) via *Xho*I/*Eco*RI. Transformation of the gene into *P. pastoris* and the fermentation of the recombinant yeast grown in a 2.5 L bioreactor were described previously [12]. Purification of the secreted protein was similar as before [7, 12, 13], with the exception that 45 % of ammonium sulfate saturation was used. The purified protein was dialyzed using 1kDa Spectra/Por 7 tubing (Spectrum Labs) and freeze-dried for storage until use. The protein is referred to as TR4K.

Light scattering

Lyophilized protein was solubilized in phosphate buffer 10 mM and incubated at 50 °C in order to disrupt the preformed helices. To study the thermo-responsive behavior of the helices, the soluble protein solutions were cooled at 5 °C for at least 10 h, and then subjected to a temperature change while performing light scattering. Xanthan (Sigma) was dispersed in phosphate buffer and heated up to 80 °C for at least 2 h to solubilize and denature any preformed structures. The electrostatic complexation of the protein with xanthan was carried out at 60 °C by titrating protein to xanthan solution at a xanthan concentration of 0.083 g/L. The charge ratio (+/-) is defined as the ratio between the concentration of positive polymeric charges (from the protein polymer) and the concentration of negative polymeric charges (from xanthan). All solutions were filtered using 0.2 μm membranes (Milipore) to prevent contamination and remove dust before measurement. Light scattering was performed with a Zetasizer (Malvern) at a scattering angle θ of 173 °, corresponding to a scattering vector $q = \frac{4\pi n}{\lambda}\sin\frac{\theta}{2}$ ~0.02 nm^{-1}, where n is the refractive index of the solvent (water). The temperature was varied between 5 °C and 60 °C.

Rheology

Protein and xanthan were solubilized in the same way as described above, in 10 mM phosphate buffer at pH 3. The xanthan hydrogels crosslinked with the protein were prepared at high temperature, and cooled to 5 °C in at least 10 h. The measurements were

carried out on a stress-controlled DHR3 rheometer (TA instruments) equipped with a Peltier temperature control system. To enable measurements on small sample quantities, it was necessary to use an 8 mm parallel plate geometry. Under these conditions, and due to the relative weakness of the gels, the rheological measurements were always performed at the edge of the sensitivity of the rheometer. About 60 µl of the gels was deposited on the Peltier-controlled bottom plate, after which the top plate was lowered and the sample squeezed in between the plates. A thin layer of tetradecane was used to cover the sample and prevent evaporation. To eliminate the formation air bubbles during loading gels onto the plate, the gels were first heated stepwise with 10 °C increment to 50 °C (in 45 min) and rapidly cooled to 10 °C. The gels were then allowed to stabilize at 10 °C for 3 h before measurements. The linear dynamic oscillatory properties of the gels were measured at different temperatures, over a frequency range between 0.1 and 100 rad/s, and at a low strain of 2 %. The stability of the gel was checked at each temperature by performing consecutive oscillatory measurements. For non-linear rheology, oscillatory shear (frequency of 1Hz) was applied, with amplitude ranging from 1 to 1000 %.

6.3.   Results and Discussion

Electrostatic complexation of xanthan and the biosynthetic protein TR4K

The triblock polymer TR4K was produced by recombinant *P. pastoris* in methanol fed-batch fermentations. The recovery of purified dry product was above 500 mg per liter of cell-free broth. The purified protein was analyzed by electrophoresis (SDS-PAGE) and matrix-assisted laser desorption/ionization time-of-flight mass spectroscopy (MALDI-TOF). The SDS-PAGE (Appendix, Figure A6.1) shows that the protein is intact and pure. The molecular mass was verified by MALDI-TOF (Appendix, Figure A6.2), which shows a monodisperse product with a mass very close to the theoretical value of 40105.

Xanthan is known to have a large molecular weight and high polydispersity [2]. The average hydrodynamic length of both the purified and unpurified xanthan samples was found to be 1250 ± 50 nm and the contour length varies between 600 and 1500 nm [14]. At a very low concentration, xanthan likely behaves like a big polyelectrolyte that can be analyzed by light scattering [14, 15]. Here, the ionic interaction between xanthan and the protein was investigated at a low xanthan concentration of 0.08 g/L at 60 °C, where the T

block did not form any triple helices. The titration of the xanthan solution by step-wisely adding the charged protein in 10 mM phosphate buffer at pH 3 was followed by means of light scattering. As shown in Figure 6.2A, xanthan alone shows very low scattering intensity, while adding a small amount of charged TR4K at the charge ratio of 0.1 results in a 10-fold increase in scattering intensity, corresponding to a similar mass increase. This demonstrates that ionic binding of multiple proteins onto xanthan backbones likely occurs. A similar increase in effective mass was observed recently for DNA molecules with added diblock protein [16]. The scattering intensity reaches a plateau value in a charge ratio range of 0.1 to 0.25. However, there is a sharp increase of scattering intensity at a charge ratio ~0.33, after which it goes back to a value similar to the plateau value. Previous studies [16, 17] with other combinations of protein polymers and polyanions (DNA and high molecular weight polystyrene sulfonate) did show similar plateau regions but not a region of aggregation. This peak is likely due to some interactions between xanthan backbones. The value of the hydrodynamic radius in this charge ratio range also has large fluctuations (Appendix, Figure A6.3). This aggregation prevents us from studying charge ratio higher than 0.4.
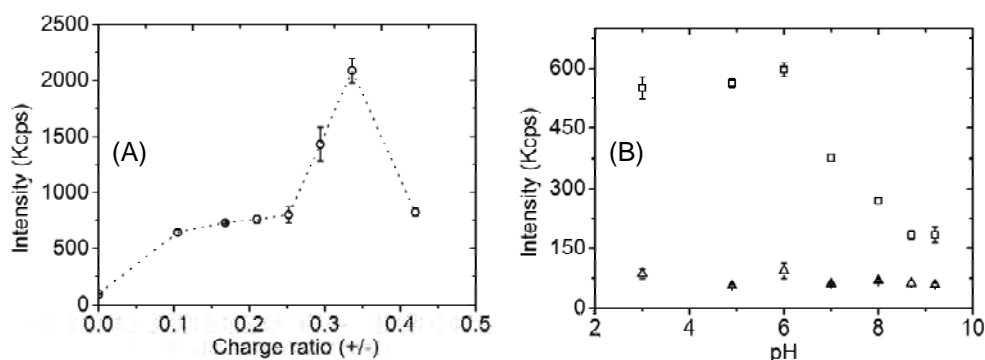
Figure 6.2 (A) Titration curve of charge-driven xanthan/TR4K complex in 10 mM phosphate buffer pH 3 at 60 °C, (B) pH-dependence of charge-driven xanthan/TR4K complex (square) and only xanthan (tri-angle) in 10 mM phosphate buffer 60 °C.

The protein TR4K interacts with xanthan with its charged K block consisting of 6 lysine residues. The protonation of the lysine residues, and therefore also their interaction with xanthan, depends on the pH of the solution. Far below the pKa of lysine, which is around 9 for isolated lysine residues, each K block is fully protonated and carries six

positive charges that can interact with the anionic xanthan. As shown in Figure 6.2B, the scattering is high in this region as a result of complex formation. Above pH 6, the scattering intensity decreases, and above pH 8 it is very low. This indicates that the complexes are already disrupted at a pH much lower than the pKa of isolated lysine, probably as a result of interactions between the neighboring lysine groups. Pure xanthan solution at the same concentration is not responsive to pH (Figure 6.2B). Therefore, the pH-dependence of xanthan/TR4K complex is due to the protonation of the K block.

Thermo-sensitive properties of xanthan/TR4K complex

The collagen-like block T is known to be thermo-responsive, which results in the formation of triple helical nodes at low temperature [13, 18]. As shown in chapter 5, a very similar system consisting of a TR4H protein (with a histidine instead of a lysine end block) and polystyrene sulfonate showed thermo-reversible aggregation of the electrostatic complexes. We expect a similar triple-helix-induced aggregation in the present system. To confirm triple helix formation, we first study solutions containing only TR4K as a function of temperature. The solutions were incubated at low temperature to induce the formation of triple helical nodes, and then these solutions were heated, while monitoring the light scattering intensity. As shown in Figure 6.3A, the scattering intensity gradually decreases with increasing temperature, indicating the dissociation of the helices into protein monomers. The melting point is estimated around 30 °C for the helices, which is in agreement with a previous report [18] and the corresponding value of the TR4H in chapter 5.

We then studied the effect of triple helix formation on the electrostatic complexes of xanthan and charged TR4K (at charge ratio of 0.2 and a pH of 3). The system was subjected to a temperature cooling step from 50 °C to 10 °C. The solutions with only xanthan were measured at high temperature (50 °C) and then TR4K was added. At 50 °C, the addition of TR4K indeed leads to remarkable increase in light scattering intensity. Cooling the charge-driven complex to 10 °C results in a doubling of the scattering intensity (Figure 6.3B). This is likely due to the formation of helical nodes between the T blocks. It was reported that there was no significant difference in the calculated weight average molar mass of xanthan in the same temperature range at a very low concentration [19]. Since the concentration used here is very low, we speculate that there is a high probability of forming helical nodes between TR4K molecules bound on the same xanthan backbone. To

further confirm the thermo-responsive properties due to the T block, the solution of xanthan/TR4K complex was incubated at 10 °C for a longer time. Figure 6.3C displays not only a decrease but also a large fluctuation of the scattering intensity in the course of time, which likely indicates that phase separation of the charge-driven xanthan/TR4K complex leads to sedimentation. The mixture of proteins and polysaccharides in aqueous dispersion is often accompanied by either segregative or associative phase separation, depending mainly on the electrical charges on the polymers [20]. The interpolymeric complexes between xanthan and β-lactoglobulin are also initiated by an associative phase separation process [8].
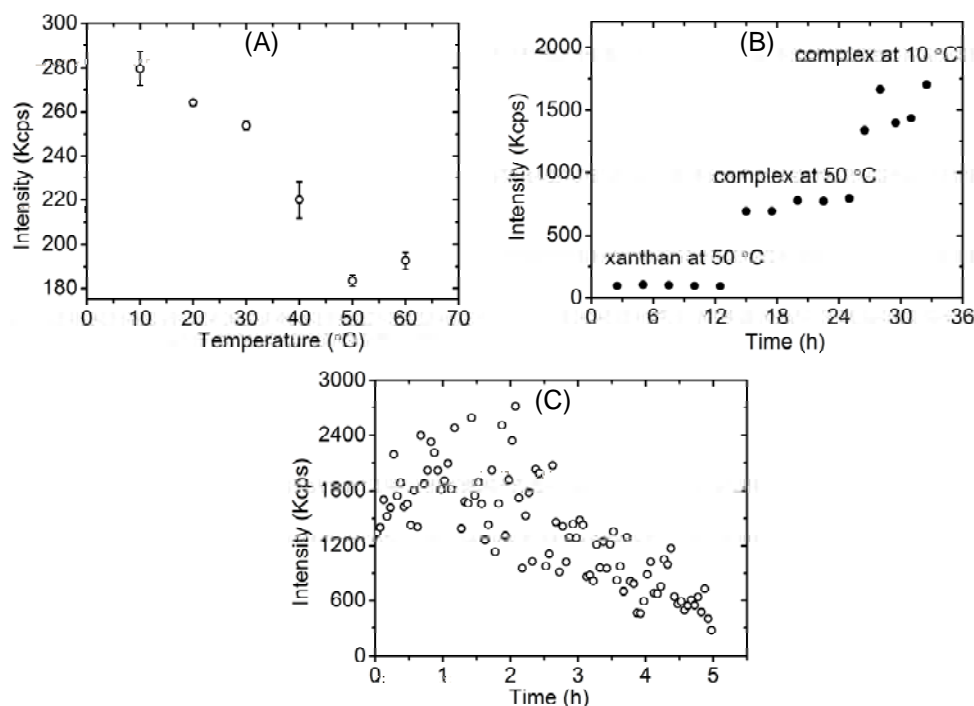
Figure 6.3 (A) Thermo-responsive melting curve of triple helical solutions, (B) Thermo-responsive properties of charge-driven xanthan/TR4K complex, and the corresponding xanthan only at 50 °C, (C) Associative phase separation of charge-driven xanthan/TR4K complex at 10 °C with time.

Electrostatic crosslinked xanthan/TR4K hydrogels

The gelation behavior of xanthan with added TR4K was studied at two xanthan concentrations (5g/L and 10 g/L). A similar range of xanthan concentration was chosen for

studying the viscoelastic characteristics of xanthan gels crosslinked by cations [21, 22] where xanthan itself is about to reach the overlap concentration (~7 g/L). Given the small sample quantities, it was necessary to perform the rheological measurements with a small 8 mm parallel geometry. Since the gels are relatively weak, the quantitative accuracy of the measurements decreases rather drastically. The small strain dynamical oscillatory data were in all cases signified by a roughly frequency independent elastic modulus G' (between 0.1 and 100 rad/s), and G' was in all cases about one decade larger than the corresponding loss modulus G''. Especially for the weakest gels, the highest frequencies (above 50 rad/s) were strongly influenced by inertial contributions from the geometry or/and rheometer. We hence choose somewhat arbitrarily to compare data for different samples and temperatures by plotting the roughly frequency independent G' at a fixed angular frequency of 1 rad/s, where inertial contributions are clearly absent and the signals are reliable. Here, at 10 °C, xanthan solutions in the absence of TR4K give a small storage modulus G' (at 1 rad/s) of about 3 Pa and 20 Pa for 5 g/L and 10 g/L, respectively (Figure 6.4A). Upon mixing with the charged TR4K in 10 mM phosphate buffer (pH 3), the corresponding modulus significantly increases. Upon adding more protein, indicated by increasing the charge ratio, the storage modulus reaches a plateau at a charge ratio around 0.6. We note that at this charge ratio, aggregation was observed in dilute solutions. Probably, the same aggregation that leads to sedimentation in dilute solutions causes gel formation in concentrated solutions. The increase of G' is probably caused by an enhancement in both entanglement of xanthan backbones due to stiffening induced by the adsorbed polymer and the crosslinks due to the TR4K protein. Figure 6.4B shows the dependence of G' of the crosslinked xanthan hydrogels (at charge ratio of 0.5) on xanthan concentration. Clearly, the modulus increases with increasing concentration.
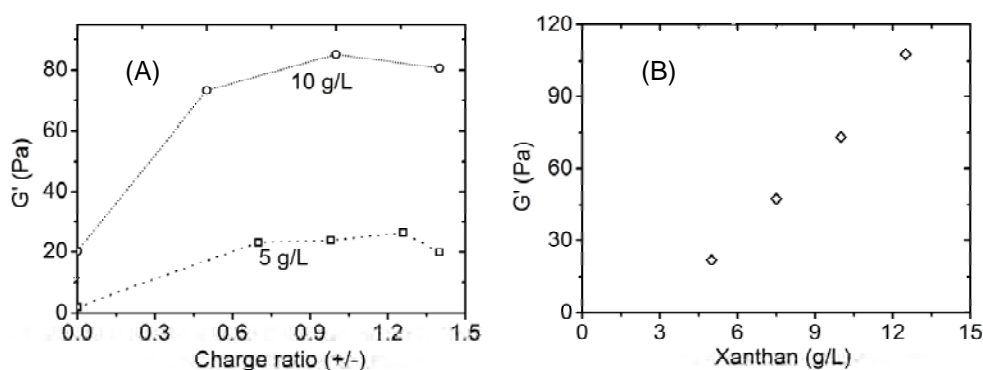
Figure 6.4 (A) Storage modulus (at 1 rad/s) of xanthan/TR4K hydrogel as a function of charge ratio for two xanthan concentration at 10 °C, (B) Storage modulus (at 1 rad/s) of xanthan/TR4K hydrogels as a function of xanthan concentration 10 °C at a charge ratio of 0.5.

Thermo-sensitive characteristics of the electrostatic xanthan/TR4K complex

As discussed above, at a low xanthan concentration, the electrostatic xanthan/TR4K complex is sensitive to temperature due to the thermo-sensitive formation of triple helices of the T block. The hydrogels formed by xanthan/TR4K complex at xanthan concentrations of 10 g/L and 5 g/L (with the same charge ratio) were introduced to temperature changes and compared with the hydrogels formed by xanthan alone at the corresponding concentrations. The resulting storage moduli (measured at 1 rad/s) as a function of temperature are shown in Figure 6.5. Xanthan gels at both concentrations show little thermo-sensitivity. The temperature dependence is enhanced in the crosslinked xanthan hydrogels, especially at the high protein concentration. Xanthan gels are reported to be relatively sensitive to temperature [2]. However, there is still debate on the complete renaturation of xanthan after heating, and this process requires the present of salt in the solution [23]. Here, we speculate that the temperature dependence is mostly contributed by the T block as there is no salt in the solution. We also note that the thermo-responsive properties of xanthan/TR4K hydrogels are entirely reversible, e.g. the storage modulus has the same value after one heating cycle to 10-50-10 °C.
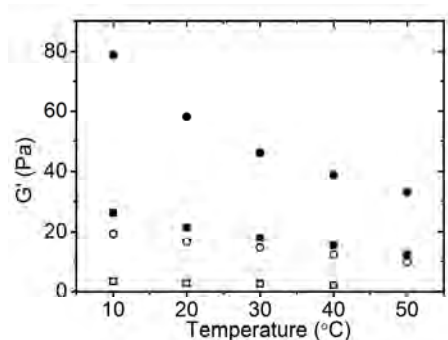
Figure 6.5 Storage modulus (at 1 rad/s) as a function of temperature for xanthan/TR4K hydrogels (charge ratio of 0.5) at xanthan concentration of 10 g/L (filled circle) and 5 g/L (filled square) in comparison with pure xanthan hydrogel at the corresponding concentration 10 g/L (open circle) and 5 g/L (open square).

Roles of the protein crosslinker observed in non-linear rheology

To study the effects of crosslinks induced by charged TR4K protein to the non-linear yielding behavior of the xanthan hydogels, amplitude sweeps were applied to the croslinked hydrogels under various conditions. As shown in Figure 6.6, xanthan hydrogels in the absence of TR4K are strain softening, both at low and at high temperature; this strain softening occurs at a strain of approximately 100 % and is probably due to the alignment and disentanglement of xanthan molecules [4]. Similar results have been reported elsewhere [24].

For the xanthan/TR4K mixtures (charge ratio of 0.5), a shoulder appears in the amplitude sweeps and the strain softening proceeds in two steps. This two-step softening occurs both at 50 °C, where triple helices are likely absent, and at 10 °C, where triple helices are present. In the presence of triple helices, the initial (linear) modulus is higher and also the first strain softening region becomes more pronounced. We hypothesized that this first strain softening regime is caused by the forced unbinding of TR4K molecules from the xanthan backbone due to the shear deformation. This unbinding leads to a decrease in stiffness of the xanthan molecules; and at 10 °C, it also results in a loss of cross-links. The second strain softening regime occurs at similar strains as for xanthan without TR4K, suggesting that this is again related to alignment and disentanglement of xanthan molecules.
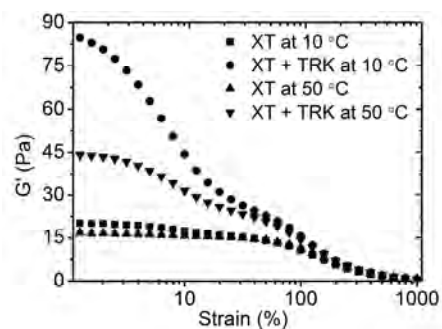
Figure 6.6 Amplitude sweeps of xanthan/TR4K hydrogels at different temperature in comparison with the corresponding xanthan hydrogels.
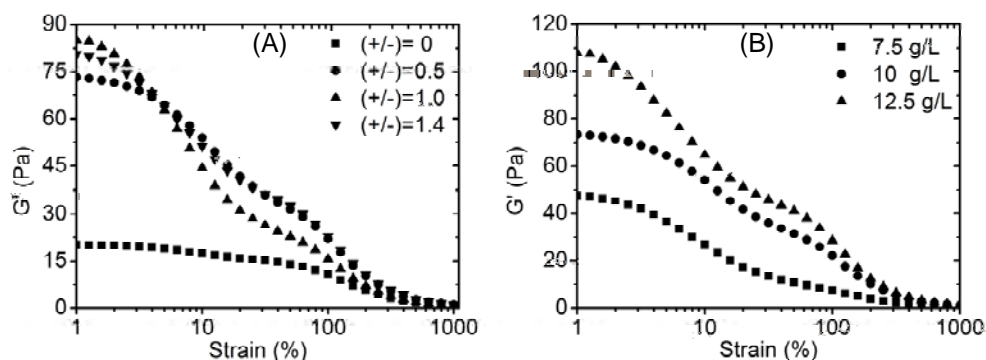
Figure 6.7 (A) Amplitude sweeps of xanthan/TR4K hydrogels for different charge ratios at 10 °C and at fixed xanthan concentration of 10 g/L, (B) Amplitude sweeps of xanthan/TR4K hydrogels for different xanthan concentrations at 10 °C and at the same charge ratio of 0.5.

The effects of the charge ratio and concentration on the non-linear rheology of xanthan/TR4K hydrogels is shown in Figure 6.7. A similar two-step strain softening is observed for all charge ratios and concentrations studied, indicating that this behavior is robust for this system.

6.4. Conclusion

The electrostatic interactions between xanthan and a biosynthetic triblock protein are analyzed by scattering and rheology. The triblock protein has two reactive end-blocks: one positively charged end-block which has ionic interactions with xanthan and another end-block which self-assembles into triple helical nodes. The results reveal both pH and

thermo-responsive properties of the crosslinked network. Such sensitive behaviors are likely introduced into the xanthan network due to the added protein polymer. Although the gel strength is highly dependent on the concentration of xanthan that serves as the backbone of the crosslinked hydrogels, the presence of the crosslinks also significantly enhances the storage modulus which becomes 5 times higher than that of the xanthan hydrogel alone. The non-linear rheology as probed with oscillatory measurements at fixed frequency and varying strain of the mixed networks shows a two-step strain softening, where the first step is probably due to unbinding of the proteins from the xanthan backbone. We anticipate that this novel type of crosslinked hydrogel represents a method to smartly modify xanthan networks into functional and sensitive biomaterials for application orientation.

References

1. V. Rana, P. Rai, A. K. Tiwary, R. S. Singh, J. F. Kennedy and C. J. Knill, *Carbohydr. Polym.*, 2011, **83**, 1031-1047.

2. Huber Company, *KELTROL® / KELZAN® xanthan gum Book*, 2001-2008, **Eight edition**.

3. G. R. Sanderson, *Brit. Polym. J.*, 1981, **13**, 71.

4. W. E. Rochefort and S. Middleman, *J. Rheol.*, 1987, **31**, 337.

5. T. Phaechamud and G. C. Ritthidej, *Drug Dev. Ind. Pharm.,* 2007, **33**, 595-605.

6. J. H. Hamman, *Mar. Drugs,* 2010, **8**, 1305-1322.

7. S. Argin-Soysal, P. Kofinas and Y. M. Lo, *Food Hydrocolloids*, 2009, **23**, 202-209.

8. S. I. Laneuville, S. L. Turgeon, C. Sanchez and P. Paquin, *Langmuir,* 2006, **22**, 7351-7357.

9. X. T. Le and S. L. Turgeon, *Soft Matter*, 2013, **9**, 3063.

10. E. Dickinson, *Soft Matter*, 2008, **4**, 932-942.

11. B. Wagner, R. Tharmann, I. Haase, M. Fischer and A. R. Bausch, *PNAS*, 2006 **103**, 13974-13978

12. M. W. T. Werten, H. Teles, A. P. H. A. Moers, E. J. H. Wolbert, J. Sprakel, G. Eggink and F. A. de Wolf, *Biomacromolecules*, 2009, **10**, 1106-1113.

13. T. T. H. Pham, P. J. Skrzeszewska, M. W. T. Werten, W. H. Rombouts, M. A. Cohen Stuart, F. A. de Wolf and J. van der Gucht, *Soft Matter*, 2013, **9**, 6391.

14. M. A. Zirnsak, D. V. Boger and V. Tirtaatmadja, *J. Rheol.*, 1999, **43**, 627.

15. D. P. Norwood, M. Benmouna and W. F. Reed, *Macromolecules,* 1996, **29**, 4293-4304.

16. A. Hernandez-Garcia, M. W. T. Werten, M. Cohen Stuart, F. A. de Wolf and R. de Vries, *Small,* 2012, **8**, 3491-3501.

17. M. D. Golinska, F. A. de Wolf, M. A. Cohen Stuart, A. Hernandez-Garcia and R. de Vries, *Soft Matter*, 2013, **9**, 6406.

18. P. J. Skrzeszewska, F. A. de Wolf, M. W. T. Werten, A. P. H. A. Moers, M. A. Cohen Stuart and J. van der Gucht, *Soft Matter*, 2009, **5**, 2057-2062.

19. C. Viebke and P. A. Williams, *Food Hydrocolloid*, 2000, **14**, 265.

20. V. Tolstoguzov, *Food Hydrocolloid,* 2003, **17**, 1-13.

21. L. Ma and G. V. Barbosa-Canovas, *J. Food Sci.*, 1997, **62**, 1124.

22. M. Marudova-Zsivanovits, N. Jilov and E. Gencheva, *J. Appl. Polym. Sci.*, 2007, **103**, 160-166.

23. T. A. Camesano and K. J. Wilkinson, *Biomacromolecules,* 2001, **2**, 1184-1191.

24. K. W. Song, H. Y. Kuk and G. S. Chang, *Korea-Aust. Rheol. J.*, 2006, **18**, 67-81.

Appendix
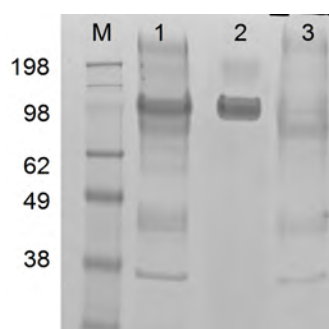
Figure A6.1 SDS-PAGE of purifying TR4K: (M) protein marker, (lane 1) fermentation broth, (lane 2) purified TR4K by precipitation with 45 % ammonium sulfate saturation, (lane 3) the remaining supernatant.
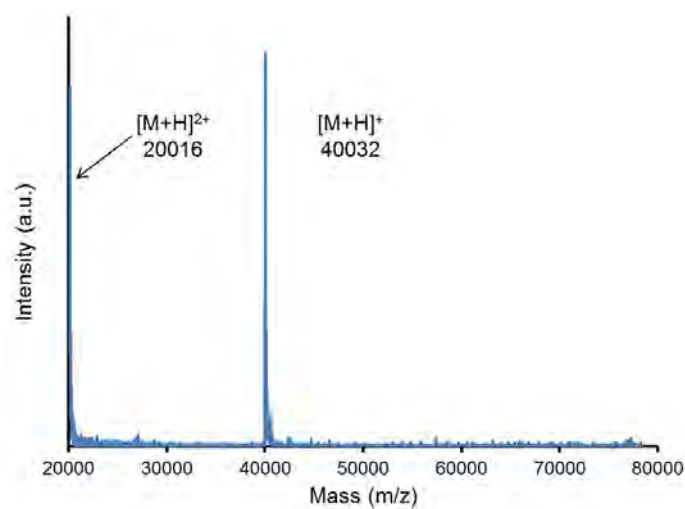
Figure A6.2 MALDI-TOF of purified TR4K. Singly and doubly charged molecular ions are indicated.
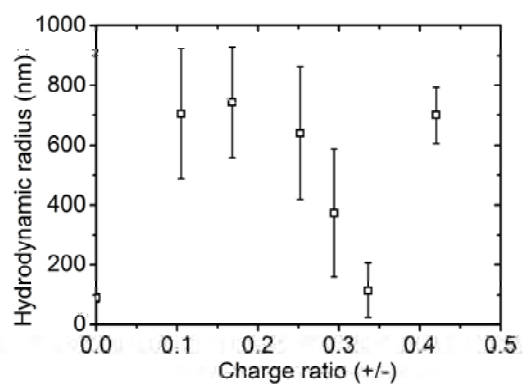
Figure A6.3 Hydrodynamic value of titration curve of charge-driven xanthan/TR4K complex in 10 mM phosphate buffer at pH 3 at 60 °C.

Chapter 7

Disulfide bond-stabilized physical gels of an asymmetric collagen-inspired telechelic protein polymer

Abstract

In this chapter, we report the production and analysis of an asymmetric collagen-inspired telechelic protein polymer with end blocks that can form triple helices of different thermal stability. Both end blocks consist of a motif that can form triple helices at low temperature, but one of these blocks carries an additional cysteine residue at the end. The cysteine residues can form disulfide bridges under oxidizing conditions, leading to dimer formation. This effectively stabilizes the triple helices, resulting in a double melting peak in differential scanning calorimetry: one corresponding to helices without disulfide bridges and one at significantly higher temperature, corresponding to stabilized helices. These disulfide bridges also lead to an increase of the elastic modulus of the helical polymer network, probably because the number of helices in the system increases, and because the disulfide bridges can crosslink different triple

7.1. Introduction

Hydrogels are chemically or physically cross-linked polymer networks filled with water. Owing to their distinctive properties, they are widely used in many applications such as drug delivery systems, tissue engineering scaffolds, wound dressing materials and thickeners in paints and cosmetics [1, 2, 3]. For all these applications, it is crucial that the properties of the hydrogels, in particular their stiffness and their erosion rate, can be tuned as precisely as possible.

An interesting class of hydrogels is that of protein-polymer based biomaterials. Using genetic engineering, it is now possible to produce well-defined, tailor-made polypeptides with a desired amino acid sequence and molecular architecture. Self-assembly motifs can be incorporated into the molecular design. Previously, we described the construction of a gene encoding the protein polymer TR4T [4]. The protein comprises three blocks. The end blocks, abbreviated as T (trimer-forming), consist of nine consecutive Pro-Gly-Pro triplets. Upon cooling, the T domains form collagen-like triple helices. The highly hydrophilic middle block R4 (consisting of four identical R monomers; each ~100 amino acids long) assumes a random coil configuration at any temperature. Upon cooling, the telechelic TR4T molecule self-assembles into a physical hydrogel with triple helices as the nodes in the network. We showed how the properties of the network can be tuned by varying concentration, temperature, and the length of both the assembly and spacer blocks [5-8].

In this paper, we adapted the TR4T design to produce a new asymmetric network former. To achieve this, one cysteine amino acid was added to the end block at the C-terminus of the polypeptides. The cysteine residue can form a disulfide bond with another cysteine, thus linking two protein molecules together. As each protein has only one cysteine residue, intra-chain loop formation by disulfide bonding is prevented. To evaluate the effect of disulfide bridge formation on the gel-forming properties of the product, the asymmetric molecules were characterized at different temperatures and protein concentrations, both in the presence and absence of a reducing agent, and compared to the properties of cysteine-free TR4T.

114

7.2.   Materials and Methods

Polymer biosynthesis

The construction of plasmid pMTL23-TR4T, which contains the gene encoding the telechelic collagen-inspired polypeptide TR4T (~42 kDa), has been described by us previously [4]. The amino acid sequence of the TR4T protein can be found in GenBank under accession number ACF33479 (mature protein starts after the sequence LEKREAEA). Here, the TR4T gene was modified so as to introduce a C-terminal Cys-Gly in the encoded protein, as well as an N-terminal Gly-Trp (not used in this work). First, a double-stranded DNA adapter was prepared by annealing of the following complementary oligonucleotides:

5'-TCGAGAAAAGAGAGGCTGAAGCTGGTTGGGGTCCACCCGGTGCTCAGCTGC CAGCCG GTGGCTGTGGTTAATAG-3' and

5'- AATTCTATTAACCACAGCCACCGGCTGGCAGCTGAGCACCGGGTGGACCCC AACCAGCTTCAGCCTCTCTTTTC-3'

The adapter was then ligated into *EcoRI/XhoI*-digested vector pMTL23 [9], to yield vector pMTL23-Trp-Cys. Vector pMTL23-TR4T was digested with *DraIII/Van91I*, after which the released TR4T gene was ligated into the correspondingly digested and dephosphorylated vector pMTL23-Trp-Cys. The resulting vector pMTL23-Trp-TR4T-Cys was then digested with *EcoRI/XhoI*, and the obtained Trp-TR4T-Cys DNA fragment was subsequently cloned into expression vector pPIC9 (Invitrogen) using *XhoI/EcoRI*. Transfection of this final vector into the yeast *Pichia pastoris* (strain GS115, Invitrogen), followed by secreted protein production in a bioreactor, and protein purification was carried out as described earlier [4]. A *yps1* protease disruptant strain derived from strain GS115 was also used. The purification of the protein from the cell-free broth was similar to the procedure we described previously. The purified protein was dialyzed using Spectra/Por tubing (Spectrum Labs) and freeze-dried for storage until use. The protein is referred to hereafter as TR4T-Cys.

Mass spectrometry

Matrix-assisted laser desorption/ionization time-of-flight mass spectroscopy (MALDI-TOF) was performed using an Ultraflex mass spectrometer (Bruker). Samples were prepared by the dried droplet method on a 600 μm AnchorChip target (Bruker), using 5 mg/ml 2,5-dihydroxyacetophenone (Sigma), 1.5 mg/mL diammonium hydrogen citrate (Sigma), 25% (v/v) ethanol and 1% (v/v) trifluoroacetic acid (Sigma) as matrix. Measurements (20 Hz) were made in the positive, linear mode, with the following parameters: ion source 1, 20000 V; ion source 2, 18450 V; lens, 5000 V; pulsed ion extraction, 550 ns. Protein Calibration Standard II (Bruker) was used for external calibration. Baselines were subtracted in Flex-Analysis v3.3 (Bruker) using the Median algorithm. The spectra were not smoothed.

Differential Scanning Calorimetry (DSC)

Differential scanning calorimetry experiments were performed with a MicroCal VP-DSC instrument. TR4T-Cys solutions were prepared at 0.48 mM in 10 mM phosphate buffer pH 3 in the presence and absence of the reducing agent tris(2-carboxyethyl)phosphine hydrochloride (TCEP) (Thermo Scientific). Degassed 0.51 ml protein solutions were loaded into the calorimeter at 50 °C. The sample was then cooled to 20 °C over a period of 1 h. For each experiment, the protein solutions were equilibrated for 15 h at 20 °C to allow complete helix formation. Then, the temperature was raised from 20 °C to 80 °C and the heat flow needed to melt the helices was recorded. To study the dependence of melting point on protein concentration, degassed 0.51 ml solutions with two different protein concentrations were loaded. To analyze the effect of scan rate, a protein solution of 0.96 mM was loaded and scanned at various scan rates (from 10 to 60 °C/h). There was always an equilibration stage of 15 h at 20 °C before each scan. The calorimetric transition enthalpy was obtained by integration of the area under the excess heat capacity peaks. The flooring of the thermogram was done by fitting the thermogram baseline with a third order polynomial.

Static light scattering (SLS)

Protein solutions were prepared by solubilising freeze-dried TR4T-Cys in 10 mM phosphate buffer at pH 7.4 to a working concentration of 195 µM and then heated at 55 °C for 30 min. TCEP was added to a final concentration of 20 mM to disrupt disulfide bonds in reducing conditions.

Light scattering at angles from 20 ° to 140 ° was performed with an ALV light scattering apparatus, equipped with a 400 mW argon ion laser operating at a wavelength of 532 nm. The measurements were performed at either low temperature (20 °C) or high temperature (40 °C), always after an equilibration period of 4 h, and the temperature was controlled by a Haake F3-K thermostat. The light scattering intensity is expressed as the excess Rayleigh ratio R_θ divided by the polymer concentration as described previously [10].

The Rayleigh ratio (R_θ) is used as an absolute measure for the scattered light intensity:

$$R_\theta = \frac{I_{sample} - I_{solvent}}{I_{toluene}} \times R_{toluene} \times \frac{n^2_{solvent}}{n^2_{toluene}} \qquad \text{(Eq.7.1)}$$

We measure R_θ as a function of the scattering vector q and extrapolate to $q=0$. Assuming that intermolecular interactions are not important at this low protein concentration, the scattering intensity can be related to the molar mass of the proteins or the apparent molar mass (M_{app}) of the protein aggregates in the solution:

$$R_0 = KCM_{app} \qquad \text{(Eq.7.2)}$$

where C is the protein concentration and K is defined as

$$K = \frac{4n^2_m \pi^2}{\lambda^4 N_{Av}} \times \left[\frac{dn}{dc}\right]^2 \qquad \text{(Eq.7.3)}$$

where n_m is the reflective index of water, dn/dc is the refractive index increment of protein, estimated to be 0.000189 kg^3/m [11], λ is the wavelength of the light source (535 nm), N_{Av} is the Avogadro's number.

Rheology

All different protein concentrations tested were prepared in the same way. A given amount of protein was dissolved in 10 mM phosphate buffer at pH 7.4 and then heated at 55 °C for 30 min, allowing the triple helices which formed during fermentation and protein purification to melt so that the percolating network is disrupted. For reducing conditions, to

break down disulfide bonds between two polypeptides, 20 mM TCEP was added to the protein solutions prior to heating. The rheological measurements were carried out on an Anton Paar Physical MCR 301 or MCR 501 rheometer equipped with a cone and plate geometry of 50 mm diameter. The temperature was controlled by a Peltier system, which allowed fast heating and cooling. A solvent trap was used to minimize evaporation. The plate was preheated to 55 °C before adding protein solutions. After lowering the cone, the temperature was quickly lowered to 15 °C. Gel formation was monitored by applying a sinusoidal deformation to the system (f=1 Hz and γ=1%). Viscoelastic dynamic analysis was performed in a frequency range of 0.01-20 Hz with deformation amplitude of 1 %, well within the linear response regime. Creep experiments were done at an applied stress of 5 Pa with duration of 1800 s. After the gel was formed at 15 °C, the temperature was increased to 20 °C, 25 °C, and 30 °C. At each temperature, the system was equilibrated for 5 h.

7.3.   Results and Discussion

Biosynthesis of intact TR4T-Cys
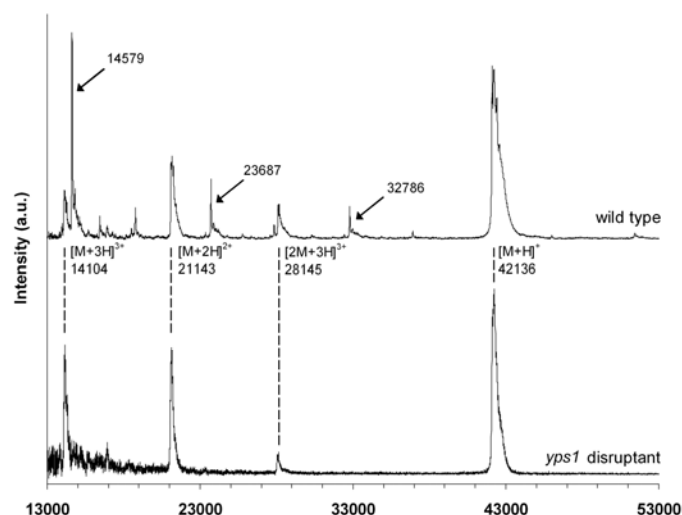
Figure 7.1 MALDI-TOF of TR4T-Cys produced in wild type *P. pastoris* (top spectrum) and in a *yps1* protease disruptant (bottom spectrum). Multiply charged molecular ions are indicated. All masses indicated refer to TR4T-Cys produced in the wild type. Arrows point to peaks discussed in the text.

118

The previously described TR4T gene [4] was adapted to code for a C-terminally cysteine-extended variant, TR4T-Cys. This protein polymer comprises three blocks: one triple helix- forming block (T) at the N-terminus, a random-coil like middle block, and another T block with a cystein residue connected to it at the C-terminus. A *P. pastoris* GS115 strain expressing TR4T-Cys as an extracellular protein was constructed and grown in a bioreactor. The protein was purified from the cell-free broth by differential ammonium sulfate precipitation, which, as described previously, routinely results in a protein purity of around 99% [4].

MALDI-TOF analysis (Figure 7.1, top spectrum) showed a main peak with a mass of 42,136 Da, which corresponds well to the theoretical mass of 42,144 Da. However, several peaks of lower mass were also visible, indicative of proteolytic degradation. After separation of the protein fragments by SDS-PAGE, several bands were subjected to N-terminal sequencing. Some of these bands showed the internal sequence NGPSQG, which occurs four times in the R4 midblock (once per R monomer, preceded in the sequence by a lysine residue). All other bands showed the N-terminal sequence expected for the intact protein, despite having different apparent masses in SDS-PAGE. This shows that these bands represent C-terminally truncated species of various lengths. Accordingly, some of the masses observed in MALDI (5,456 Da, 14,579 Da, 23,687 Da, and 32,786 Da) match the theoretical masses of parts of the sequence spanning from the N-terminus to the location of the aforementioned lysine residues in the R4 mid block (5,472 Da, 14,580 Da, 23,689 Da, and 32,798 Da, respectively). This points to endoproteolysis at specific lysine residues, just as we have reported before, for a triblock very similar to TR4T but having longer $(PGP)_{16}$ triple helix-forming end blocks [12] . The observed degradation in that case was found to be linked to the higher thermo-stability of the longer end blocks relative to the $(PGP)_9$ end blocks of TR4T. Apparently, the occurrence of stable triple helices in vivo directly or indirectly triggered proteolysis of the triblock protein. This problem was solved by using a *yps1* protease disruptant of *P. pastoris*, deficient in the lysine- and arginine-specific endoprotease *yapsin 1* [12, 13].

We reasoned that formation of disulfide (S-S) bridges by the cysteine residue in TR4T-Cys may have a triple helix-stabilizing effect similar to that of using longer end blocks, and might thus trigger similar degradation in vivo as observed previously for $(PGP)_{16}$ end blocks. To verify this hypothesis, we transformed the *yps1* protease disruptant with the

TR4T-Cys construct, and produced the protein as before [4]. The protein yield was 400 mg from one litter of fermentation supernatant. MALDI-TOF analysis (Figure 7.1, bottom spectrum) no longer showed significant secondary peaks, which indicates that the TR4T-Cys is intact in the *yps1* disruptant. Accordingly, the protein also visibly formed strong self-supporting gels at 40 g/L, whereas TR4T-Cys produced in the wild type strain did not form self-supporting network at 50 g/L. These findings suggest that the C-terminal cysteine indeed stabilizes the trimer-forming end blocks in vivo to such an extent that the wild type cells respond with yapsin-mediated degradation, as was seen previously for the triblock with $(PGP)_{16}$ end blocks [12].

Disulfide bond-stabilized triple helices
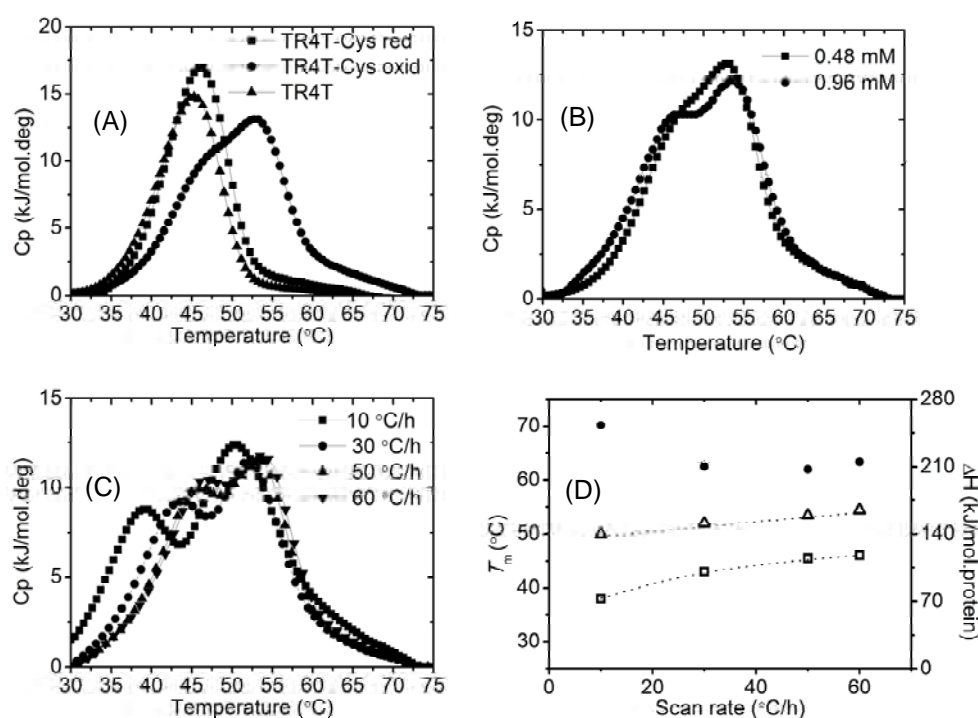
Figure 7.2 DSC scans (A) TR4T-Cys at both oxidizing and reducing conditions at a concentration of 0.48 mM at a scan rate 60 °C/h ; symmetric TR4T is shown for comparison at a scan rate 60 °C/h, (B) TR4T-Cys at different concentrations in oxidation state at a scan rate of 60 °C/h, (C) Scans with different scan rates for 0.96 mM TR4T-Cys protein, (D) Melting temperature: high T_m (open triangle), low T_m (open square) and enthalpy (filled circle) as a function of scan rate.

In previous work, we have seen that the symmetric TR4T protein forms gels due to triple helix formation and that melting of these triple helices is an endothermic process [4, 6]. The heat effect upon melting of the asymmetric TR4T-Cys was analyzed with DSC. Figure 7.2A shows DSC scans of TR4T-Cys in both oxidizing (e.g. TR4T-Cys-oxid) and reducing conditions (e.g. TR4T-Cys-red) at a protein concentration of 0.48 mM. In reducing conditions, the melting point occurred at approximately the same temperature as for the unmodified TR4T, around 45 °C at a scan rate of 60 °C/h. The melting temperature is slightly higher than that measured previously for TR4T (around 42 °C at a scan rate of 15 °C/h) [4, 6], probably due to the higher scan rate. Interestingly, in oxidizing conditions, when there are disulfide bonds between the polypeptides, the DSC scan of TR4T-Cys displayed *two* melting points, one at 45 °C and one at 56 °C. The total enthalpy change of the two melting steps together is approximately the same as the melting enthalpy under reducing conditions, which indicates that the total amount of triple helices is the same. The first melting step occurs at a similar temperature as the melting point of TR4T and reduced TR4T-Cys. The second melting step occurs at a higher temperature and likely represents the disulfide bond-stabilized helices. Apparently, the formation of disulfide bonds in TR4T-Cys stabilizes a fraction of the triple helices, resulting in a higher melting temperature.

Figure 7.2B shows the melting point of TR4T-Cys at two different protein concentrations. At the higher protein concentration, two obvious melting points are seen. As expected [6, 8], the apparent melting points were not much shifted and the total enthalpy (area under the curve) remained the same ($\sim$ 200-220 kJ· protein mol^{-1}).

By deconvolution of the two melting peaks for TR4T-Cys at the scan rate of 10 °C/h (Figure 7.2C), we estimate the enthalpies of the two fractions to be around 98 kJ/mol.protein for the first peak, 155 kJ/mol.protein for the second peak, respectively and the total is 253 kJ/mol.protein. This indicates that there are more triple helices stabilized with disulfide bonds (Figure 7.3A) in the network than there are triple helices without disulfide bridges. The total concentration of triple helices in the system is maximally $2C_p/3$, with C_p the total protein concentration. If all disulfide bridges would be formed between two cysteine residues inside one and the same triple helix, with the third strand in such a helix coming from a C-terminal T block, then the maximum number of disulfide bridge-stabilized helices would be $C_p/2$. In that case, the ratio between the amount of

121

stabilized and non-stabilized triple helices would be equal to 3. What we find is much less than that. This indicates that there are also disulfide bridges that cross-link different triple helices, which leads to hexameric (Figure 7.3B) or even larger nodes in the network (Figure 7.3C). Note that the melting temperature of such larger nodes with disulfide bridges only between different triple helices (as in Figure 7.3B and C) is expected to be not significantly different from the melting temperature of a single triple helix without disulfide bridge. Note also that it cannot be excluded that the lower ratio was partly caused by incomplete disulfide formation.

(A)

S-S bridge-stabilized triple
helical knot

(B)

Hexamers of two triple helical knots
formed by S-S brides

(C)

Formation of larger knots
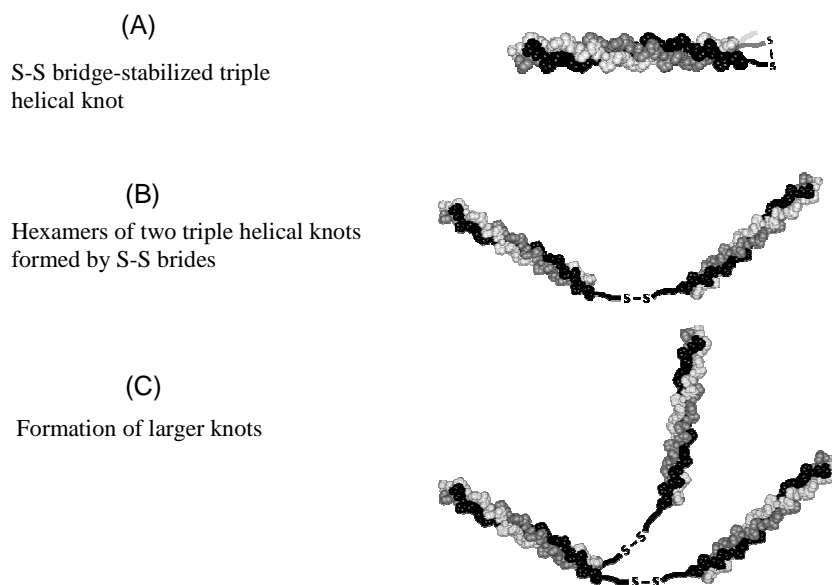
Figure 7.3 Formation of disulfide-bridge (S-S bridge) stabilized triple helical knots and cross-linked trimers.

The apparent melting temperature of the protein polymer (Figure 7.2C) reveals a dependence on the scan rate, similarly to the results for TR4T described previously. At higher scan rate, the melting peak shifts to higher temperatures (Figure 7.2D). This indicates that the system is not in equilibrium during the melting cycle. By extrapolating to zero scan rate, we estimate the equilibrium melting temperature of the helices without disulfide bridges to be around 34 °C and that of disulfide bridge-stabilized helices around 48 °C.

The triple helix – single coil equilibrium can be characterized with an equilibrium association constant:

$$K = \frac{[H]}{[C]^3}$$ (Eq.7.4)

where H is helix and C is the concentration of free end blocks. The equilibrium constant is related to the change in standard Gibbs free energy of helix formation, $-RT \ln K = \Delta G^0 = \Delta H^0 - T\Delta S^0$, where R is the gas constant. The T_m is usually defined as the temperature where the fraction of the end blocks taking part in triple helices is 0.5, which implies that $C = 3H = C_e/2$ and $K = 4/(3C_e^2)$, where C_e is the total concentration of T end blocks, equal to $2C_p$. With this value of K, which determines the free energy of triple helix formation at T_m, the entropy of triple helix formation (ΔS^o) can be calculated at any value of C_e from the measured values of ΔH^o and T_m (see above):

$$\Delta S^0 = \frac{\Delta H^0}{T_m} - R \ln\left(\frac{3(C_e)^2}{4}\right)$$ (Eq.7.5)

where R is the gas constant. Thus, a ΔS^o value of ~ 600 J·K^{-1}·mol^{-1} is found for the reduced state of TR4T-Cys. The present values of ΔS^o, ΔH^o and T_m for the reduced state of TR4T-Cys are approximately equal those previously observed for cysteine-free TR4T [8], which shows that the amino acids added to TR4T for the creation of TR4T-Cys did not detectably stabilize or destabilize the triple helix.

The increase in melting temperature in the oxidized state can be related to a change in the entropy. Assuming that ΔH^o is the same for oxidizing and reducing conditions (as suggested by the measured helices), we find a ΔS_{ox}^0 value of ~ -579 J·K·mol^{-1}, which is, in absolute sense, 21 J·K·mol^{-1} less than in the reduced state. Accordingly, the effect of disulfide bridging on the free energy of triple helix formation, calculated as:

$$\Delta G^0 = -T \times \Delta S_{ox}^0 - (-T \times \Delta S_{red}^0)$$ (Eq.7.6)

was about -7 kJ·mol^{-1}, a clear stabilizing effect.

Probably, this stabilizing effect is due to a reduction of the translational entropy of the dimerized molecules, as compared to the free molecules. In the oxidized state, when two T blocks are attached end to end through a disulfide bridge, that pair of T blocks is confined to a spherical volume with a radius limited to the length of one T block, i.e one (PGP)$_9$ in stretched conformation (approximately 8 nm, corresponding to a length of 0.3 or

maximally 0.35 nm per amino acid). Accordingly, the local concentration of end blocks, attached to a common S-S bridge, can be calculated as:

$$C_{S-S} = \frac{2}{(27 \times l)^3 \times \frac{4}{3}\pi \times 10^3 \times N_{Av}}$$

(Eq.7.7)

where l is the length per amino acid of the extended conformation and N_{Av} is Avogadro's number. Including the free blocks, the total local concentration of end blocks at the Cys-containing C-terminus is:

$$C_{S-S}^o = C_{S-S} + C_e$$

(Eq.7.8)

At a bulk TR4T-Cys concentration (Cp) of 0.96 mM, C^o_{s-s} would be ~3.4 mM, and from this local concentration C^o_{s-s}, the local K of the disulfide-stabilized triple helices can be calculated as $4/[3(C^o_{s-s})^2]$, at 50 % helix formation, and in combination with the values of ΔH^o and ΔS^o determined above, a theoretical T_m value specific for the disulfide-stabilized triple helices can then be calculated as:

$$T_m^{S-S} = \frac{\Delta H^o}{\Delta S^o + R\ln\left(\frac{3(C_{S-S}^o)^2}{4}\right)}$$

(Eq.7.9)

With the values of ΔS^o and ΔH^o obtained above, this gives a T_m of the stabilized helices of approximately 47-48 °C, in good agreement with the experimentally found value. This suggests that the stabilizing effect of the disulfide bridges can indeed be explained in terms of a local enhancement of the T block concentration.

Disulfide bonding of TR4T-Cys studied with light scattering

To study the formation of disulfide bond formation between two cysteine amino acids, static light scattering was carried out. We measured the intensity of scattered light as a function of the angle of detection and determined the normalized Rayleigh ratio KC/R_0, which is proportional to the mass of scattered objects (Appendix, Figure A7.1). By extrapolating to $q=0$, and using equation 2, we can estimate the apparent mass (M_{app}) of the protein clusters. We assume that we can interpret increases in the M_{app} at different conditions in terms of cluster formation. Before measurements, protein solutions were heated up to 55 °C in 30 min to melt the triple helices. At high temperature and under reducing conditions, when there are no triple helices and no disulfide bridges, we expect

only protein monomers. However, our light scattering results indicate an apparent mass of 91 kg/mol in this case, which is about a factor of 2.3 times higher than the mass of a protein monomer. This may be due to excluded volume interactions between proteins, or to uncertainties in the refractive index increment of the protein. Nevertheless, we estimate the average cluster size $<n>=M_{cluster}/M_o$ as the relative increase in scattering intensity compared to the sample in reducing conditions and at high temperature. The results are shown in table 7.1, for both oxidizing and reducing conditions, and both above and below the melting temperature of the triple helices. At high temperature and under reducing condition, $<n>=1$. At high temperature (40 °C) and in oxidizing conditions, $<n>$ is about a factor of two higher than in reducing conditions. This suggests that dimers are formed between proteins due to disulfide bonds. At low temperature (20 °C) and under reducing condition, there is formation of triple helices, which leads to the formation of small clusters with an average $<n> \approx 4$. The clusters are larger ($<n> \approx 7$) in oxidizing conditions due to the disulfide bridges.

Conditions	R/KC	$<n>$	Interpretation	Configuration
at 40 °C - red	91	1	No disulfide bonds, no triple helices: monomers	
at 40 °C - oxid	172	2	Disulfide bonds, no triple helices: mainly dimers	
at 20 °C - red	392	4	No disulfide bonds, triple helices: small cluster of 3 molecules	
at 20 °C - oxid	649	7	Disulfide bonds, triple helices: bigger cluster ≈ 6 molecules	Figure 7.3B and 3C

Table 7.1 Estimated changes in M_{app} expressed as ratio $<n> = M_{cluster}/M_o$.

Gelation of TR4T-Cys depends on concentration and oxidation states.

At temperatures above 50 °C, solutions of TR4T-Cys were viscous without detectable elastic response. When the solutions were cooled down from 50 °C to 15 °C, physical gels

were formed as a result of triple helix formation. A similar behavior was observed previously for symmetric TR4T [6]. Figure 7.4 shows the storage modulus of TR4T-Cys gels of different concentrations in both oxidizing and reducing conditions. Obviously, the elastic modulus of the gels increases with protein concentration. In addition, the modulus of TR4T-Cys gels was approximately two times higher than that of TR4T at similar concentration. When disulfide bonds were removed, the modulus of the TR4T-Cys gel was comparable to that of TR4T at the same concentration. Hence, triple helix-based networks become more rigid in the presence of disulfide bonds. The reason for this reinforcement is probably that the stabilization by the disulfide bridges shifts the helix-coil equilibrium towards more helices. In addition, disulfide bridges can cross-link different triple helices, leading to hexameric (Figure 7.3B) or even larger nodes (Figure 7.3C). In this way, inactive loops can be connected to become active network strands.
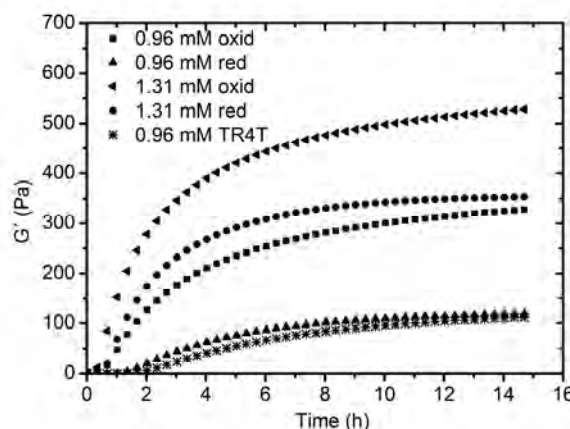
Figure 7.4 Storage modulus as a function of gel age at different protein concentrations, and with or without the presence of disulfide bonds (oxid: oxidizing; red: reduction).

Frequency sweeps were used to investigate the dynamic viscoelastic properties of TR4T-Cys gels. Storage and loss moduli as a function of frequency for different protein concentrations under both oxidizing and reducing conditions are presented in Figure 7.5A and 7.5B, at 15 °C and 20 °C, respectively. In all cases, the elastic behavior (G') dominates over the viscous behavior (G''). The storage modulus does not depend on the frequency in the range between 0.01 and 100 rad/s. The loss moduli decrease with frequency, go

126

through a minimum and then increase again. These behaviours are similar to those of TR4T gels and gelatin [6].

Creep experiments were carried out to get more insight in the behaviour at time scale above 100s. A constant stress was applied to the gels and the resulting deformation was measured as a function of time. The deformation is presented as a time-dependent compliance J(t) (Figure 7.5C and 7.5D). The creep curves are characterized by a rapid elastic response followed by a slow viscous response. The latter observation implies that we still have physical gels and the new covalent disulfide bonds do not lead to a percolating covalent network.
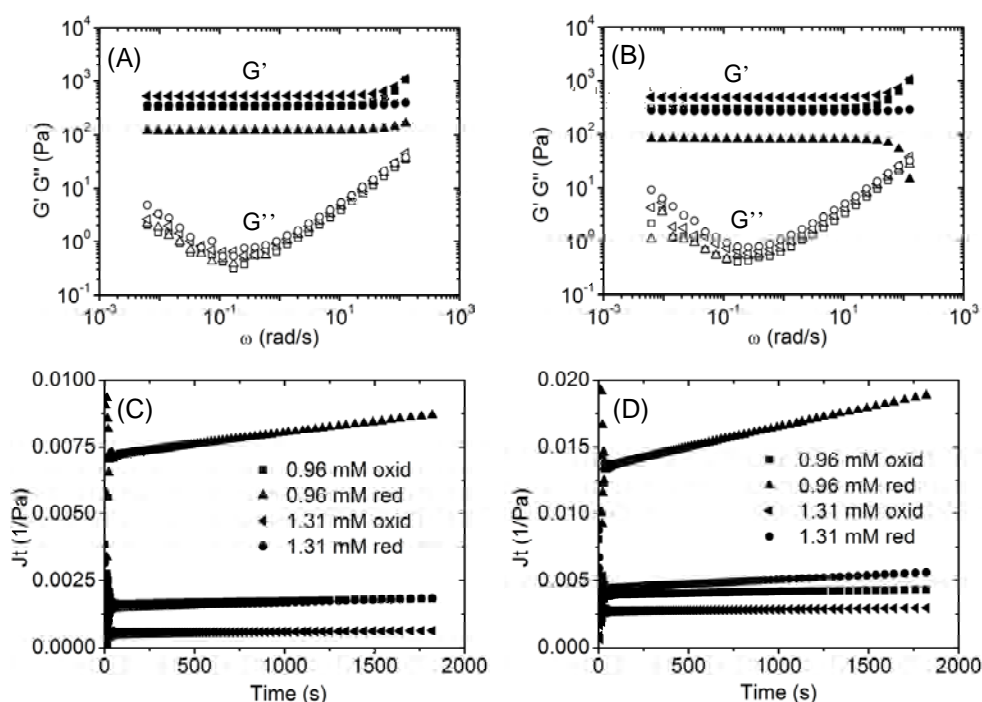
Figure 7.5 (A) Frequency sweeps at 15 °C with storage moduli (filled markers) and loss moduli (open marker) of TR4T-Cys at 0.96 mM oxid (square), 0.96 mM red (up-pointing tri-angle), 1.31 mM oxid (left-pointing triangle), 1.31 mM red (circle); (B) Frequency sweep at 20 °C; (C) Creep experiments at 15 °C; (D) Creep experiments at 20 °C for different protein concentrations under both oxidizing and reducing conditions.
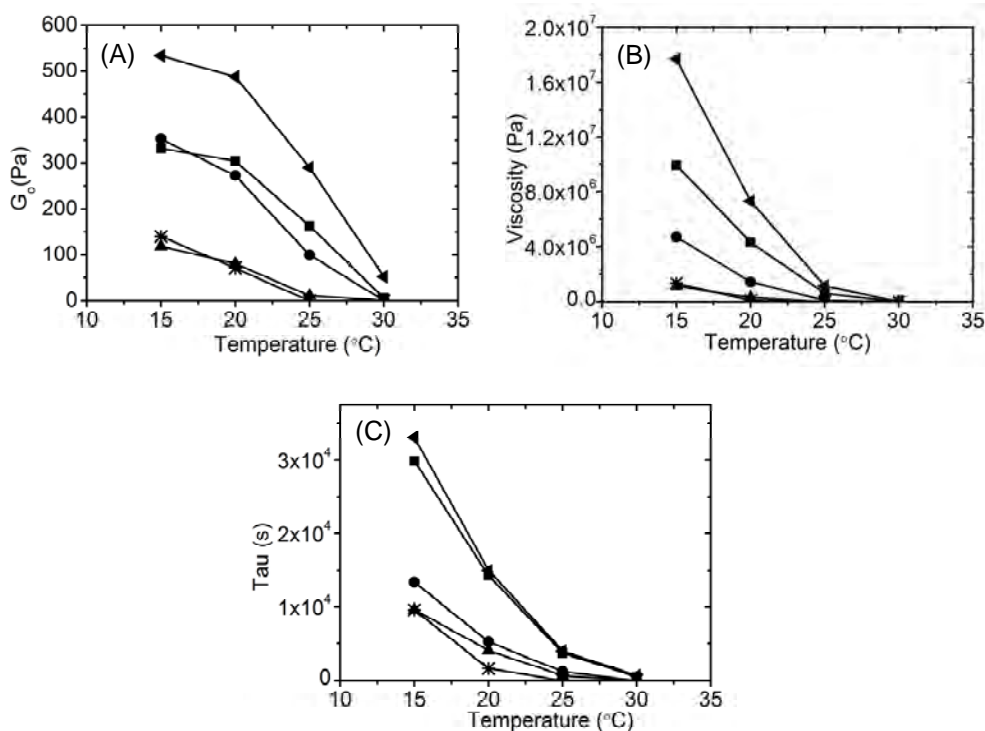
Figure 7.6 (A) Plateau storage modulus as a function of temperature; (B) Viscosity as a function of temperature; (C) Relaxation time as a function of temperature for different protein concentrations under both oxidizing and reducing conditions for: 0.96 mM TR4T-Cys oxid (square), 0.96 mM TR4T-Cys red (up-pointing tri-angle), 1.31 mM TR4T-Cys oxid (left-pointing triangle), 1.31 mM TR4T-Cys red (circle) and 0.96 mM TR4T as the symmetric molecule (star).

From the data in Figure 7.5, we calculated the plateau modulus G_0, the zero-shear viscosity η (the inverse slope of J=f(t) at long deformation times) and the relaxation time of the gels τ (η divided by G_0). In Figure 7.6, G_0, η and τ are plotted as a function of temperature for two different concentrations and in both oxidizing and reducing conditions. Under both oxidizing and reducing conditions, the storage modulus, the viscosity, and the relaxation time increased with concentration. As shown previously for TR4T, this increase is due to an increasing ratio between bridges and loops. As discussed above, the modulus of TR4T-Cys in oxidizing conditions is almost two times higher than that of TR4T gels, while in reducing conditions, removal of disulfide bonds resulted in a decreased of G_0 of the TR4T-Cys gels to the same value to the symmetric TR4T gels. Upon increasing the temperature, the gels melt and the modulus, viscosity and, relaxation time decrease rapidly.

The temperature where the gel melts is more or less the same in oxidizing and reducing conditions. The reason for this is that the gel properties already disappear as soon as the non-stabilized triple helices melt. After this, small clusters are probably still present, but these cannot form a percolating network. Moreover, the relaxation time (Figure 7.6C) almost triples under oxidizing conditions, which implies that triple helical knots are also kinetically stabilized by disulfide bonds, probably by suppressing two dangling ends in a triple helix with an intra-helical bond.

7.4. Conclusion

Using a protease disruptant of *Pichia pastoris*, we successfully produced the asymmetric block copolymer TR4T-Cys; a C-terminally cysteine-extended variant of our previously reported symmetric triblock TR4T. The gelation of the asymmetric TR4T-Cys is based on the formation of a physical network with triple helical nodes upon cooling. Besides, disulfide bonds between cysteine amino acids in TR4T-Cys strengthen and stabilize the triple helical nodes. Firstly, the presence of these disulfide bonds in TR4T-Cys resulted in a second melting temperature which was higher than that of the triple helical knot without the disulfide bonds. Secondly, the disulfide bonds dramatically strengthened the network as demonstrated by an almost two-times increased storage modulus, relaxation time and viscosity compared with values in the absence of disulfide bonds. Thus, we have created a dual-responsive physical network which is sensitive to temperature and the ambient redox potential. These physical gels might be promising biomaterials for tunable biomedical applications where multiple stimuli are used to trigger the physical properties. The redox potential is a particularly interesting stimulus for use in biomedical applications. For example, it has been demonstrated that the redox conditions between the intracellular and extracellular spaces are very different. Moreover, redox stimuli can be applied highly localized by using electrodes. Recent work has shown that the gel properties, such as the melting temperature, can be taiolerd further by changing the molecular design, for example by using longer T blocks [8].

References

1. M. Sutter, J. Siepmann, W. E. Hennink, W. Jiskoot, *J. Controlled Release*, 2007, **119** (3), 301-312.

2. B. S. Kim, D. J. Mooney, *J. Biomed. Mater. Res*., 1998, **41** (2), 322-332.

3. J. Kim, S. S. Kim, K. H. Kim, Y. H. Jin, S. M. Hong, S. S. Hwang, B. G. Cho, D. Y. Shin, S. S. Im, *Polymer,* 2004, **45** (10) 3527-3533.

4. M. W. T. Werten, H. Teles, A. P. H. A. Moers, E. J. H. Wolbert, J. Sprakel, G. Eggink, F. A. de Wolf, *Biomacromolecules,* 2009, **10** (5), 1106-1113.

5. P. J. Skrzeszewska, F. A. de Wolf, M. W. T. Werten, A. P. H. A. Moers, M. A. Cohen Stuart, J. van der Gucht, *Soft Matter,* 2009, **5** (10), 2057-2062.

6. P. J. Skrzeszewska, F. A. de Wolf, M. A. Cohen Stuart, J. van der Gucht, *Soft Matter,* 2010, **6**, 416-422.

7. H. Teles, P. J. Skrzeszewska, M. W. T. Werten, J. van der Gucht, G. Eggink, F. A. de Wolf, *Soft Matter,* 2010, **6**, 4681-4687.

8. C. I. F. Silva, H. Teles, M. D. Golinska, M. W. T. Werten, G. Eggink, F. A. de Wolf, *Biomacromolecules,* 2012, **13** (5), 1250-1258.

9. S. P. Chambers, S. E. Prior, D. A. Batstow, N. P. Minton, *Gene,* 1988, **68** (1), 139-149.

10. J. Wang, M. A. Cohen Stuart, A. T. M. Marcelis, M. Colomb-Delsuc, S. Otto, J. van der Gucht, *Macromolecules,* 2012, **45** (17), 7179-7185.

11. H. Zhao, P. H. Brown, P. Schuck, *Biophys. J.,* 2011, **100** (9), 2309-2317.

12. C. I. F. Silva, H. Teles, A. P. H. A. Moers, G. Eggink, F. A. de Wolf, M. W. T. Werten, *Biotechnol. Bioeng.,* 2011, **108** (11), 2517-2525.

13. M. W. T. Werten, F. A. de Wolf, *Appl. Environ. Microbiol.,* 2005, **71** (5), 2310-2317.

Appendix
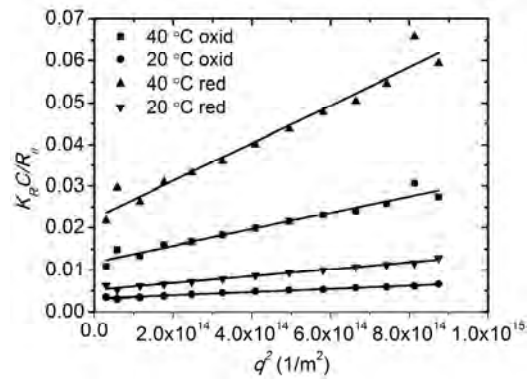
Figure A7.1 Dependence of $K_R C/R_\theta$ on detection angle at different temperature in both oxidizing and reducing conditions.

Chapter 8

Summary and General Discussion

8.1.   Summary

The increasing demand of functional biomaterials for medical applications has boosted the development of new types of hydrogels based on bio-mimetic polymers. These polymers surpass the synthetic ones in many aspects due to their lower toxicity, and better biocompatibility and biodegradability. Breakthroughs in genetic engineering have provided new approaches to design such materials. Recombinant techniques allow the combination of different motifs from various natural proteins into one polypeptide molecule which may thereby acquire selected properties and functionalities of the original protein domains. Moreover, many aspects such as precise composition and tunable regulation of length and amino acid sequence are achievable. Such tools also help the creation of highly repetitive polypeptide blocks merged together into a unique artificial protein molecule. The materials produced using these recombinant techniques are called protein-engineered materials [1].

Many of the bio-inspired motifs used in these materials are responsive to a certain stimulus. For example, their self-assembly may be induced by a change in temperature or pH, or by adding an additional component. Multi-stimuli responsive materials can also be made by combining motifs that respond to different stimuli in one design.

In this thesis, we present the design, production and characterization of biomimetic network formers (Table 8.1) which are based on an asymmetric triblock design. The two end-blocks, which are sensitive to different stimuli, reversibly self-assemble upon triggering, leading to network formation. All polymers are designed by genetic engineering and produced by fermentation of genetically modified *Pichia pastoris*, as described in **chapter 2**. The amino acid sequences of the two reactive end-blocks are based on natural protein motifs including elastin, silk, collagen-like triple helix and poly cationic domains. An inert random-coil block is used as a spacer between the two end blocks. Different kinds of asymmetric triblocks are discussed in this thesis.

A triblock copolymer protein (SCE) inspired by silk and elastin is analyzed in **chapters 3 and 4**. The silk-like block (S) is comprised of 12 (GAGAGAGE) repeats and forms a pH-sensitive beta-roll (beta-sheet like) structure that further stacks into long fibrils. The elastin-like block (E) consists of 40 (VPGXG) repeats and has thermo-responsive properties; above the lower critical solution temperature (LCST), it forms aggregates. In **chapter 3**, we find that polymers that have both silk and elastin-like domains show

temperature-dependent fibril formation. At high temperature, the elastin blocks irreversibly induce bundling and aggregation of the fibrils. The presence of a random-coiled spacer (C) between the functional blocks helps to decouple their mutual interactions, thus reducing the sensitivity to temperature somewhat. We also find that the presence of the elastin block changes the kinetics of fibril formation. Whereas silk-like proteins without elastin blocks form monodisperse fibrils, the presence of the elastin-like block leads to polydisperse fibrils with a length that depends on concentration. This suggests that homogeneous nucleation can take place in the asymmetric triblocks, whereas the symmetric S-C-S or C-S-C triblocks, without elastin, could not nucleate homogeneously.

Name	Structural information
SCE	S: silk-like block, C: random coil, E: elastin-like block
TR4H	T: collagen-like triple helix, R: random coil, H: poly(histidine), hexamer
TR4K	T: collagen-like triple helix, R: random coil, K: poly(lysine), hexamer
TR4T-Cys	T: collagen-like triple helix, R: random coil, Cys: cysteine

Table 8.1 Asymmetric triblock protein polymers studied in this thesis.

In **chapter 4**, the self-assembly of the silk-elastin-like polymer SCE is further characterized in the presence of NaCl. We find that the thermo-responsive aggregation of the E block is strongly dependent on the salt concentration. At high salt concentration, the aggregation transition is much more pronounced. At high pH, where the S block does not self-assemble, the polymer forms micellar aggregates upon heating in the presence of NaCl. At low temperature, lowering the pH leads to fibril formation. When both blocks are induced to self-assemble, the final structure reveals a pathway-dependence. Heating the solution of fibrils formed at low temperature results in fibril aggregates which do not dissociate upon cooling. The pH-triggered fibril formation of preheated protein solutions leads to the formation of large objects, which likely cause sedimentation. The structural difference is also demonstrated clearly in the morphology of gels formed at high protein concentration: whereas the gel formed in the first pathway (first lower the pH, then increase the temperature) is transparent, the gel formed in the latter pathway (first increase the temperature, then lower the pH) is milky and has a higher elastic modulus.

In **chapter 5 and 6**, we characterize an asymmetric triblock copolymer (TR4H or TR4K), which has a collagen-like, triple-helix-forming motif at one end, and a poly cationic block at the other. The collagen-like end-block T consists of 9 (PGP) repeats and forms thermo-responsive triple helices upon cooling. Such helices are reversibly disrupted when the temperature is raised above the melting temperature. The other end-block has 6 positively charged amino acids (histidine-H or lysine-K) and forms micelles when a negatively charged polymer is added. The charge-driven complexation of this block depends on its degree of deprotonation, which is determined by the pKa and the pH. The additives used in this study are a flexible polyanion (polystyrene sulfonate, PSS) and a semi-flexible polyanion (xanthan). **Chapter 5** describes the micelle-to-network transition of the triblock TR4H with PSS. First, the self-assembly of each end-block is studied separately. As expected, the collagen-like block reversibly forms triple helices upon cooling. The cationic H block forms charge-driven complexes upon adding PSS, leading to micelles with an aggregation number that depends on ionic strength. At high concentration, the micellar TR4H/PSS solutions form a viscoelastic gel upon cooling (Figure 8.1 A), which melts at high temperature, indicating the formation of helical junctions between the micelles. Liquid-liquid phase separation is observed when the concentration is below the gelation point (around 90 g/L). This leads to a dilute phase on top of a concentrated gel phase (Figure 8.1 B). The phase separation is driven by the attraction between charge-driven micelles caused by the triple helices. It disappears when the solution is heated or when the ionic strength is increased.

Charge-driven complexation of the same type of triblock copolymer, TR4K, with xanthan, a semi-flexible polyelectrolyte is presented in **chapter 6**. Xanthan is a negatively charged polysaccharide with a contour length of about 1.5 µm and high polydispersity. At high temperature and at very low xanthan concentration, the TR4K binds to the xanthan backbone via the charged block K, leading to charge-driven bottle brushes, as indicated by a significant increase in light scattering intensity due to the increased mass. This interaction is dependent on the pH, due to protonation of the cationic K block. The xanthan/TR4K complex shows thermo-sensitivity due to the helical interaction of the collagen-like blocks. At a xanthan concentration around the overlap concentration (7 g/L), the presence of the triblock results in an increase in elastic modulus of xanthan gels. At high temperature, the elastic modulus increases by 3 times after adding the triblock. As triple helices do not

136

form, this must be due to changes in the entanglement of the bottle brushes. Also the non-linear rheology of the xanthan/triblock gels differs significantly from that of xanthan alone. While xanthan gels are known to be shear-softening and melt at a strain of 100 % due to the alignment of xanthan molecules, the xanthan/TR4K gels have two-step strain softening, in which the first step is probably due to unbinding of the proteins from the xanthan backbone. At low temperatures when the helical junctions are formed, the elastic modulus increases even further approximately two times compared with the corresponding value at high temperature. This is ascribed to the formation of crosslinks induced by the proteins between the xanthan molecules.
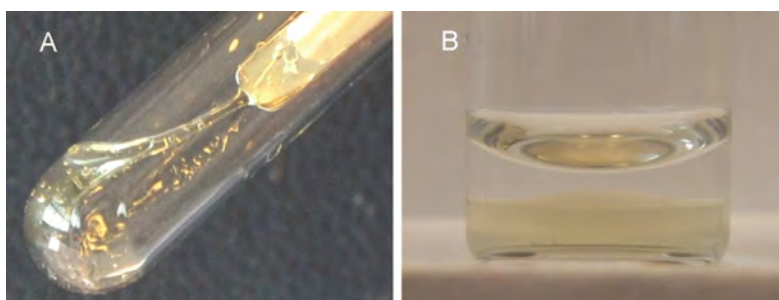
Figure 8.1 (A) A physical gel formed by thermo-triggering TR4H/PSS complexation at high concentration (150 g/L). (B) Phase separation upon thermo-triggering TR4H/PSS complexation at low concentration (40 g/L).

In **chapter 7**, we discuss an asymmetric triblock copolymer, which has two triple helix forming end-blocks, with a cysteine residue added to one of these [2]. Under oxidizing conditions, the cysteine residues can form disulfide bonds between two polymers whereas reducing conditions restore the thiol groups. Since cysteine can form only one S-S bridge, intramolecular loops are prevented. The presence of S-S bonds significantly enhances the thermal stability of the triple helical network. This results in the appearance of two melting temperatures, of which the higher one is due to the S-S stabilized triple helices. The elastic modulus of the physical gels in the presence of S-S bonds is almost 2 times higher than that of the physical gels in the absence of S-S bonds. The relaxation time also triples under oxidizing conditions, which indicates that triple helical knots are also kinetically stabilized by S-S bonds.

8.2.   General discussion

We started our study on bio-inspired hybrid networks by designing and producing dual-responsive (or multi- responsive) asymmetric triblock protein polymers. This concept is relatively new; and after finishing this thesis, there are still many questions to be answered. We first discuss some of these questions for the three specific protein polymers studied in this thesis. Then we discuss more generally what the problems and promises are of asymmetric protein polymers.

Silk-elastin based hybrid network (SCE)

The combination of domains from natural silk and natural elastin was first explored by Cappello a few decades ago [3]. These studies have attracted other researchers to further engineer these motifs into different block copolymers [4, 5] and manipulate them into various structures [6-8]. The structures formed by the elastin-like blocks are typically quite dynamic and relatively weak, so that they can easily reorganize. The silk-like blocks, by contrast, organize in a more stable way into crystalline arrays, which can therefore be kinetically directed towards different structures. This substantial difference of the two self-assembling blocks likely plays a key role in the resulting structures. In this thesis, we report a hybrid molecule which has two end blocks spaced by a large hydrophilic random coil. The spacer decouples the local interactions between the silk-like and elastin-like blocks, but its high hydrophilicity increases the transition temperature of the elastin-like block. With regard to optimizing the design, the length of the spacer block deserves more attention. Indeed, the effects of the fused domain on the transition temperature in elastin-containing block copolymers have been reported elsewhere [9, 10]. However, the estimation of such effects might have large variations depending on the composition of the elastin-like block. To reduce the transition temperature of the elastin-like block, the (VPGXG) peptides should contain hydrophobic amino acids at the X position. The fused middle block might have less interference on the transition temperature, when it would be less hydrophilic; in polymer jargon: when it is closer to the θ-temperature. Varying the length ratio between the two reactive blocks might also be interesting. The silk-like block might contribute to the overall hydrophobicity of the protein polymer, thus affecting the transition temperature as well.

The pH-sensitive self-assembly of silk-like block can also be controlled by changing the charged amino acid.

In the conditions that both S and E blocks are triggered, the self-assembly of this hybrid network is a non-equilibrium process. We find that the final structures highly depend on the triggering order. This opens a whole new variety of kinetic self-assembly, which also implies more difficulties to precisely control the processes. Thus, it is necessary to regulate the involved parameters, and the relative reaction rates become important. Many factors such as pH, ionic strength, solvent and surface induction, might affect the assembling processes, resulting into various final structures [11-14]. Perhaps, one way to systematically investigate silk-elastin hybrid network is to mix the asymmetric SCE polymer with the symmetric silk block which forms strong fibrillar and pH-responsive gels at low protein concentration [15]. Most likely, the two species will co-assemble to composite fibrils. Mixture of these two polymers might therefore allow varying the thickness of the fibrils and probably the mechanical properties, and the temperature-responsiveness of the mixed gels as well.

Collagen-like triple helix and poly-cationic hybrid network (TR4H or TR4K)

Since the discovery of the ordered-triple helices in gelatin, their properties have been exploited and adapted into many engineered-block copolymers [16-19]. Their thermo-sensitive properties make them promising materials. In this research, we combined a triple helix-forming domain with a charged-block, which co-assembles with an oppositely charged additive, thus making the physical gels responsive to multiple stimuli. The charge complex can serve as thermo-sensitive nano-carrier [20] or nanoparticle vaccine [21]. It would be interesting, therefore, to study the electrostatic binding of the triblock with different types of molecules such as DNA, di(triblock) polymer, or other charged proteins. Preliminary experiments show that our triblock can indeed be used to condense DNA (Figure 8.2).

Without an added polyanion, the triblock TR4H can only form triple helix, while the random coil and charged block cannot self-assemble. This means that this molecule would acts as a gel stopper in a system of symmetric TR4T molecules. Mixtures of the two molecules might lead to microgel dispersions that may be comparable to natural casein micelles (Figure 8.3). The mixtures might also have interesting rheological features depending on the average domain size and the mixing ratio. The crosslinks induced by

TR4K triblock polymer on semi-flexible polyelectrolytes (xanthan) results in storage modulus and shear-thinning property of xanthan gels. The xanthan/TR4K system might possibly share the exciting property of nonlinear elasticity with biological gels such as actin, fibrin, and neurofilament.
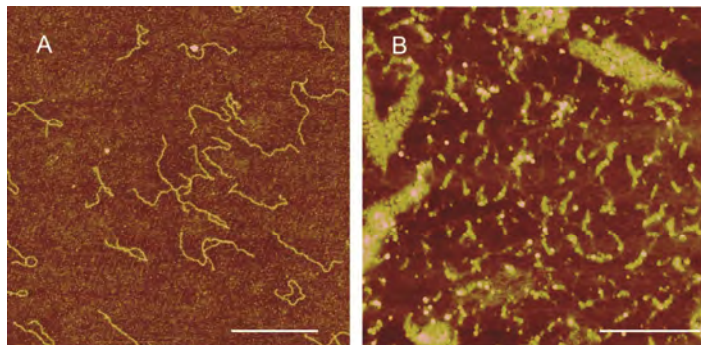
Figure 8.2 DNA coated with TR4K. (a) DNA bottle brushes at high temperature (b) Condensation of coated DNA at low temperature. Scale bars correspond to 500 nm.
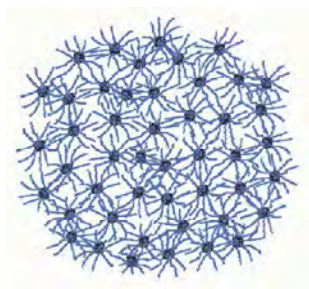
Figure 8.3 Casein micelles (adapted from a book [22]).

As a design parameter, we can consider the length of various blocks. A shorter spacer might provide less steric hindrance, thus allowing the end-blocks to associate more easily. The cationic block can be elongated to improve the electrostatic interaction or replaced by a different amino acid so that the charge-driven complexation can occur at a desired pH. The length of the triple helix block can be tuned to optimize the melting temperature of the physical gel [23] .

Triple helix-based triblock modified with cysteine (TR4T-Cys)

Physical gels formed by symmetric triple helix-forming triblocks, TR4T, without cysteine have been well-characterized [18, 24]. The addition of one cysteine at one end of the polymer results in a significant improvement in visco-elastic properties and thermo-stability. Collagen triple-helix folding consists at least of two slow steps: nucleation and zipper-like propagation. Both of them require the cis–trans isomerization of numerous prolines/hydroxyprolines, a process with high activation energy and temperature dependence [25, 26]. The dimerization due to S-S bonds might lead to acceleration of the nucleation step. Furthermore, it has been reported that S-S bridges contribute to the formation of collagen-like fibrils [27] from short synthetic collagen fragments with sticky ends, in which the three strands are held in a staggered array by disulfide bonds via intermolecular triple-helix formation. In nature, the type XIII collagen and the cartilage matrix protein, i.e. matrilin-1, are subsequently stabilized through interchain disulfide bonds, resulting in a stable trimer [28]. There might be the formation of helical nodes larger than trimers in synthetic collagen-like peptides [27] or natural collagen VII [29]. Therefore, further investigations might be needed to reveal the contribution of S-S bridges to structural properties of this triple helical gel, but it is beyond any doubt that they stabilize the helices in their vicinity.

The added cysteine residue may also be useful for specific labeling, for example maleimide-linked dyes [30]. It also serves as a ligand-binding site to other thiol-modified surfaces, particles or molecules [31], which is of interest for applications including medical implants and cell supports. Similarly, our triblock could be used as thermo-sensitive biocompatible shell to modify nanoparticles [32].
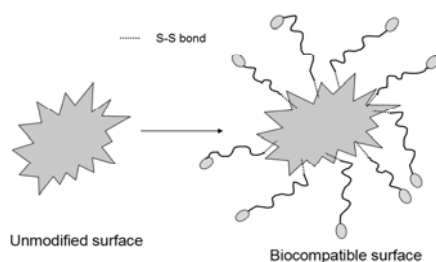
Figure 8.4 Modified nanoparticle/surface for biocompatibility.

8.3. Motivation aspect of the hybrid networks

With the increasing demands of high performance biomaterials, network-forming components must be able to build a physical gel under narrowly defined conditions. The well-known class of telechelic polymer S-C-S (S: functional end-block, C: connector) displays various interesting dynamic behaviors including shear banding, self-assembly, rheochaos, and phase-separation [18, 33, 34]. Another aspect is the functionality of the end-block which self-assembles upon triggering. However, connectors often return to the same nodes, resulting in loop formation. Loop formation is a structural imperfection that weakens network connectivity and lowers the material's elasticity. The asymmetric triblock with two different end-blocks is designed in order to: (1) prevent unimolecular loops and improve mechanical properties (2) achieve multi-responsiveness: this allows us to observe different assembling pathways. In this work, with respect to (1), we indeed observed the decrease in loop formation in physical gels formed by TR4T-Cys due to the formation of S-S bridges. With respect to (2), we indeed obtained multi-responsive hydrogels with all three asymmetric triblock proteins. However, we have only scratched the surface as understanding kinetics of self-assembly and pathway dependent processes. Further investigations are needed to get more insights into how to manipulate various parameters in controlling the final structures.

Regarding the design aspect, alternative motifs for the end-block might also be 'coil-coil', a versatile protein folding motif [35]; 'leucin zipper' , common three-dimensional structural motif in proteins [36]; 'β-hairpin secondary structure' (MAX1, a 20-residue peptide) via a pH-promoted intramolecular folding event [37]. The thermal stability of the coiled-coil containing proteins can also be manipulated in a predictable way by substituting amino acids in the coiled-coil domain [38]. Besides cysteine, tyrosine can be incorporated to obtain di-tyrosine crosslinks [39] between polymers.

8.4. Toward application

Although this research does not focus on a specific application, it presents a novel design of protein-engineered materials directed toward the preparation of high performance materials. It gives examples illustrating some promises of recombinant protein engineering as a tool for material synthesis. The engineered materials combine several of the

advantages of natural and synthetic materials. While natural materials are chosen for biotechnological applications because of their known bioactivity, biocompatibility and susceptibility to denaturation or degradation, synthetic materials offer improved control over material composition and resultant properties together with flexibility in design [1]. Protein-engineered biomaterials may combine all these advantages. One of the fields, where these materials may have impacts is in biomedicine.

Tissue engineering

Materials for tissue engineering have to mimic the *in vivo* cellular environment, and implant materials provide a scaffold to help tissue healing. The key engineering strategy focuses on soft materials in which recruitment of endogenous progenitor cells, endothelial cells and osteoblasts takes places. This improves healing process and avoids immunogenic responses in the host. For instance, in bone implant, the materials should be not only biodegradable but adaptable to the site and shape of the wound. A fluid cell-recruitment system that can be easily injected from a needle, allowing a minimally invasive procedure would be desired.

Challenges confronted by medicine today include the increasing demand for sensitive, efficient systems and approaches, which will improve responses to pathology. Hence, responsive protein-based materials which can adapt to the environment, and are capable of conformational changes on receiving an external signal such as a change in pH or temperature, attract a lot of attention. Crosslinkable elastin-like polypeptide (ELP) gels were applied to cartilage matrix repair in critically sized defects in goat knees [40]. These studies showed an ability of the crosslinked ELP to support cell infiltration, and to be resorbed from the defect site. Collagen gels are attractive, since they can act as a "cage" to retain cells or as gene delivery complexes, which are larger than drugs and therapeutic proteins [41]. Condensed cellular seeded collagen gel was used as a matrix scaffold for treatment of focal defects of articular cartilage [42]. Collagen-based gels are approved by the FDA for wound healing under the commercial name Excellagen. The potential of our novel hydrogel design is mostly in cases where the sol-gel transition is important. For example, in many tissue engineering applications, a stimuli responsive system is needed for injection and in-situ gelation. In most cases, a thermo-responsive material is used, in which the change from room temperature to body temperature induces gelation [43]. The hydrogels

formed by hybrid triblocks SCE and TR4T-Cys are mostly suitable for tissue engineering as manipulated scaffolds. The gel structure and the resulting mechanical properties depend on concentration, temperature, and pH. Hydrogels formed by TR4T-Cys seem to be suitable for soft tissue implants where fluid-gel transition is needed in gelation. The protein solution is fluid above a certain melting temperature (T_m) and forms a gel below T_m in the course of time. SCE might be suitable for hard tissue implants where the materials can form stiff gels. Besides, the physical gels formed by SCE highly depend on the crystalline process of silk fibers that serves as scaffolds similar to the dense fibrillar networks in vivo-like tissues. Moreover, two-component systems which gel in a reasonable time after mixing are also an option for bone tissue engineering [44] or cell encapsulation [45]. Thus, a mixture of the TR4K (or TR4H) micellar solution with an appropriate charged component might be applicable.

Drug delivery

One of the essential goals of medical treatment is to ensure that the required amount of an agent is available at the target location at a specific time. Therefore, efforts have been made to increase the precision of delivery system and its adaption to the external environment such as pH and temperature. It is not surprising that regenerative medicine and drug delivery are utilizing similar responsive strategies in a bio-mimetic fashion. Different organs, tissues and cellular compartments may have differences in pH, which makes the pH a suitable stimulus. In oral delivery, for example, pH-sensitive hydrogels are selected for the specific pH of colon or intestine where the charge-driven complexes dissociate, which results in drug release.

Cationic polymers are excellent carriers for gene therapy. For example, PAMAM-PEG-mannose dendritic-linear hybrid polymer is an effective system for DNA delivery with low toxicity [46]. The thermally responsive polymer is designed to be systemically soluble when injected in vivo, but to become insoluble and accumulate in a locally heated tumor. Two polymer systems that exhibit a LCST phase transition, namely poly(N-isopropylacrylamide) and elastin-like polypeptides, are both suitable for hyperthermia [47]. The use of a redox-responsive material is applicable for intracellular protein therapeutics, for example a disulfide-containing crosslinker can be used for making responsive single-protein nanocapsules [48].

144

Although permanent gels are widely used for drug release, they have some disadvantages such as incomplete release, poor biodegradability and even cellular toxicity. Such problems might be overcome by using physical hydrogels formed by dissociable joints. The potentials of our designed physical hydrogels for drug delivery can be found in all three hybrid networks. The pH-responsive SCE hydrogels would be fit for drug delivery to the intestine system or the colon. The hybrid can be designed so that the hydrogels can be dissociated at a specific pH. The LCST of elastin-like block in SCE might also be considered for hyperthermia. The TR4K network former can bind to charged molecules, thus providing a possibility for DNA delivery or for any other charged agent. The hydrogels formed by TR4T-Cys that are simultaneously responsive to temperature and redox-potential are perhaps applicable for intracellular therapeutics. Moreover, the cysteine can be used to incorporate an active agent via the thiol group to be slowly released at the target site.

In summary, we have focused on the concept of multi-responsive gelation in this thesis. For real applications, the designed systems definitely need various improvements so that the sensitive soft materials form at physiological conditions. Other aspects of the gel properties would also have to be considered such as erosion rate, life span and probably biocompatibility as well.

8.5. Conclusion

In this chapter, we have discussed the perspectives for further investigation of our bio-inspired network formers and their future applications. There lie many challenging research opportunities ahead and there is a necessity to improve the engineered materials to meet desired application criteria. Nevertheless, the outcomes of this thesis pave a way to future development of high performance materials. We hope our presented work provides useful and informative suggestions to inspire and encourage deeper studies on such bio-inspired hybrid networks.

References

1. R. L. DiMarco and S. C. Heilshorn, *Adv. Mater.*, 2012, **24**, 3923-3940.

2. M. W. T. Werten, H. Teles, A. P. H. A. Moers, E. J. H. Wolbert, J. Sprakel, G. Eggink and F. A. de Wolf, *Biomacromolecules,* 2009, **10**, 1106-1113.

3. J. Cappello, J. Crissman, M. Dorman, M. Mikolajczak, G. Textor, M. Marquet and F. Ferrari, *Biotechnol. Prog.*, 1990, **6**, 198-202.

4. M. Haider, V. Leung, F. Ferrari, J. Crissman, J. Powell, J. Cappello and H. Ghandehari, *Mol. Pharm.*, 2005, **2**, 139-150.

5. X. X. Xia, Q. Xu, X. Hu, G. Qin and D. L. Kaplan, *Biomacromolecules*, 2011, **12** 3844-3850.

6. Y. Ner, J. A. Stuart , G. Whited and G. A. Sotzing, *Polymer,* 2009, **50**, 5828-5836.

7. W. Hwang, B. H. Kim, R. Dandu, J. Cappello, H. Ghandehari and J. Seog, *Langmuir*, 2009, **25**, 12682-12686.

8. R. Anumolu, J. A. Gustafson, J. J. Magda, J. Cappello, H. Ghandehari and L. F. Pease, *ACS Nano*, 2011, **5** 5374-5382.

9. K. Trabbic-Carlson, D. E. Meyer, L. Liu, R. Piervincenzi, N. Nath, T. LaBean and A. Chilkoti, *Protein Eng. Des. Sel.*, 2004, **17**, 57-66.

10. T. Christensen, W. Hassouneh, K. Trabbic-Carlson and A. Chilkoti, *Biomacromolecules,* 2013, **14**, 1514-1519.

11. N. J. Edwin, R. P. Hammer, R. L. McCarley and P. S. Russo, *Biomacromolecules*, 2010, **11**, 341-347.

12. B. Dai, S. g. Kang, T. Huynh, H. Lei, M. Castelli, J. Hua, Y. Zhang and R. Zhou, *PNAS* 2013, **110**, 8543-8548.

13. Z. Shao and F. Vollrath, *Polymer,* 1999, **40**, 1799-1806.

14. M. Schor, A. A. Martens, F. A. de Wolf, M. A. Cohen Stuart and P. G. Bolhuis, *Soft Matter*, 2009, **5**, 2658-2665.

15. A. A. Martens, G. Portale, M. W. T. Werten, R. J. de Vries, G. Eggink, M. A. Cohen Stuart and F. A. de Wolf, *Macromolecules,* 2009, **42**, 1002-1009.

16. S. B. Ross-Murphy, *Polymer*, 1992, **33**, 2622.

17. L. E. R. O'Leary, J. A. Fallas, E. L. Bakota, M. K. Kang and J. D. Hartgerink, *Nature Chemistry,* 2011, **3**, 821-828.

18. P. J. Skrzeszewska, F. A. de Wolf, M. W. T. Werten, A. P. H. A. Moers, M. A. Cohen Stuart and J. van der Gucht, *Soft Matter*, 2009, **5**, 2057-2062.

19. H. J. Lee, J. S. Lee, T. Chansakul, C. Yu, J. H. Elisseeff and S. M. Yu, *Biomaterials,* 2006, **27**, 5268-5276.

20. M. T. Calejo, A. M. S. Cardoso, A. L. Kjøniksen, K. Zhu, C. M. Morais, S. A. Sande, A. L. Cardoso, M. C. P. de Lima, A. Jurado and B. Nyström, *Int. J. Pharm.*, 2013, **448**, 105-114.

21. J. H. van den Berg, K. Oosterhuis, W. E. Hennink , G. Storm, L. J. van der Aa, J. F. J. Engbersen, J. B. A. G. Haanen, J. H. Beijnen, T. N. Schumacher and B. Nuijen, *J. Control. Release*, 2010, **141**, 234-240.

22. C. G. De Kruif and C. Holt, *Advanced Dairy Chemistry, Proteins (3 rd edition)* 2003, **Kluwer Academic/Plenum Publishers, New York**, 233-276.

23. C. I. F. Silva, P. J. Skrzeszewska, M. D. Golinska, M. W. T. Werten, G. Eggink and F. A. de Wolf, *Biomacromolecules,* 2012, **13**, 1250-1258.

24. P. J. Skrzeszewska, F. A. de Wolf, M. A. Cohen Stuart and J. van der Gucht, *Soft Matter*, 2010, **6**, 416-422.

25. H. P. Bachinger, P. Bruckner, R. Timpl and J. Engel, *Eur. J. Biochem.*, 1978, **90**, 605-613.

26. Y. Xu, T. Hyde, X. Wang, M. Bhate, B. Brodsky and J. Baum, *Biochemistry,* 2003, **42**, 8696-8703.

27. F. W. Kotch and R. T. Raines, *PNAS,* 2006, **103**, 3028-3033.

28. A. Snellman, A. Tuomisto, A. Koski, A. Latvanlehto and T. Pihlajaniemi, *J. Biol. Chem.*, 2007, **282**, 14898-14905.

29. M. Chen, D. R. Keene, F. K. Costa, S. H. Tahk and D. T. Woodley, *J. Biol. Chem.*, 2001, **276**, 21649-21655.

30. Y. Kim, S. O. Ho, N. R. Gassman, Y. Korlann, E. V. Landorf, F. R. Collart and S. Weiss, *Bioconjugate Chem.*, 2008, **19**, 786-791.

31. M. M. Stevens and J. H. George, *Science,* 2005, **310**, 1135.

32. D. Suzuki and H. Kawaguchi, *Langmuir*, 2005, **21**, 8175-8179.

33. S. Manneville, A. Colin, G. Waton and F. Schosseler, *Phys. Rev. E,* 2007, **75**, 061502.

34. A. Finne, N. Andronova and A. C. Albertsson, *Biomacromolecules,* 2003, **4**, 1451-1456.

35. C. Xu and J. Kopecek, *Pharmaceut. Res.*, 2008, **25**, 674.

36. W. Shen, J. A. Kornfield and D. A. Tirrell, *Macromolecules,* 2007, **40**, 689-692.

37. J. P. Schneider, D. J. Pochan, B. Ozbas, K. Rajagopal, L. Pakstis and J. Kretsinger, *J. Am. Chem. Soc.,* 2002, **124**, 15030-15037.

38. J. Kopeček, *Biomaterials*, 2007, **28**, 5185-5192.

39. J. G. Jee, S. J. Park and H. J. Kim, *Rapid Commun. Mass Spectrom.*, 2000, **14**, 1563-1567.

40. D. L. Nettles, K. Kitaoka, N. A. Hanson, C. M. Flahiff, B. A. Mata, E. W. Hsu, A. Chilkoti and L. A. Setton, *Tissue Eng. Part A.*, 2008, **14**, 1133-1140.

41. D. G. Wallacea and J. Rosenblatt, *Adv. Drug Deliv. Rev.*, 2003, **55**,1631-1649.

42. R. Mueller-Rath, K. Gavénis, S. Andereya, T. Mumme, M. Albrand , M. Stoffel , D. Weichert and U. Schneider, *Bio-Med. Mater. Eng.*, 2010, **20** 317-328.

43. D. Schmaljohann, *Adv. Drug Deliv. Rev.*, 2006, **58**, 1655-1670.

44. I. C. Bonzani, R. Adhikari, S. Houshyar, R. Mayadunne, P. Gunatillake and M. M. Stevens, *Biomaterials,* 2007, **28**, 423-433.

45. C. T. S. Wong Po Foo, J. S. Lee, W. Mulyasasmita, A. Parisi-Amon and S. C. Heilshorna, *PNAS*, 2009, **106**, 22067-22072.

46. K. C. Wood, S. R. Little, R. Langer and P. T. Hammond, *Angew. Chem. Int. Ed.,* 2005, **44**, 6704-6708.

47. A. Chilkoti, M. R. Dreher, D. E. Meyer and D. Raucher, *Adv. Drug Deliv. Rev.*, 2002, **54**, 613-630.

48. M. Zhao, A. Biswas, B. Hu, K. I. Joo , P. Wang , Z. Gu and Y. Tang, *Biomaterials,* 2011, **32**, 5223-5230.

Samenvatting

De toenemende vraag naar functionele biomaterialen voor medische toepassinge heeft een sterke stimulans gegeven aan de ontwikkeling van nieuwe typen hydrogelen gebaseerd op biomimetische polymeren. Deze polymeren overtreffen de synthetische polymeren in veel opzichten, dankzij hun lagere toxiciteit, betere biocompatibiliteit, en bio-afbreekbaarheid. Doorbraken in gentechnologie hebben nieuwe mogelijkheden geopend om zulke materialen te ontwerpen. Recombinant technieken maken het mogelijk karakteristieke stukjes (motieven) uit verschillende natuurlijke eiwitten te combineren tot een enkele polypeptide molecuul dat daardoor bepaalde en geselecteerde eigenschappen en functionaliteiten van de oorspronkelijke eiwitten verkrijgt. Bovendien kan men veel aspecten van het ontwerp, zoals de samenstelling, de lengte en de aminozuurvolgorde, nauwkeurig bepalen. Het is dan ook mogelijk langs deze weg sterk repetitieve polypeptide blokken te creëren en die samen te voegen tot een uniek kunstmatig eiwitmolecuul. De materialen die met deze recombinant methode worden geproduceerd noemt men eiwit-technologische materialen.

Veel van de bio-geïnspireerde motieven die in deze materialen gebruikt worden reageren op een bepaalde stimulus. Ze kunnen bijvoorbeeld zelf-assemblage vertonen die op gang wordt gebracht door een verandering in temperatuur of pH, of door toevoeging van een component. Materialen die op meerdere stimuli reageren kunnen eveneens worden gemaakt, door motieven met verschillende stimuli samen te brengen in een ontwerp.

In dit proefschrift presenteren we het ontwerp, de productie en de karakterisering van biomimetische netwerkvormers (tabel 8.1) die gebaseerd zijn op een asymmetrische blokkenstructuur. De beide eindblokken zijn zo gekozen dat ze gevoelig zijn voor verschillende stimuli, en reversibel associëren; wanneer ze dat beide doen ontstaat een netwerk. Alle polymeren zijn ontworpen met behulp van gentechnologie en geproduceerd door middel van fermentatie van de genetisch gemodificeerde gist *Pichia Pastoris*, zoals beschreven in **Hoofdstuk 2**. De aminozuursequenties van de twee reactieve eindblokken zijn veelal gebaseerd op natuurlijke eiwitmotieven en secundaire structuren zoals die voorkomen in elastine, zijde en collageen (bijvoorbeeld een drievoudige helix), maar omvatten ook meer kunstmatige sequenties zoals een polykationisch blok. Een inert blok, dat een wanordelijke (statistische) kluwen vormt wordt gebruikt als verbinding tussen de

twee eindblokken. Verscheidene soorten asymmetrische triblokken worden in dit proefschrift besproken.

Naam	Strucuur
SCE	S:zijde-achtig blok, C: statistische kluwen, E: elastine-achtig blok
TR4H	T: collageenachtige drievoudige helix, R: statistische kluwen, H: poly(histidine) hexameer
TR4K	T: collageenachtige drievoudige helix, R: statistische kluwen, K: poly(lysine) hexameer
TR4T-Cys	T: collageenachtige drievoudige helix, R: statistische kluwen, Cys: cysteine

Tabel 8.1 Asymmetrische triblok eiwitpolymeren die in dit proefschrift bestudeerd worden.

Een triblok copolymeer eiwit (SCE) geinspireerd op zijde (S) en elastine (E) wordt geanalyseerd in de **Hoofdstukken 3 en 4**. Het zijde-achtige blok is opgebouwd uit 12 herhalingen van de sequentie GAGAGAGE en vormt een pH-gevoelige beta-rol (een structuur die lijkt op de bekendere beta sheet) die vervolgens zijdelings kan associeren tot lange fibrillen. Het elastine-achtige blok bestaat uit 40 herhalingen van de sequentie VPGXG (waarin X een hydrofoob aminozuur is), en heeft thermoresponsieve eigenschappen; boven een bepaalde temperatuur (zg Lower Critical Solution Temperature of LCST) wordt het slecht oplosbaar en vormt het aggregaten. In **Hoofdstukken 3**, we vinden dat polymeren die zowel zijde-achtige als elastine-achtige domeinen hebben temperatuur-afhankelijk fibrilleergedrag vertonen. Bij hoge temperatuur geven de elastineblokken aanleiding tot irreversibele bundeling en aggregatie van de fibrillen. De aanwezigheid van een kluwenachtig middenblok (C) tussen de functionele blokken vermindert de wederzijdse wisselwerking, en helpt zo de blokken te 'ontkoppelen', waardoor de temperatuurgevoeligheid wat afneemt. We vinden ook dat door de aanwezigheid van het elastineblok de kinetiek van de fibrilvorming verandert. Terwijl zijde-achtige eiwitten zonder elastine blokken monodisperse fibrillen vormen, leidt de inbouw van het elastineblok tot polydisperse fibrillen met een concentratie-afhankelijke lengte. Dit is een aanwijzing dat de asymmetrische triblokken homogene nucleatie kunnen

vertonen, terwijl de fibrillen van de symmetrische triblokken S-C-S of C-S-C, zonder elastine, niet homogeen kunnen kiemen.

In **Hoofdstuk 4** wordt de zelf-assemblage van het zijde-elastine polymeer nader gekarakteriseerd in aanwezigheid van opgelost zout (NaCl). We vinden dat de thermoresponsieve aggregatie van het E blok sterk afhangt van de zoutconcentratie. Bij hoge zoutconcentratie is de aggregatie veel uitgesprokener. Bij hoge pH, waar het S blok niet assembleert, vormt het polymeer micellen bij verwarming, wanneer er genoeg zout is. Bij lage temperatuur leidt het verlagen van de pH tot fibrilvorming. Wanneer beide blokken worden gestimuleerd tot associatie dan zien we dat de structuur die ontstaat afhankelijk is van het experimentele protocol, dwz van de volgorde waarin de stimuli worden toegepast. Wanneer men bij lage temperatuur verkregen fibrillen verwarmt dan ontstaan aggregaten die bij afkoelen niet weer uiteen vallen. De pH-gestimuleerde fibrilvorming van voorverwarmde eiwitoplossingen daarentegen leidt tot de vorming van grote deeltjes, die gemakkelijk sedimenteren. Het structuurverschil manifesteert zich ook duidelijk in de morfologie van gelen die bij hogere concentratie worden gevormd: terwijl via de route 'eerst pH verlagen, dan verwarmen' een transparant gel gevormd wordt, komen we via de route 'eerst verwarmen, dan pH verlagen' uit bij een turbide gel, dat ook een hogere elastische modulus heeft.

In **Hoofdtsuk 5 en 6** karakteriseren we een asymmetrisch triblokcopolymeer (TR4H, TR4K) dat een drievoudige helixvormer (T) heeft aan een eind, en een kort kationisch blok (H, K) aan het andere. Het T blok bestaat uit 9 herhalingen van de sequentie PGP en vormt helices bij lage temperatuur. Deze helices worden weer verbroken wanneer men ze verwarmt tot boven de smelttemperatuur. Het andere eindblok heeft zes positief geladen aminozuren (histidine, H, of lysine, K) en vormt micellen wanneer een negatief geladen polymeer wordt toegevoegd. De ladingsgedreven complexering van dit blok hangt af van de mate van protonering, die op zijn beurt afhangt van de pH. De additieven die in deze studie zijn gebruikt zijn een flexibel polyanion (polystyreen sulfonaat, PSS) en een semiflexibel polyanion (xanthaan). **Hoofdstuk 5** beschrijft de micel-netwerk overgang van het triblok TR4H met PSS. Eerst wordt de assemblage van ieder eindblok apart bestudeerd. Zoals verwacht vormt het collageenachtige blok drievoudige helices bij afkoeling. Het kationische H blok vormt polyelectrolytcomplexen bij toevoeging van PSS, wat leidt tot micellen met een ionsterkte-afhankelijk aggregatiegetal. Bij hoge concentratie vormt de

micellaire TR4H/PSS oplossing, na afkoeling, een visco-elastisch gel (fig. 8.1.a), dat weer smelt bij hoge temperatuur, hetgeen de helix-verbindingen tussen de micellen aantoont. Wanneer de concentratie onder het gelpunt (ca 90 g/L) blijft, wordt bij afkoeling vloeistof-vloeistof fasescheiding waargenomen; men ziet dan een verdunde fase boven een geconcentreerde visceuze gelfase (fig. 8.1b). De fasescheiding wordt gedreven door de aantrekking tussen de micellen, en die wordt uiteraard veroorzaakt door helices die zich vormen tussen de micellaire coronas. Ze verdwijnt wanneer de oplossing wordt verwarmd, of als de micellen uiteenvallen, dwz wanneer de ionsterkte wordt verhoogd.
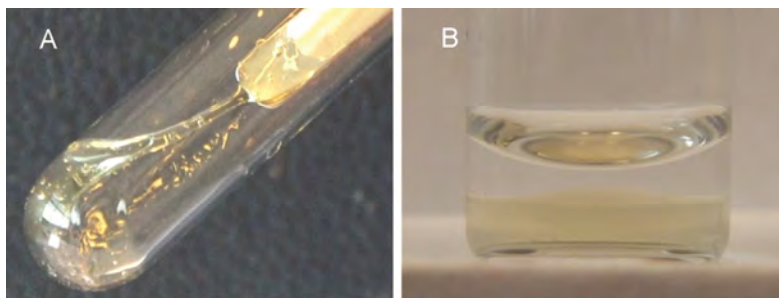

Fig. 8.1 (A) Een fysisch gel gevormd door thermisch stimuleren (afkoelen) van een TR4H/PSS complex bij hoge concentratie (150 g/L). (B) Fasescheiding door thermische stimulatie (afkoelen) van een TR4H/PSS complex bij lage concentratie (40 g/L).

De ladingsgedreven complexering tussen een gelijksoortig triblokcopolymeer, TR4K, en xanthaan, een semi-flexibel polyelectrolyt, wordt gepresenteerd in **Hoofdstuk 6**. Xanthaan is een natuurlijk, negatief geladen polysaccharide met een contourlengte van ongeveer 1.5 micrometer en een hoge polydispersiteit. Bij hoge temperatuur en zeer lage xanthaan concentratie bindt TR4K aan de xanthaan hoofdketen via het geladen blok K, en dat leidt tot 'flesseborstel' structuren bijeengehouden door electrostatische interactie. Dat manifesteert zich als een sterke toename van de lichtvertrooiing, door complexdeeltjes met een hoge molaire massa. De vorming van de flesseborstels hangt af van de pH vanwege de protonering van het kationische K blok. Het xanthaan/TR4K complex vertoont voorts thermogevoeligheid door de helices die het T blok kan vormen. Bij een xanthaanconcentratie rond de overlapconcentratie (7 g/L) resulteert de aanwezigheid van het triblokcopolymeer in een toename van de elastische modulus van het xanthaangel. Bij hoge temperatuur is de toename ongeveer een factor 3. Aangezien er dan geen helices zijn,

moet dit komen van de verstrengeling van de flesseborstels. Het niet-lineaire reologisch karakter van de xanthaan/triblok gelen is ook significant anders dan dat van xanthaan alleen. Terwijl xanthaan gelen eenvoudig pseudoplastisch (shear-thinning) zijn en smelten bij een vervorming van ca 100%, door de oplijning van de moleculen, vertoont het xanthaan /TR4K gel een tweestaps pseudoplasticiteit, waarbij de eerste stap waarschijnlijk het loskomen van de eiwitten van de xanthaanketen is. Bij lagere temperatuur, als er wel helices zijn, is de modulus nog ongeveer een factor 2 hoger dan bij hogere temperatuur. Dit wordt toegeschreven aan de vorming van crosslinks tussen de flesseborstels, ook weer via helices gevormd door de eiwitmoleculen.

In **Hoofdstuk 7** bespreken we tenslotte een asymmetrisch copolymeer dat twee helixvormende eindblokken heeft, met een cysteïne-residu aan een van deze twee. Onder oxiderende condities kan het cysteïne disulfidebindingen maken tussen twee polymeren, terwijl bij reducerende omstandigheden deze bindingen breken en thiolgroepen terugkomen. Aangezien cysteïne slechts een S-S brug kan vormen, is vorming van intramoleculaire lussen uitgesloten. De aanwezigheid van S-S bindingen verbetert de thermostabiliteit van het helix-netwerk aanzienlijk. Dit wordt duidelijk door het verschijnen van twee smelttemperaturen, waarvan de hoogste komt van de S-S-gestabiliseerde helices. De elastische modulus van het fysische gel in de aanwezigheid van S-S bindingen is bijna 2 maal zo hoog als die van het netwerk zonder die bindingen. De relaxatietijd wordt eveneens een factor 3 langer, hetgeen erop wijst dat helix-knooppunten ook door S-S bindingen worden gestabiliseerd.

Acknowledgment

The study presented in the book would not be finished without supports from many people. Therefore, I would like to show my appreciation to them in the last pages.

I would like to thank Martien for choosing me as the PhD researcher for this project and as one of his students. Martien, during the busy time as the Chair of our Group, you often tried to manage your time to supervise me and share your scientific interests. I am very grateful that you always have a trust in me, and give me lots of freedom to work. I also appreciate that you appointed Jasper to be my weekly supervisor who has really made my research significantly move forward! Thank to your passion, we have finished this project, eventually.

Jasper, it is my privilege to be one of your students. I really appreciate your patience to teach me the basic rheology, your continuous supports and encouragement. With your practical planning, my study is indeed finished on time in spite of many scientific failures and arrangement inconvenience as well. It is hard to express how much debt I owed you.

Frits, I would like to thank for your arrangement so that I have sufficient conditions to work in FBR. Although your time is occupied with different projects and responsibilities, you are always approachable to supervise me. I also appreciate that you are always present in my project meetings at FOM.

Marc, as my weekly supervisor in FBR, you have shared your incredibly deep experiences in molecular biology and fermentation. I appreciate a lots that you patiently helped me firstly to adapt your lab, and secondly to well carry out my project there with many useful discussions. I also thank Emil, Anton and other colleagues in FBR for their supports in FBR.

During my long time being abroad, I have finally arrived at "Fysko home". I would like to thank all Fysko colleagues who indeed silently help me to fulfill my job here. Josie, thank so much for your sweet heart; you are the one that raises me up in Fysko, especially when the researches are going down. I would love to talk with you continuously about everything in life. You transfer your warm-hearted encouragements and your strong believes in a good life to me. I would like to thank Renco, Franks, Marlene and Mieke for being available to support me whenever I need you. And Remco, I really appreciate your knowledge and your enthusiasm to help me with DLS and SASX. You always support me

with your highest responsibility. I also enjoyed sharing with about other non-scientific stuffs. I sincerely thank Mara with her quick supports whenever I need it. She always tries to make things go smoothly. I also appreciate supports from Ronald, Anton for technical helps, Jan for teaching arrangement, Anita and Bert for management work, and Diane for friendly joining us all non-scientific activities (e.g. lunch/coffee break time, bar). I also appreciate all other Fysko staff members for silently making this lab a pleasant working environment.

Certainly, "Fysko home" can not be established without the presence of my friends (also my colleagues) who make my life here much more colorful. Firstly, thank all guys of '2009-2013 batch'. We are coming to "Fysko home" and maybe leaving it almost the same time. I can start to count from the first floor at the furthest point of the lab. Huanhuan and Liyakat, you are the sincere friends I am happy to have. I would never forget the jokes and stories we shared behind the closed door of our room 1014. Thank you very much for your being there. Armando, thank you for being my first Fysko-FBR colleague, you have supported me a lots when I started my project. During this 4-year job, we have gone through some difficult moments in "our protein polymer group''. Thank you for the passion you have shared with me. Yunus, thank so much for sharing with me your passion in both science and "strange" music. Dmitry, a real gentleman! Thank you so much for being one of my friends here. You are the one that I can always ask for help without hesitation. Soumi, thank you for lots of sweet time we have spent together including organizing the 2011-PhD trip, the activities in the 2013-PhD trip, and all non-scientific discussions. I also thank Surrender for various pleasant talks. As a FOM-WUR employer, we also shared FOM meeting and scientific interest. Thank you for the very excellent Indian dinner as well. Lennart, the "angry guy", who always tries to tease on people, but is willing to help everyone, thank you for helping me the first AFM imaging and all other things. We had also made a very nice trip to Washington together. Thank so much for your arrangement and sweetness during that time. Emilia, Harke, Monika! Thank you for good time we had both in lab and in the 2011 PhD-trip.

Paulina, I still remember and keep the videos in which you were explaining to me how to do rheological experiments. I really appreciate your supports in Fysko and the time we worked together in FBR. Yuan (Coconut girl), thank so much for our friendship, I would love to recall all memorial 'events' with you. Evan, thank so much for your warm care and

nice time in organizing and during the 2011-PhD trip. Wolf and Gosia ('long hair'), I was so happy that you started your work in FBR when I was still working there. Your presence in the worst period of my project indeed had somehow a meaningful impact on me. Thank you for your encouragement. Gosia, outside of lab, I also enjoyed the nice time with you and your husband. I also want to 'meet' your favorite horse in near future. And Wolf, I still remember your first days working in FBR, you (with very specially Dutch red hair !!), a newcomer, who was learning to adapt to the fermentation world, voluntarily offered to carry the fermentors and push heavy carts (full of water-containing bottles) for me. I am always grateful to your persistence to convince me to do more fermentation of my clones. Jacob, Sabine and Johan, my office neighbors, thank a lot for your sweetly sharing with me (and my office mates) happy time and funny jokes. Certainly, we (and Wolf) shared good time in the same car during 2013-phD trip together as well. Frank (Snijkers), you helped me to do rheology in your last 2 months in Fysko, though you were busy with many unfinished works; thank you very much for your patience and sharing with me your deep experiences in experimental rheology. Katarzyna, my lovely bench mate, I love the time when we shared the corner between your bench and mine. Thank you so much for your sweet care, the funny time and the nice shoes. Junyou, I am so happy to have you to help me with static scattering. I am grateful to your generosity of offering supports without asking for reward. Besides, thank you very much for other non-scientific discussions. Inge, thank you for very pleasant time we shared during the 2011 PhD trip. Kamuran, Celine, I really enjoy talking to you guys. Your sense of humor makes the lunch time better to join. Gosia (short hair), Nadia and Helene, thank you for the very nice time together in Rome and also your warm care to me when I was lost. Christian, Jeroen, Maria, Marten, Rui! I like to listen to your funny (sometimes a bit crazy) jokes during lunch or coffee break (sometimes in bars). Hande, Natalia, although we have not had chances to work together yet, I enjoyed talking to you about both fun and bad moments on protein projects. Merve, my new office mate, thank you for many discussions we are sharing in our office now; and thank you for understanding my moody moments during the last stage of my thesis. Juan and Ran, thank you for the good time we shared sport activities. Certainly, thank all Fysko fellows who I have or have not had opportunities to (talk) work with.

I also sincerely thank Maria and other FOM staff members for their supports. Maria, you have organized IND (my Dutch residence permit) from the beginning of my PhD and

clarified all other management stuffs during these 4 years, although I have not met you yet. I also acknowledge BRM Committee A for their presence during all my project meetings and scientific comments on my project progress.

I would like to thank my family for having faith in me and continuous supports from far away. I also want thank my longtime friends (chi Le, anh Trung, My, Trong, Giang) for encouraging and sharing with me bad and good moments of being abroad.

Phuoc, I always highly appreciate your standing by me, and respect on my decisions. Thank you very much for everything.

Thao

About the author

Thao (Thi Hien) Pham was born on the 31st of January 1982 in Quang-Ngai, Vietnam. In 1999, she started her undergraduate in Biotechnology in Hochiminh University of Natural Science. In 2004, she got Samsung Scholarship to study Master in Biomedicine in Sungkyunkwan University, South Korea. After finishing her Master study, she worked as a research assistant in College of Enginnering, Sungkyunkwan University, with the research interest in nanoparticles for biomedical applications. In 2008, she moved to Germany to work in Life & Brain Center, Bonn University. In the end of 2008, she moved to Belgium to work as pre-doctoral student in K.U. Leuven. In December 2009, she started her PhD research funded by Stichting FOM in the group of Physical Chemistry and Colloid Science, Wageningen UR. The results of this PhD study are presented in this book. In December 2013, she will continue her scientific work as a postdoc in the same group.

List of publications

M. D. Golinska †, **Thao T. H. Pham** †, M. W. T. Werten, F. A. de Wolf, M. A. Stuart and J. van der Gucht, Fibril formation by pH and temperature responsive silk-elastin block copolymers. *Biomacromolecules*, 2013, 14 (1), 48-55. (†: equal contribution)

Thao T. H. Pham, P. J. Skrzeszewska, M. W. T. Werten, W. H. Rombouts, M. A. Cohen Stuart, F. A. de Wolf and J. van der Gucht, Disulfide bond-stabilized physical gels of an asymmetric collagen-inspired telechelic protein polymer. *Soft Matter*, 2013, 9, 6391-6397.

Thao T. H. Pham, F. A. de Wolf, M. A. Cohen Stuart and J. van der Gucht, Pathway-dependent properties of a multi-stimuli sensitive biosynthetic hybrid network. *Soft Matter*, 2013, 9, 8737-8744.

Thao T. H. Pham, Junyou Wang, M. W. T. Werten, Frank Snijkers, F. A. de Wolf, M. A. Stuart and J. van der Gucht, Multi-responsive gels formed by a biosynthetic asymmetric triblock protein polymer with a polyanion. *Soft Matter*, 2013, 9, 8923-8930.

Thao T. H. Pham, Frank Snijkers, F. A. de Wolf, M. A. Stuart and J. van der Gucht, Enhanced properties of xanthan hydrogels through electrostatic crosslinking with a biosynthetic triblock protein polymer. *Submitted*

Overview of completed training activities (VLAG)

Discipline specific activities (courses, workshops, symposia, summer schools etc.)

Dutch Soft matter day (WUR)	2010
European School on Rheology KU Leuven, Belgium	2011
FOM Young Scientist day, FOM, Utrecht	2011
Han-sure-Lessse winter school, Belgium	2012
ECI Conference, Crete, Greece	2012
Gordon research Conference, Davidson College, USA	2012
FOM Bio-related workshop, Utrecht	2010-2013
DPD Lunteren, The Netherlands	2013
ISMC conference, Rome, Italy	2013
FOM-biophysics days, Veldhoven, The Netherlands	2013

General courses

FOM- Taking charge of PhD projects	2010
Scientific Writing, WUR	2011
FOM- Nyenrode Business orientation program	2013
FOM- Career planning course	2013

Optionals (discussion groups, PhD excursions, MSc courses, etc.)

PhD excursion PCC, WUR (Singapore, Malaysia, Vietnam)	2011
PhD excursion organizing committee PCC, WUR	2011
Advance Soft Matter PCC, WUR	2011
PhD excursion PCC, WUR (California, USA)	2013
Group meetings PCC, WUR	2010-2013
FOM- BRM project meeting (bi-yearly)	